Aramco Journal of Technology

SUMMER 2019

Aramco
Journal
of Technology

The *Aramco Journal of Technology* is published quarterly by the Saudi Arabian Oil Company, Dhahran, Saudi Arabia, to provide the company's scientific and engineering communities a forum for the exchange of ideas through the presentation of technical information aimed at advancing knowledge in the hydrocarbon industry.

Editor

William E. Bradshaw
william.bradshaw.1@aramco.com.sa
tel: +966-013-876-0498

Production Coordination

Richard E. Doughty

Design

Graphic Engine Design Studio
Austin, Texas, U.S.A.

The *Aramco Journal of Technology* gratefully acknowledges the assistance, contribution and cooperation of numerous operating organizations throughout the company.

ISSN 1319-2388

Dear Readers,

Welcome to Saudi Aramco's newly redesigned *Aramco Journal of Technology*.

We welcome your comments and feedback.

Please email your comments to the editor:

William.bradshaw.1@aramco.com

Contents

Laser Gun:
The Next Perforation Technology

Dr. Sameeh I. Batarseh, Dr. Damian P. San-Roman-Alerigi, Omar M. AlObaid, and Dr. Haitham A. Othman

Abstract /

Establishing communication between the wellbore and hydrocarbon-bearing formations is critical to ensure optimal production. Laser technology utilizes the power of light to perforate rocks and achieve this goal. The technology is non-damaging, safe (nonexplosive), and affords precise control over the perforation's geometry (size and shape). The technology has been successfully demonstrated in the lab environment. The process creates an enhanced tunnel that improves the flow and increases production. The results have guided the development of a field deployment strategy. In the field, the laser source will be mounted on a coiled tubing unit on the surface and the beam transmitted downhole via optical fibers. Downhole, the beam will be out-coupled and directed to the target using an optical bottom-hole assembly (oBHA). This tool combines optical and mechanical components to control the beam and produce multiple shots per foot as needed to create the desired perforation network. High power laser perforation is the next intelligent perforation generation that will change current well perforation.

Laser-rock interaction drives in the transformation of electromagnetic (EM) energy into thermal energy. This results in a highly localized and controllable temperature surge that can melt or vaporize the rocks. These properties make the technology a unique alternative to current perforation techniques based on shaped charge guns. The thermal process induced by the laser enhances the flow properties of the rock, especially in tight formations. Laser perforation has been tested on all types for rocks, including unconventional tight sands. This has been proven through extensive pre- and post-perforation characterization over the last two decades.

This work presents the development and evolution of the high power laser tools for subsurface applications. These tools provide innovative and non-damaging alternatives to current downhole technologies. In the lab, the laser technology has been proven to improve the flow properties; therefore, it can improve communication between the wellbore and formation. To achieve this efficiently in the field, it is necessary to develop different tool designs and configurations, manufacture prototypes, conduct extensive tests, and optimize each part before upscaling for field operations.

The laser source is mounted in a coil tubing rig at the surface; the coil contains the optical fiber cable used to convey the energy to the downhole tool. The tool combines mechanical and optical components to transform, control, and direct the laser beam. The design and configuration of each tool assembly varies depending on the targeted application. For example, the perforation tool converts and splits the beam into several horizontal beams; whereas the drilling tool emits a straight beam with a controlled size for deeper penetration. They also incorporate purging capabilities to circulate fluids to clean the hole from the debris and carry the cuttings. The entire assembly must be made to fit in slim holes as small as 4", and be ruggedized to operate in a complex environment with high-pressures and high temperatures.

The technology improves reach and provides versatility in a compact and environmentally friendly manner. For example, it is a waterless technology when it is used for fracturing, and a nonexplosive-based perforation when it is used to perforate. The unique features of the technology enable a precise, controlled, and oriented delivery of energy in any direction, regardless of the reservoir stress orientation and magnitude. Therefore, it enhances reach to produce from pay zones that are bypassed by current conventional technologies and practice. The motivations to search alternative technologies are the advancement of technologies, including elevated higher power laser systems, and the need to enhance several applications in deeper wells in an environmentally friendly manner.

Introduction

Perforation is needed to establish communication between the wellbore and the reservoir, bypass the damage zone caused by drilling, and open pathways for future stimulation, if needed.

Early inventions of perforating devices can be traced to the early 1900s. In 1902, Thomas E. Clark invented a tool to perforate through casing and formation that used a mechanism to drive a lever through the casing and then

Fig. 1 *A simplified design of the shaped charge gun.*

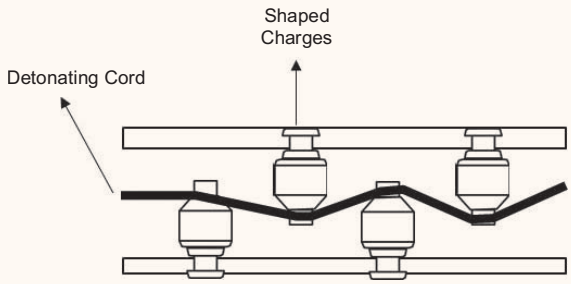

Fig. 2 *The main components of the shaped charge bullet.*

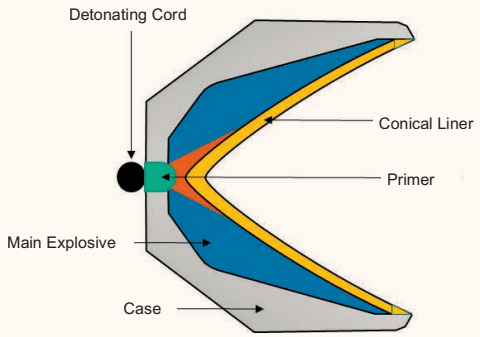

retract it to allow for fluid to flow into the well[1]. Clark and several other invertors investigated other methods to perforate the casing; those methods were implemented in the early 1900s, however, these showed little success.

By the 1930s, the industry needed a new method to establish wellbore to reservoir communication and increase production at the same time. Ira J. McCullough designed a tool called the gun perforator, which was capable of firing bullets through the casing and formation[2], and it was capable of firing bullets simultaneously through the casing. Thereby providing the needed communication and increasing production. The method was quickly adopted by the industry. Variations on it continue to be used and led to the development of the shaped charge perforation.

Figure 1 depicts a simplified design of the shaped charge gun for illustration. Figure 2 presents the main component of the shaped charge bullet. The underlying technology was invented during the Second World War as an anti-tank weapon by Henry Mohaupt. He was recruited by Fort Worth to modify the technology for perforating oil and gas wells[3].

The main components of a shaped charge are: detonating cord, primer, main explosive, case, and conical liner. The function of the detonating cord is to deliver an electric charge to detonate the primer, which contains small quantity of a high explosive material. The case is made of steel or zinc and houses the explosive material, and the liner presses the main explosive. This main explosive provides most of the energy to create the perforation. The explosion pushes the liner material to form a jet, which perforates the casing and formation[4]. Notably, the performance of the shaped charge depends on the design of the case and not necessarily the amount of explosives. For example, 25 grams of explosives can create a perforation with a depth of 25" and 2⅜" diameter, or a depth of 6" and ¼" diameter.

Perforations are meant only to create a channel between the reservoir and wellbore to allow oil and gas to be produced. Subsequently, explosive perforation methods can create a compacted zone, which significantly reduces permeability. In 1987, Syed M. Tariq showed the effect of shaped charge perforations on the efficiency of hydrocarbon production. The study discussed the effects of different parameters on the productivity ratio, such as perforation depth, diameter, angle phasing, and length[5]. The study demonstrated that the productivity increases in relation with perforation length, density, and phasing. Therefore, productivity can be significantly improved by optimizing these variables. The perforation diameter is another important parameter in increasing the productivity ratio.

In most cases, a deep and large perforation is desired; however, achieving it is challenging with current technology. The explosive and liner of the shaped charge may yield either deep or large diameter perforation. A deep perforation is desired because it bypasses the damaged zone caused by drilling; whereas, a large hole is preferred to decrease the hydraulic differential pressure and produce more hydrocarbons. Subsequently, the diameter of the perforation tunnel should be optimized to minimize the friction pressure (ΔP)[6].

$$\Delta P = 0.2369 \times \rho \left[\frac{Q}{N \times D_p^2 \times C_d}\right]^2 \quad (1)$$

where ρ is the density of fluid, N is the number of perforations, Q is total pump rate, D_p is the perforation

Fig. 3 *Perforation friction pressure (ΔP), as a function of the perforation diameter (D) for the case Q = 30 bbl/min, p = 10 lb/gal, N = 1, Dp = 2", and Cd = 0.87.*

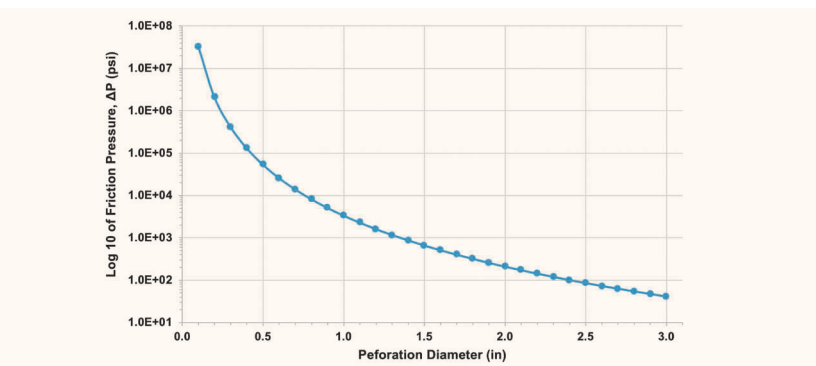

dimeter, and C_d the coefficient of discharge. These parameters can also change with time; for example, due to abrasion by the fracturing fluids or the injection-induced perforation friction decrease. Figure 3 presents the vertical hole pressure drawdown as a function of the perforation diameter. The results show that the optimized diameter should be large ($D \gtrsim 2$") to reduce the friction pressure, although this is difficult to achieve using current shaped charge technology. High power overcomes these limitations, it can create perforations with large diameters and long depth; for example, perforations in sandstone using a laser can attain large diameters ($D = 4$") and long depth ($L = 24$")[7].

In the oil and gas industry, this technology offers a unique solution to resolve challenges in many areas, ranging from stimulation to drilling[8]. Research in these areas has been continuously growing over the last two decades. These efforts described the interaction of a laser with subsurface materials (rocks and fluids), identified key laser sources for downhole applications, and drive the development of unique solutions to enable subsurface transmission of the high power beam[9]. Research in this area has grown significantly in the recent years due to the evolution in the laser industry. High power laser generation has become more efficient, reliable, powerful, and cost-effective. Thereby, bringing about a wide range of applications and the opportunity to take the technology downhole.

High Power Laser Tool Development

In the field, the laser source will be placed at the surface and the beam transmitted downhole via optical fibers. Downhole, the beam can be out-coupled and directed to the target using an optical bottom-hole assembly (oBHA). This tool combines optical and mechanical components to control the beam for different applications.

Laser and Fiber Optics

The word laser means "light amplification by stimulated emission of radiation." Lasers are used in many industries due to their reliability, precision, accuracy, efficiency, safety, and power. The first laser was demonstrated at the Hughes Research Laboratory in California by Theodore Maiman in 1960[10]. The idea was posited by Einstein in 1916. The technology has evolved significantly since its inception. Nowadays, the laser industry offers a wide range of laser classes with different output power, frequency, and profiles in space and time — continuous and pulsed. These characteristics define the applicability and limitations of laser technology for any application.

A fiber laser is a special kind of solid-state laser where the gain medium is an optical fiber doped with rare earths, e.g., erbium, ytterbium, neodymium, dysprosium, praseodymium, or thallium. Conceived as laser amplifiers in optical telecommunication networks, fiber-based lasers have evolved to become a pivotal technology for a wide array of applications in industry and research. Fiber lasers are candidates (now) for oil and gas applications due to their properties; e.g., portability, high power output up to 100 kW[11], and delivery via fiber optic cables.

Concerning delivery, the tool will require a specially built optical fiber to transmit the high power beam several miles below the ground. While traditional fibers for telecommunications can reach several kilometers, these are not designed for the transmission of multi-kilowatt lasers. The limiting factors in fiber optic transmission of high power laser beams are attenuation (loss) due to the materials' absorption and scattering; therefore, material selection, fiber design, and fabrication, are crucial to create low-loss and high quality optical waveguides that are defect-free and immune to [stimulated] nonlinear effects like Brillouin and Raman scattering. These last two effects are of particular importance to overcome in high energy applications, where nonlinear effects can potentially kill the beam transmission[12-15].

Optical Bottom-Hole Assembly (oBHA)

Figure 4 depicts the configuration of the high power laser gun. The system is different in principle and functionality than the conventional shaped charge gun. The main components of the laser gun are optical component or assembly, rotational assembly, laser/purge perf-port, and laser/purge straight-port.

Optical assembly. Most optical systems for subsurface application are based on lenses, mirrors, and prisms. These are combined to create different optical systems for subsurface operations, including optical heads to focus, de-focus, collimate, and expand or contract the beam.

Fig. 4 *The configuration of a laser perforation gun showing two laser ports.*

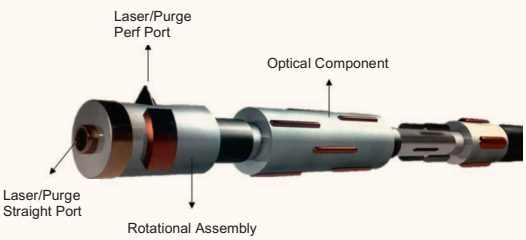

Fig. 5 *Irradiance for a Gaussian beam with beam waist of 30 mm, wavelength 1,064 nm, and power 10 kW.*

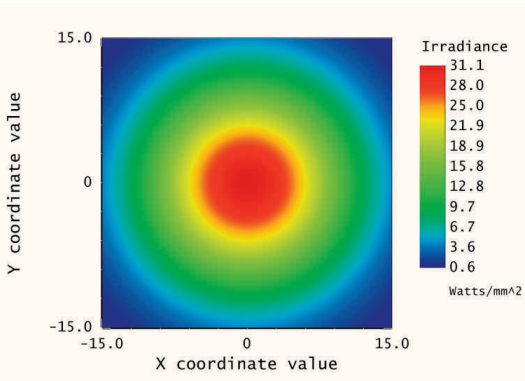

Figures 5 to 8 plot the ray tracing and irradiance (energy distribution) for the beam in each of these applications. In all cases, the input beam is a 30 mm Gaussian laser beam with a wavelength of 1,064 nm and the power is 10 kW. Note, the calculated irradiance (light distribution) for the output beams shows the distortion effects due to the optical system at the given image (visualization or work) plane.

Fig. 6 *Light focusing using a bi-convex lens: (a) ray pattern, and (b) output beam irradiance. Note, the calculated irradiance (light distribution) for the input (b) and output (c) beams shows the distortion effects due to the lenses.*

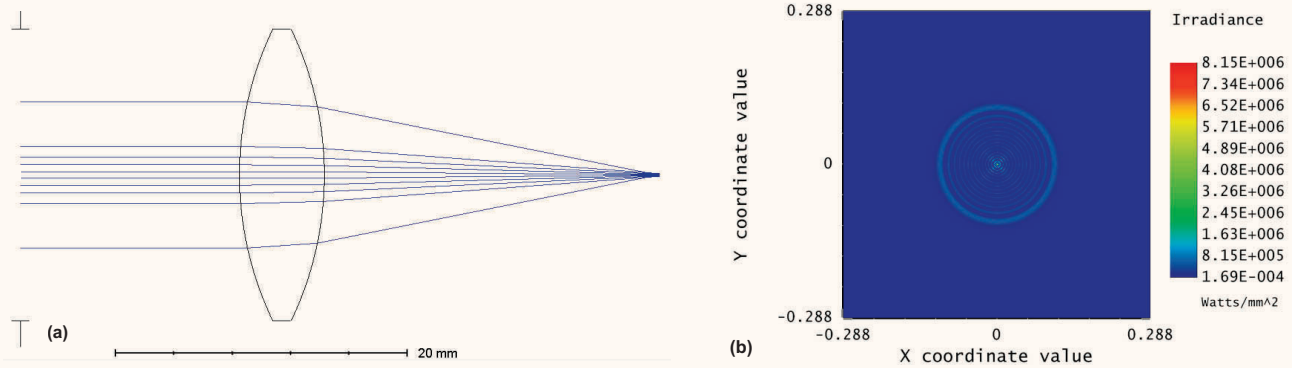

Fig. 7 *Light focusing using a bi-convex lens: (a) ray pattern, and (b) output beam irradiance.*

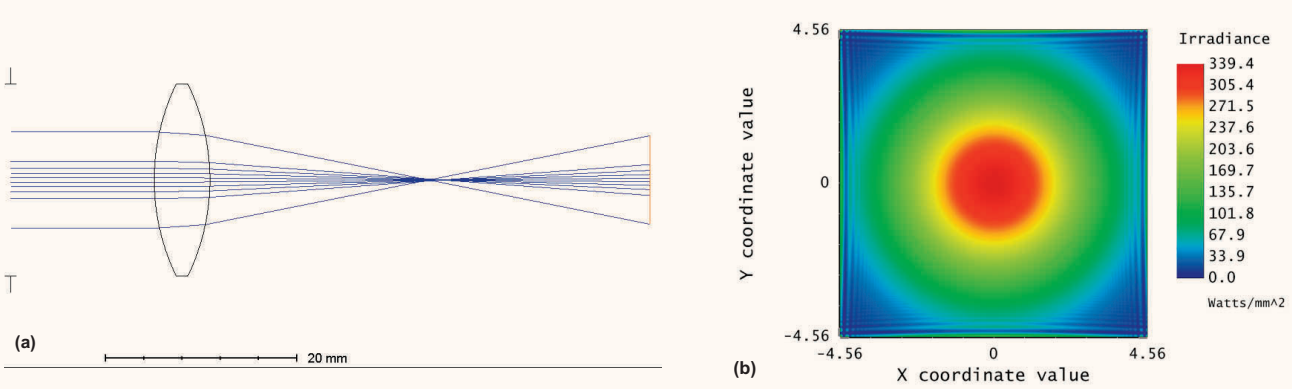

Fig. 8 *Light collimation using two bi-convex lenses: (a) ray pattern, and (b) output beam irradiance. Note, the calculated irradiance (light distribution) for the output beam shows the distortion effects due to the lenses.*

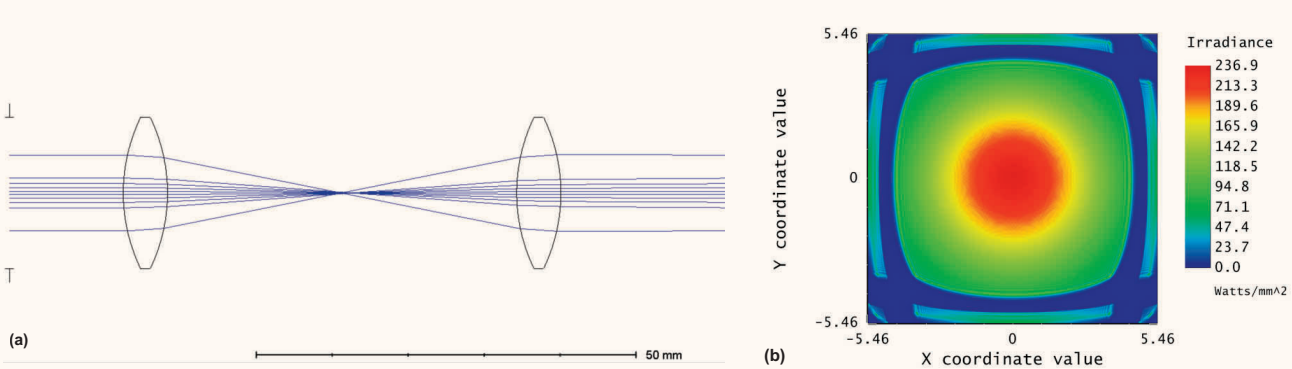

Rotational assembly. When the beam exits from the optical component, the controlled beam (size and shape) enters the rotational assembly. The function of this part is to control and orient the beam to the target into the formation — through casing and cement. Figure 9 displays the cross-sectional of the tool with the beam exiting straight for drilling applications. There is a mirror that slides back and forth to activate or deactivate the output; when the mirror is in a flat position it allows the beam to exit straight through the port.

For perforation mode, the mirror is activated. It orients the beam at an angle exiting through the perforation port as seen in Fig. 10.

The excitation of the beam is done by switching the beam on and off as much as needed, which means there are no shaped charges to load and unload to achieve a number of shots per foot. The tool moves to the target zone, perforates, rotates, and moves up or down to perforate again. In another configuration, the tool splits the beam into several beams simultaneously to achieve multiple shots per foot.

Purge. The purge serves different functions within the system. It carries cuttings, clears the beam path, and cool downs the assemblies. The purging fluid can be gas or liquid and must have enough viscosity to transport the debris out of the hole and be transparent to electromagnetic (EM) radiation, at least around the beam's wavelength.

Purging has several functions, including:

- Lubrication and cooling of the optical assembly, which heats up due to the absorption of the high power laser beam by the optics. Thermal management is critical to secure the integrity of the optics and mitigate changes in the optical properties due to heating.
- Clear the laser pathway: The laser-rock interaction drives a process that transforms EM energy into thermal energy. This thermal energy causes a localized temperature surge and provides the energy required to melt, spall, dissociate, evaporate, and even sublimate the rock. The thermal dynamics depend on the thermal and EM properties of the rock. The ablated material, debris and particles, flows and blocks the beam. The design of the purge is critical to maintain a flow that carries away the debris to

Fig. 9 *Laser perforation gun showing straight beam orientation mode.*

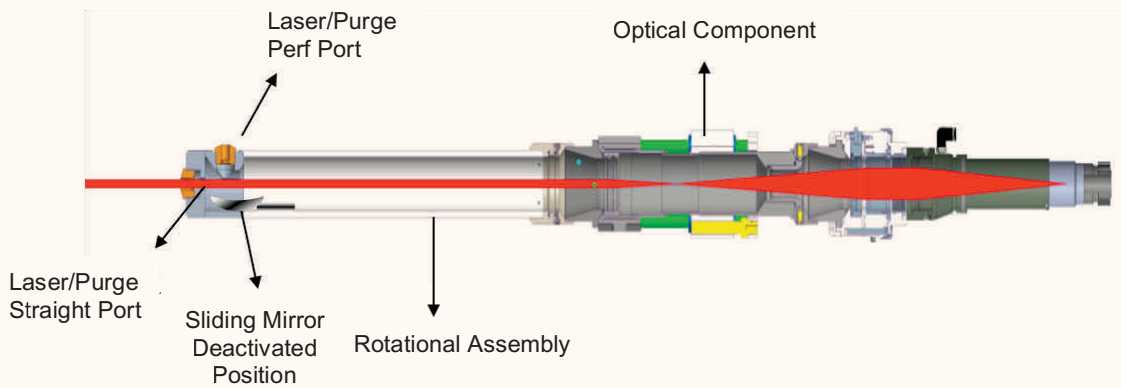

Fig. 10 *Laser perforation gun showing angle beam orientation mode.*

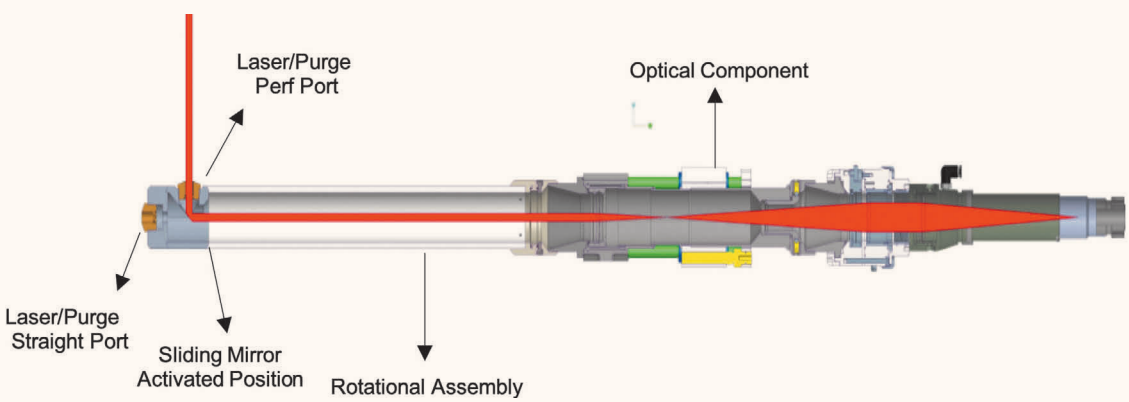

Fig. 11 *Reflection and scattering at an oblique incidence.*

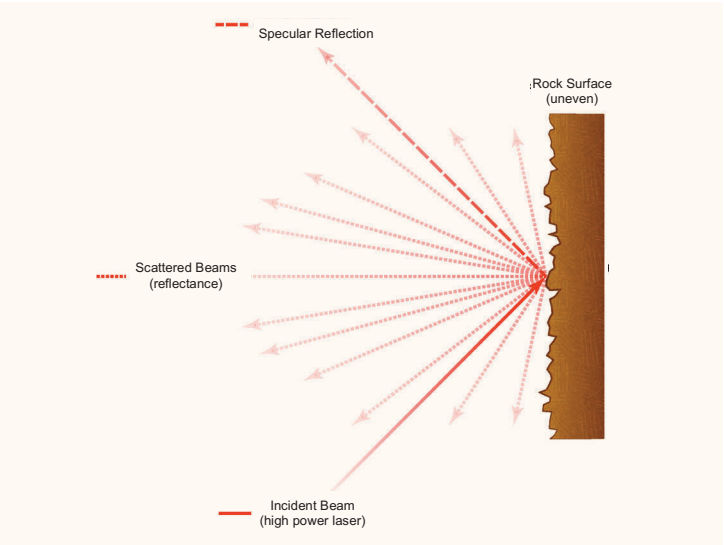

Fig. 12 *Reflectance and scattering at a normal incidence.*

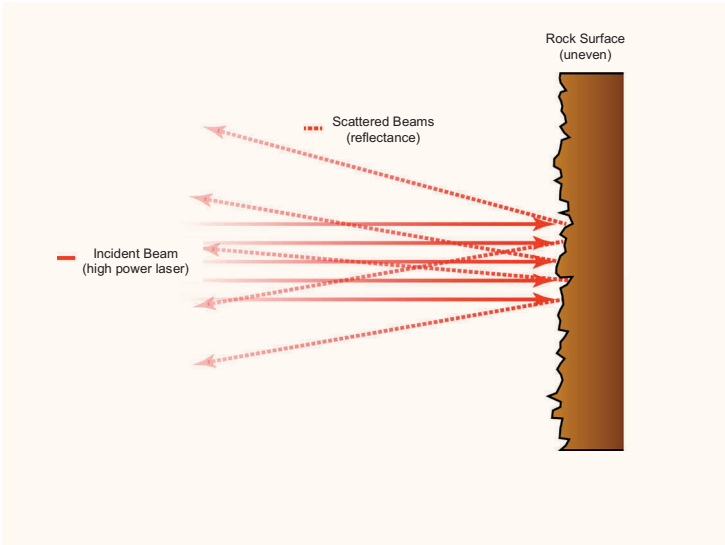

ensure a clear path for maximum interaction. The most efficient purge is coaxial, i.e., where the fluid flows in the same direction as the beam.

- Formation phase control: The purging media also controls the phase of the rock, for example, if fracturing is required to be initiated in the formation, then cooler fluid or gas can be used to provide thermal shocking to the formation, and fractures are created.

Interaction Results and Analysis

The laser beam incident on the surface of the rock may be partly reflected regularly (specular reflection) by the sample surface, partly scattered diffusely, and partly absorbed by the material. In practice, all three types occur at the same time, although with different contributions. This process depends on the characteristic of the surface and its environment. Mineral materials are generally polycrystalline so at each interface, inhomogeneity or imperfections can deviate, reflect, or scatter the high power laser beam.

The absorption and diffraction processes occur within a volume of the material, rather than strictly at the surface. This is because as the light interacts with the material it will be partially reflected, absorbed, and scattered by the first particle; the light scattered forward will interact with the particle beneath and undergo a similar process. This is a cascading process that takes place within a few micrometers from the surface. The net result is an absorption volume and light scattered in multiple directions, even for a beam at normal incidence. Figures 11 and 12 depict the process for an oblique and a normal incidence, respectively. In every case, the process results in a diffuse reflectance spectrum.

Figure 13 shows the reflectance spectra for different rock types and samples encountered in the subsurface. Notably, similar types of rocks may exhibit different behaviors due to their porosity, concentration of organic matter, bedding, and heterogeneities.

These spectra are critical because it shows how different rocks will absorb the high power beam. Low reflectance values mean that the sample absorbs more EM radiation; whereas higher values imply the opposite. Absorption occurs when the energy of the light beam is absorbed by

Fig. 13 *Average reflectance for different rock types and samples: anhydrite (AH), calcium carbonate (CB), concrete/cement (CR), dolomite limestone (DLe), Indiana limestone (LSi), desert pink limestone (LSp), yellow limestone (LSy), Saudi yellow limestone (LSsy), steel (MSt), and shales (SH) of varying origins.*

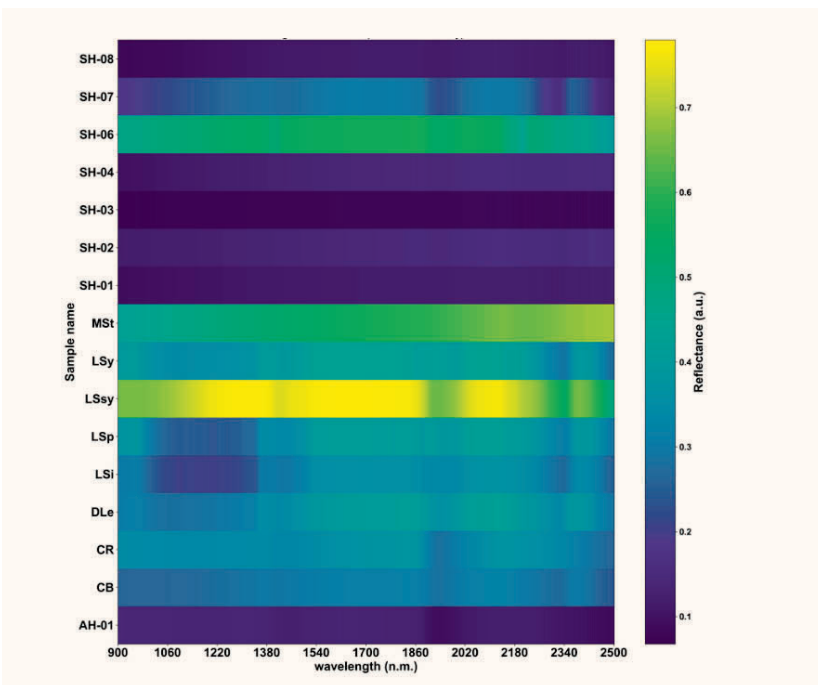

Fig. 14 *Kubelka-Munk spectra for a shale sample with different TOC.*

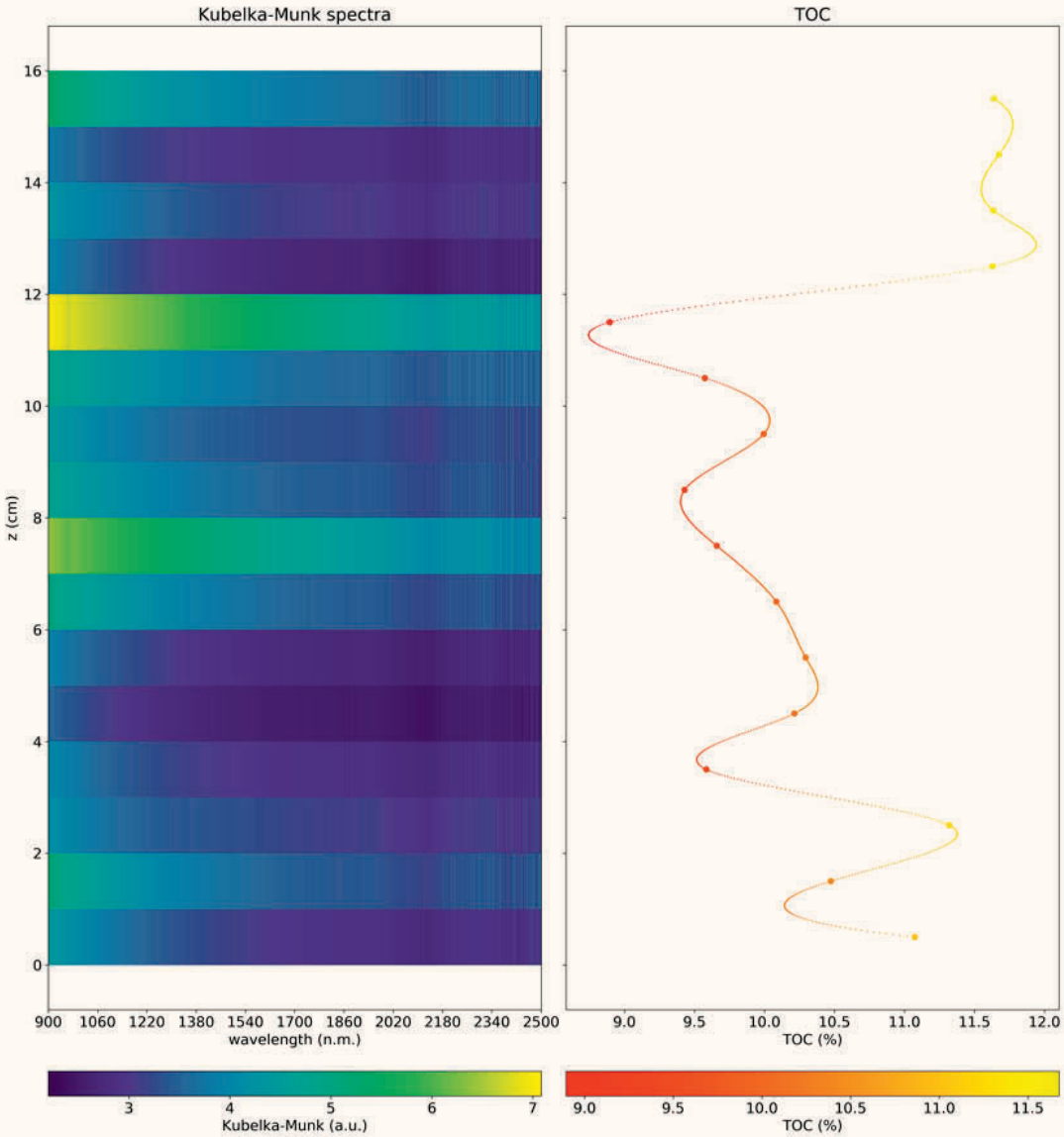

the material. In this way the light´s energy is transformed into potential energy in the atoms of the material. The result is typically heat, which causes the material to warm, and in some cases induce phase changes. There are two regimens of absorption: (1) linear absorption, the energy transfer does not depend on the intensity of the beam only in its frequency, and (2) nonlinear absorption, where absorption changes with the intensity resulting in absorption saturation.

There are different factors which contribute to overall absorbance or reflectance, and even for similar rock types results may vary. This is due to the heterogeneities, polycrystalline structure, morphology, and impurities, e.g., presence of organic matter, water, etc. Figure 14 shows the correlation of average absorption, measured using the Kubelka-Munk factor, and the total organic content (TOC) within each corresponding sample. The results show that there is some correlation between these parameters; the relation has been observed and used to characterize kerogen maturity on shale cuttings[16].

For high power laser applications, this information is critical because it determines how the laser propagates and is absorbed by the rock. In some instances, the rock or the material may have a high absorption, e.g., anhydrite and some shales, or low absorption, e.g., Saudi yellow limestone and some shales. Particularly for perforation, the beam will encounter several layers of casing, made of steel and cement layers of different thickness, and rocks with different saturation and conditions. Therefore, the beam will be absorbed differently at every stage

and the penetration rate will vary. Furthermore, the environmental conditions also play a role and may impact the evolution of the interaction.

Gas Purge on Dry Rocks

The purge provides thermal and kinetic energy to the process. The latter is used to remove material from the beam's path and carry cuttings. The former helps cool down the lased material through convection. This is because the purge gas has a high velocity, and therefore, a low temperature. Subsequently, it can also have an impact on the evolution of the laser process.

The combined effect of the process can be summarized using the specific energy. It measures the laser performance and the efficiency of the perforation. The specific energy is defined as the amount of energy required to remove volume of rock per unit of energy input. Its unit is kilo joule per cubic gram. This is similar to the thermal enthalpy, since it describes the amount of energy required to transform a quantity of the rock from one state into another, e.g., solid to liquid.

The energy consumed by the process must be balanced,

$$E_{in} = E_{thermal\ loss} + E_{absorbed} + E_{reflected}, \quad 2$$

where the input energy, E_{in}, includes the contribution of the high power laser beam and purging fluids. The right side of Eqn. 2 encompasses the portion of energy reflected by the material, the energy absorbed, and the thermal energy dissipated to the environment. The amount of energy absorbed will depend on the efficiency of the EM thermal coupling between the laser and the rock; this energy in turn drives the transport phenomena that changes the host rock and creates the perforation. Subsequently, the energy absorbed is divided into that used in (a) thermal processes, and (b) chemical reactions.

Salehi et al. (2007)[17] studied the effect of different purge gases on the performance of perforation on limestone and sandstone rocks. In particular, the study used argon, nitrogen, air, and helium. In all the experiments the laser parameters were kept constant, the power at 5.37 kW, time 4 seconds, and beam spot 0.35".

Figure 15 presents the effect of the four gases on Berea sandstone, where the range of the specific energy is between 45 kJ/cc to 50 kJ/cc. In this case, helium purge consumed the less energy to perforate, while argon and air consumed more energy. This might be due to the effect of these gases on the chemical reaction at elevated temperatures. Sandstone samples consists of different minerals, and quartz dominates the Berea sandstone. These minerals react differently when they are heated in different atmospheres. Alternatively, the temperature of the different purging gases may have changed the thermal dynamic processes. The net result is that different gas purges lead to variations in the measurable performance of the perforation[17].

Figure 16 summarizes the same experiment for a limestone rock[17]. In this case there seems to be no advantage to using one gas or the other. The sample consists mainly of calcium carbonate and the laser drives a high rate calcination process that liberates large quantities of carbon dioxide (CO_2). This liberated gas could have saturated the perforation and immediate environments; thereby, in effect decreasing the effect of different purging gases.

In the latter case, the laser drives a calcination process, which is the thermal decomposition of carbonate through calcination. The process is known to liberate high volumes of CO_2 as a gas. It can be described in two steps: (a) rock heating to calcination temperature, and (b) calcination. The results suggest that large volumes of CO_2 were generated during the calcination reaction; therefore, the calcination took place in a CO_2 atmosphere. The energy budget depicts the complex dynamics in these processes, which are governed by the efficiency of EM thermal coupling and the transport phenomena in the host rock of the perforation itself. These phenomena encompass mineral dissociation, chemical reactions,

Fig. 15 *The effect of gas purging on Berea sandstone[17].*

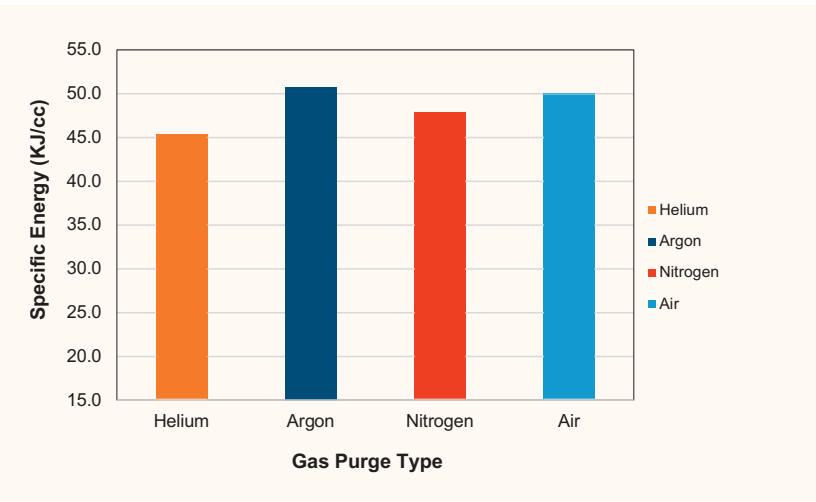

Fig. 16 *The effect of gas purging on limestone[17].*

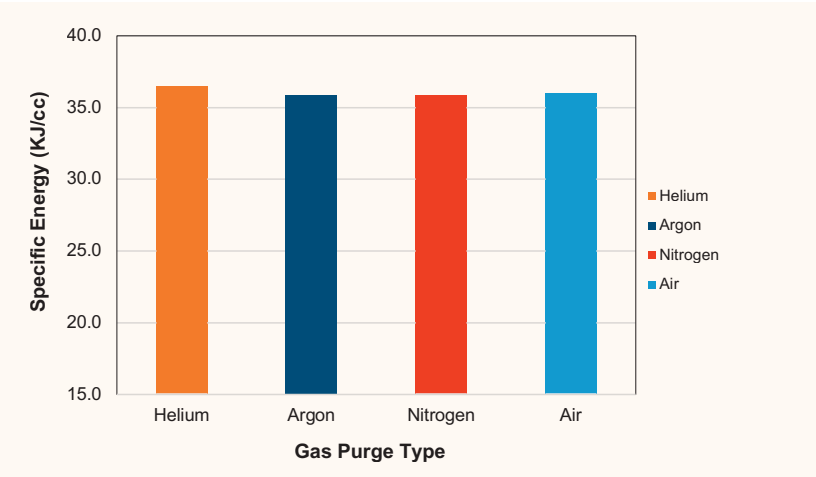

Fig. 17 *Laser perforation of a large sample, 4" in diameter and 24" deep.*

phase change, and convective flow.

Flow Improvement

The advantage of the laser perforation is the precise control of the perforation tunnel shape, depth, and quality. A laser is nonexplosive, therefore, it does not cause compaction or cruising to the formation. Figure 17 shows the perforation tunnel created using the high power laser tool. This perforation would overcome the requirements[6] described earlier on the text.

Table 1 summarizes the permeability and porosity characterizations of different rock types before and after perforation. In all cases, the experimental results demonstrate that a laser can improve the properties of rocks, even in tight formations.

Conclusions

A high power laser perforation gun has the potential to change the conventional perforation technology. It provides an alternative to explosive-based technologies. The process relies on the EM thermal coupling to create a controlled temperature rise and drive a localized phase transition process. The net result is the removal of material to create perforation tunnels of a controllable aspect ratio. A large perforation and tunnel can be created with the laser gun; this size — more than 2" in diameter and 24" deep — reduces the pressure drop across the tunnel for maximum hydraulic fracturing operation.

The system is compact, efficient, and reliable. The laser gun can generate a beam with controlled power that can melt, spall, or vaporize the formation. It creates a controlled perforation and a non-melt tunnel for maximum flow. Partial or permeable melt can also be created to form a permeable cased tunnel that allows the hydrocarbon to flow, this is beneficial in unconsolidated formations where the tunnel stability can be an issue.

Acknowledgments

The authors would like to thank the management of Saudi Aramco for their support and permission to publish this article.

This article was presented at the Middle East Oil & Gas Show and Conference, Manama, Kingdom of Bahrain, March 18-21, 2019.

References

1. Clark, T.E.: "Device for Perforating Well Casings," U.S. Patent 702,128, 1902.
2. Mccullough, I.J.: "Gun Perforator," U.S. Patent 2,155,322, 1939.
3. Mohaupt, H.H.: "Penetrating Projectile System and Apparatus," U.S. Patent 4,123,975, 1977.
4. Satti, R., Betancourt, D., Harvey, W., Zuklic, S., et al.: "Beginning with the End in Mind: Shaped Charges Designed for Reservoir Conditions," SPE paper 183915, presented at the SPE Middle East Oil & Gas Show and Conference, Manama, Kingdom of Bahrain, March 6-9, 2017.
5. Tariq, S.M.: "Evaluation of Flow Characteristics of Perforations Including Nonlinear Effects with the Finite-Element Method," *SPE Production Engineering*, Vol. 2, Issue 2, May 1987, pp. 104-112.

Table 1 *Permeability and porosity increase measurements of pre- and post-laser[7].*

Sample	Permeability Increase %	Porosity Increase %
Berea Yellow	2	57
Berea Gray	22	50
Reservoir Tight Sandstone	171	150
Limestone	33	15
Shale 1	28	700
Shale 2	11	250

6. Eberhard, M.J. and Schlosser, D.E.: "Current Use of Limited-Entry Hydraulic Fracturing in the Codell/Niobrara Formations — DJ Basin," SPE paper 29553, presented at the Low Permeability Reservoirs Symposium, Denver, Colorado, March 19-22, 1995.

7. Batarseh, S.I., Graves, R., San-Roman-Alerigi, D.P. and Chand, K.: "Laser Perforation: Lab to the Field," SPE paper 188729, presented at the Abu Dhabi International Petroleum Exhibition and Conference, Abu Dhabi, UAE, November 13-16, 2017.

8. Batarseh, S.I., Graves, R., Al Obaid, O., Al Hartih, A., et al.: "High Power Laser Technology in Downhole Applications, Reshaping the Industry," SPE paper 188507, presented at the Abu Dhabi International Petroleum Exhibition and Conference, Abu Dhabi, UAE, November 13-16, 2017.

9. Batarseh, S.I., San-Roman-Alerigi, D.P., Reece, J. and Othman, H.: "Downhole High Power Laser Tools Development and Evolutions," SPE paper 193064, presented at the Abu Dhabi International Petroleum Exhibition and Conference, Abu Dhabi, UAE, November 12-15, 2018.

10. Hecht, J.: "A Short History of Laser Development," *Applied Optics*, Vol. 49, Issue 25, September 2010, pp. 99-122.

11. Jauregui, C., Limpert, J. and Tunnermann, A.: "High Power Fiber Lasers," *Nature Photonics*, Vol. 7, October 2013, pp. 861-867.

12. JDSU: "Technical Note: Suppression of Stimulated Brillouin Scattering," 2006, 7 p., *www.jdsu.com*.

13. Kovalev, V.I. and Harrison, R.G.: "Suppression of Stimulated Brillouin Scattering in High Power Single Frequency Fiber Amplifiers," *Optics Letters*, Vol. 31, Issue 2, 2006, pp. 161-163.

14. Kim, J., Dupriez, P., Codemard, C., Nilsson, J., et al.: "Suppression of Stimulated Raman Scattering in a High Power Yb-doped Fiber Amplifier Using a W-type Core with Fundamental Mode Cutoff," *Optics Express*, Vol. 14, Issue 12, June 2006, pp. 5103-5113.

15. Zmuda, M.W.: "Stimulated Brillouin Scattering (SBS) Suppression Techniques," Final Report, AFRL-DE-PS-TR-2007-1127, July 2007, 22 p.

16. Charsky, A. and Herron, M.M.: "Quantitative Analysis of Kerogen Content and Mineralogy in Shale Cuttings by Diffuse Reflectance Infrared Fourier Transform Spectroscopy," paper SCA2012-27, presented at the International Symposium of the Society of Core Analysts, Aberdeen, Scotland, U.K., August 27-30, 2012.

17. Salehi, I.A., Gahan, B.C. and Batarseh, S.I.: "Laser Drilling — Drilling with the Power of Light," Technical Report, U.S. Department of Energy, Office of Scientific and Technical Information, May 2007, 318 p.

About the Authors

Dr. Sameeh I. Batarseh

Ph.D. in Petroleum Engineering, Colorado School of Mines

Dr. Sameeh I. Batarseh joined Saudi Aramco in 2011 as a Petroleum Engineering Specialist working with the Production Technology Team of Saudi Aramco's Exploration and Petroleum Engineering Center – Advanced Research Center (EXPEC ARC). Currently, he is leading the High-Power Laser Program and serving as Lead Engineer for Unconventional Resources. Sameeh's area of interest is to develop an in situ laser application in drilling, perforation and fracturing, among many other applications with a focus on unconventional reservoirs.

He is an active member of the Society of Petroleum Engineers (SPE), serving the society for several years while holding different positions, including sitting on the SPE Executive Advisory Committee, chairing the Program Committee and serving as session chair. He was also the board and vice chair for the Western Region USA San Joaquin Valley. Sameeh's service is recognized worldwide as he received the SPE President Section Award of Excellence, Regional Service Award, and is a SPE Distinguished Lecturer (DL). He has organized over 54 SPE technical workshops.

Sameeh has authored or coauthored more than 68 articles with high-impact publications, and has an H-Index of 34. He holds 12 granted patents and has 31 patents in progress.

Sameeh received his Ph.D. degree in Petroleum Engineering from the Colorado School of Mines, Golden, CO.

Dr. Damian San-Roman-Alerigi

Ph.D. in Electrical Engineering, King Abdullah University of Science and Technology

Dr. Damian San-Roman-Alerigi is a Petroleum Scientist working with the Production Technology Team of Saudi Aramco's Exploration and Petroleum Engineering Center – Advanced Research Center (EXPEC ARC). His focus is on developing the next generation of subsurface photonic and electromagnetic tools.

Damian's previous research focused on the interaction of waves with complex media and its application to subsurface technologies. His work encompasses different areas of science and engineering, from oil and gas to applied mathematics; he has published papers in various international journals and conferences around the world.

Damian received his B.S. degree in Physics from the National Autonomous University of Mexico, Mexico City, Mexico. In 2008, he enrolled in King Abdullah University of Science and Technology (KAUST) as a founding class student where he completed his M.S. degree in 2010, and his Ph.D. degree in 2014, both in Electrical Engineering.

Omar M. AlObaid

B.S. in Petroleum Engineering, University of Louisiana at Lafayette

Omar M. AlObaid is a Petroleum Engineer working with the Production Technology Team of Saudi Aramco's Exploration and Petroleum Engineering Center – Advanced Research Center (EXPEC ARC). He has 2.5 years of experience working on the development of the high power laser program targeting production challenges to enhance productivity in Saudi Aramco's reservoirs. Omar is also involved in other research targeting unconventional resources, including microwave and acoustics studies.

He received his B.S. degree in Petroleum Engineering from the University of Louisiana at Lafayette, Lafayette, LA.

Dr. Haitham A. Othman

Ph.D. in Petroleum Engineering, Texas Tech University

Dr. Haitham A. Othman is a Petroleum Engineer working with the Production Technology Team (PTT) of Saudi Aramco's Exploration and Petroleum Engineering Center – Advanced Research Center (EXPEC ARC). Upon graduation in 2015, Haitham joined the High Power Laser Team. He is now the Champion of PTT's Unconventional Resources Focus Area. Haitham and his team are working on developing tools and methods for high power laser applications to tackle several Upstream production challenges.

He has published several technical papers in international conferences.

Haitham received his Ph.D. degree in Petroleum Engineering from Texas Tech University, Lubbock, TX.

Newly Designed Flow Activated Pulsation Tool for Coiled Tubing Deployed Matrix Acidizing Stimulation Applications in Extended Reach Carbonate Reservoirs

Hussain A. Al-Saiood, Laurie S. Duthie, Ahmed H. Albaqshi, and Moumien Ali

Abstract /

Matrix acid stimulation throughout a well's life cycle is a common technique applied to wells with impaired productivity. Coiled tubing (CT) is often chosen as the conveyance means for delivering the acid treatment in horizontal wells to the damaged zones, and in applying an effective chemical divergent for highly permeable zones. Due to the nature of helical buckling, weight stacking, and wellbore geometry, the CT operation is often limited in its ability to reach total depth (TD).

In short horizontal wells with slight reservoir contact, conventional methods such as pumping lubricant fluid are used to overcome the effect of drag and friction on the CT. For extended reach wells, a downhole pulsation tool is placed on the bottom-hole assembly (BHA) adding axial vibration, which reduces the frictional forces, delaying the onset of CT helical buckling. The compounding increase in friction as more coil is introduced significantly reduces the effect of the pulsation tool, often resulting in its inability to advance the coil to TD.

To tackle this challenge, a more responsive flow activated pulsation tool (FAPT) was developed, providing excitation over an increased length of coil to continuously break the friction at each new contact point without sacrificing frequency and pulse magnitude. The new generation flow activated pulsation tool was developed by re-thinking the design philosophy, creating a new pulsation mechanism to meet the objective of extending the CT reach in restricted extended reach wells. The development was completed after testing a series of different valve section designs to determine the optimum generated pulse magnitudes that would increase the overall pull force. The developed tool produces stronger and higher performing pulses. Additionally, the new design focuses on reducing the activation flow rate of the tool down to approximately one barrel per minute. This improves the operational efficiency and reduces the total volume of fluid required on the job location.

This study focuses on the FAPT development and the results of using the new tool on the first two global trial runs. The two wells were drilled as oil producing horizontal wells with 19,000 ft to TD. The wells were completed as open hole with electric submersible pumps (ESPs) and a 2.44" restriction to allow well intervention. The intended goal was achieved in both runs by reaching TD, which allowed for effective acid treatments.

Introduction

As the complexity of well profiles has increased in the pursuit of cost-effective and efficient oil and gas production, technology in the oil industry has equally advanced. This increased well complexity, i.e., long horizontal sections, tortuous well paths, high reservoir contact, deep wells, etc., has led to even more challenging intervention runs requiring continual development to the conventional reach extending equipment[1].

Matrix stimulation is one of the key intervention treatments that is performed to increase well productivity in carbonate formation reservoirs, when well productivity decreases due to damage in the formation or because of poor permeability quality, stimulation techniques are applied to create a conductive flow path influencing the production rate[2].

In carbonate matrix acid stimulations there are variant fluids such as hydrochloric acid, solvents and other treatment chemicals that are pumped at a pressure lower than the reservoir formation fracture pressure. The pumped treatment fluid works by dissolving and breaking down the materials that is plugging oil/gas passage to the wellbore, and by creating new flow paths through the carbonate rock bypassing the damage[3].

Coiled tubing (CT) is often the preferred method to conduct acidized matrix stimulation intervention operations, especially when accurate placement of the stimulation treatment is necessary to provide good zonal coverage in

long horizontal wells[4].

The authors examine the reach challenges for CT in extended reach wells, and discuss the latest development of the tools in operation to extend the reachability in these applications.

Challenges

In acid stimulations, the purpose is to convey and pump the acid matrix in the open hole section at different stages in the reservoir zone to enhance field productivity. Intervention runs with maximum reservoir coverage will provide better production enhancement, which makes the CT reach a critical part in the success of any intervention[1].

One of the challenges during intervention for CT is reaching the total depth (TD) in extended reach wells. Extended reach wells are defined[5] as any well with a measured depth (MD) to true vertical depth ratio greater than 2.0. Additional factors contribute in this challenge such as the well depth, horizontal lateral length, open hole interval, drag and/or friction between the wellbore and the string, hole size and the clearance between the inner hole diameter and coil through restriction.

The deployment of CT in a horizontal well has several challenges due to friction and drag between the CT and wellbore. As the run in hole depth increase, the friction forces on the CT also increase. This friction increase induces sinusoidal buckling, which is followed by helical buckling, Fig. 1, when additional CT insertion takes place. This ultimately results in lockup, where no further progression in depth can happen[6]. The helical buckling stage plays the most significant role in lockup occurrence, thereby preventing the CT from reaching deeper into the well. The lockup status depends on different system characteristics, such as the material of the CT, well profile and applied force at the surface to inject the string into the well[7].

In field runs, the flow activated pulsation tool (FAPT) proved to break and reduce static friction between the CT and the wellbore by generating pressure pulses that travel along the coil string. This friction reduction extended the CT reach.

Theory

The theory behind the CT FAPT is that imparting additional dynamic energy into a string in a buckled state delays the onset of the helically buckled state. This is accomplished by creating continuous CT movement in a dynamic friction state, which is a relatively lower friction state when compared to static friction. The friction reduction results in more efficient weight transfer, quicker CT travel downhole, and increased overall downhole reach. The benefit of the tool is proportional to the amount of friction that is present between the CT and the wellbore and what proportion of that friction can be reduced by the FAPT's presence.

In CT applications, the tool works by generating pressure pulses that excite the CT. This causes an axial movement of the CT, which aids in breaking the static friction between the CT and the wellbore. Pressure pulses generated by the FAPT are created by a power section and reciprocating valve section, which work together to convert the hydraulic energy of the pumped fluids into pressure pulses that reflect up and down the coil.

Fig. 1 *Helical buckling.*

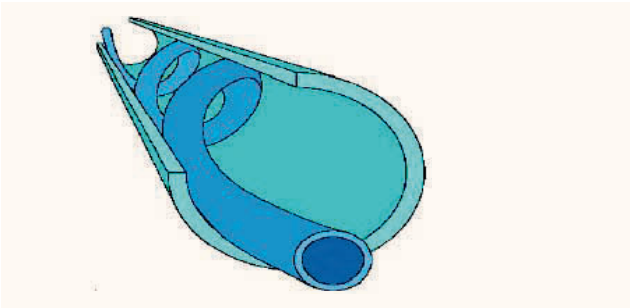

After evaluating different well profiles, job parameters, and results of previous field runs, it was theorized that a higher level of friction reduction could be achieved through development of a more optimized valve section in the FAPT. This could then be paired with updated job modeling and planning that would result in delivering higher energy into the CT string and bottom-hole assembly (BHA) when most needed. These changes would enable the CT to consistently reach the target zone requiring acid stimulation.

Application Overview

The CT reach progression using a 2" CT string equipped with FAPT is determined by the covered open hole length percentage; the target is to provide more than 90% coverage from the open hole section.

In the intervention runs with the legacy FAPT, the tool helped to get to TD in most of the runs with maximum open hole length of 3,659 ft, from Well-1 to Well-5, Fig. 2. In more challenging wells with more than 4,000 ft of open hole length, such as Well-8, the coverage percentage was less than 60%.

In the interest of trials, the newly designed FAPT would be tested in more challenging wells, Well-9 and Well-10, compared to Well-1 to Well-8, where the legacy FAPT was used.

Well-9

Well-9 is a 6⅛" open hole horizontal oil producer well, completed with 4½" production tubing and an electric submersible pump (ESP) with a minimum pass through internal diameter (ID) restriction of 2.441". The casing shoe of the well is at 15,123 ft, the open hole length is 3,876 ft, and there is an 8,761 ft horizontal section to the TD, 18,999 ft MD, Fig. 3.

Well-10

Well-10 is a 6⅛" open hole horizontal oil producer well, completed with 4½" production tubing and an ESP with a minimum pass through ID restriction of 2.441". The casing shoe of the well is at 13,748 ft, the open hole length is 5,739 ft, and there is a 9,252 ft horizontal section to the TD, 19,487 ft MD, Fig. 4.

Fig. 2 *Legacy FAPT runs and application details, and the results using the new design FAPT in trial wells.*

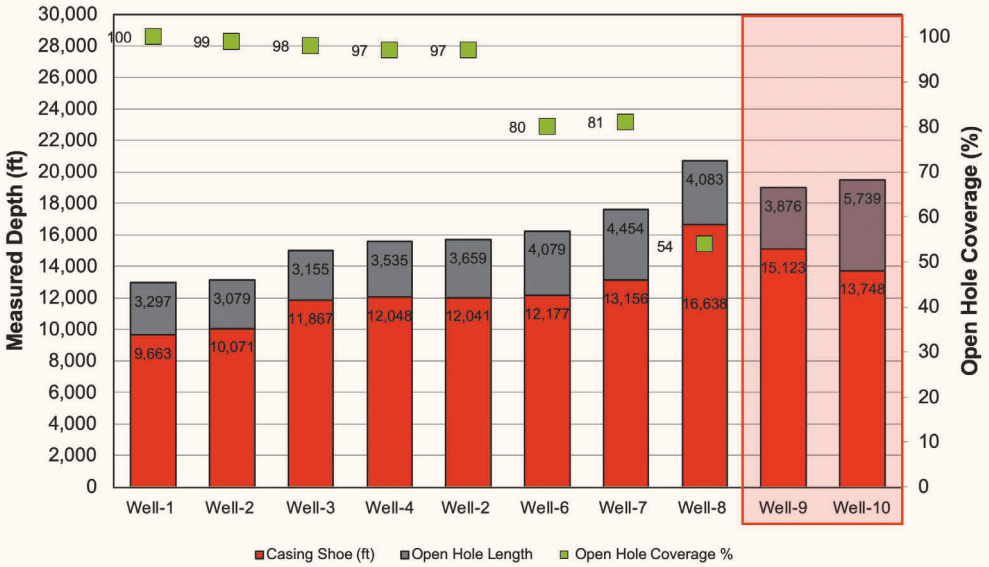

Design

In all generations of the FAPT, the power section would drive a valve plate, Fig. 5, in a dynamic path relative to a stationary valve plate, creating fluctuating fluid velocities resulting in an overall pressure differential across the tool and a secondary pressure pulse that travels upstream until it reaches a refraction point or degrades due to friction inside the CT string. This pulse would act on the CT string and BHA to create physical motion and drive the system into a dynamic energy state that is required to reduce the higher friction levels that occur when the system is static.

The next generation of the FAPT required a design optimization to perform these same tasks, but more impactful and more specifically for the well conditions found in medium to long reach wells. It was determined that the valve section of the tool would need to capture additional hydraulic energy in the form of pressure wave magnitudes to further reduce friction and reach the target zone(s). It was additionally determined that further optimization as it related to the activation flow rate could be beneficial. In other words, relative to the current FAPT, the new design requirements were a need to activate at a specific flow rate and to also capture higher hydraulic energy in the form of pulses. Those pulses then needed to be delivered to the system in a manner that physically impacted the CT string and BHA in a way that created higher dynamic energy.

To achieve the design intent, an iterative design and testing plan was implemented that could inform each

Fig. 3 *A 3D image of the well trajectory of Well-9.*

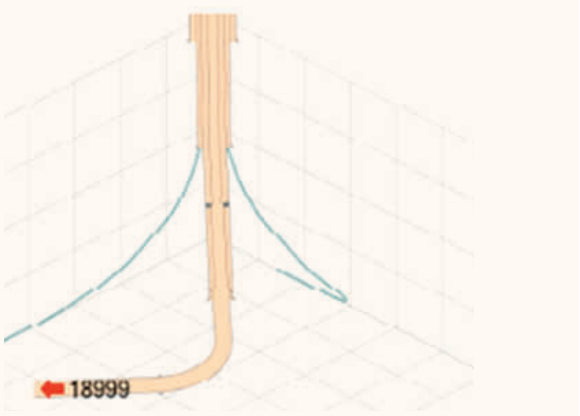

Fig. 4 *A 3D image of the well trajectory of Well-10.*

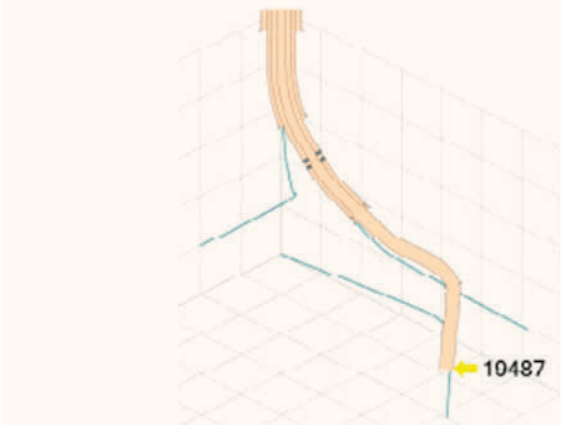

other during the development process. It was first necessary to fully research the effects of flow rate on the overall hydraulic energy available for capture, pressure differential across the tool, as well as the speed at which the valving system would act to create pulses for previous valve designs. This allowed the first phase of valve optimization. It was necessary to test and benchmark a variety of optimized design options given that any change in valve design, Fig. 6, resulting in higher localized fluid velocity changes for higher pulse creation could also create higher turbulence, and thereby generate negative effects on efficiencies and energy capture. The study of these results informed each other and allowed a full understanding of the valve design and how various changes could positively or negatively affect one another.

In the final iteration, the valve section was varied by reducing the area through the oscillating valve relative to the flow area through the stationary valve to drive max efficiency in the desired flow rates. Simultaneously, the stationary valve and oscillating valve areas were reduced to achieve the desired activation flow rate and overall higher energy capture in the form of hydraulic pulses.

Testing

Lab testing for the FAPT was done using a dynamometer (dyno test stand). A dyno test stand is a closed loop flow system that continuously circulates flow through the FAPT at different flow rates and produces real-time measurements of pressure, frequency, and flow, along multiple areas of the system. Pressure is measured by placing digital pressure transducers at the flow inlet and outlet locations, as well as multiple locations along the FAPT. This provides the ability to map out the pressure pulses generated for a unique valve configuration and quantify the different properties of each wave over a given time. Various plots can then be generated and compared, with an emphasis placed on which one the design team is focusing on.

Figure 7 shows the dyno test stand with a FAPT assembled for testing. The dyno test stand is operated from a control unit, which also houses all the data acquisition equipment.

Figures 8, 9, and 10 provide information collected during the test from the data system demonstrations, including typical upstream and downstream pressure outputs of the FAPT over time with varying flow rates being pumped through the tool. This allows the designer to measure the differential pressure across the FAPT, the amplitude and pulse ratio of the pressure pulses, and the efficiency of the valve system. Multiple tests were performed using different valve iterations to determine which valve combination best fits the design objectives.

Figure 9 shows multiple valve configuration curves that were evaluated as part of the testing for this generation of the FAPT. It is also critical to evaluate the actual signature and dwell time of the pressure pulse. Figure 10

Fig. 5 *FAPT components.*

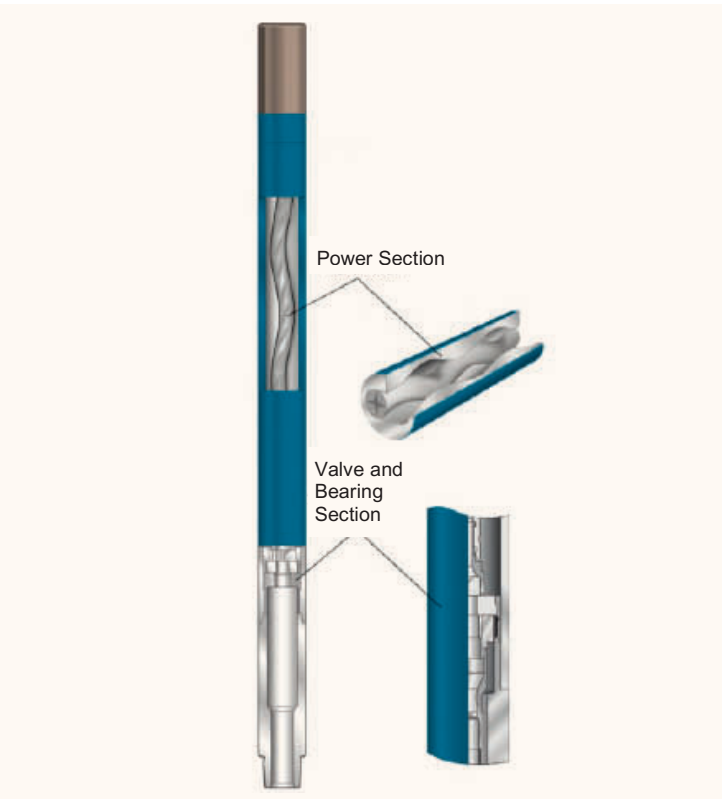

Fig. 6 *Valve plate positions during operation.*

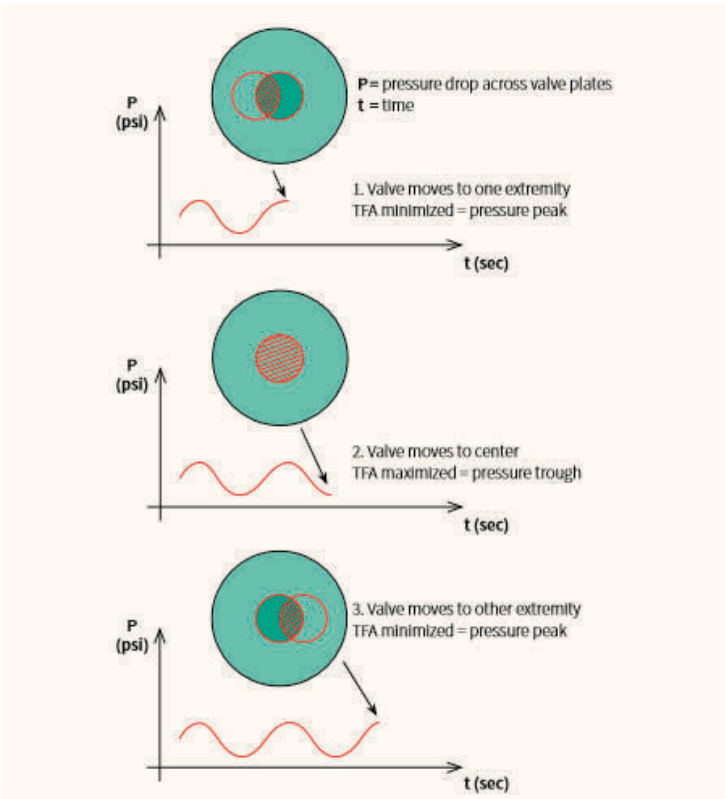

Fig. 7 *Dyno test stand with a FAPT ready for testing.*

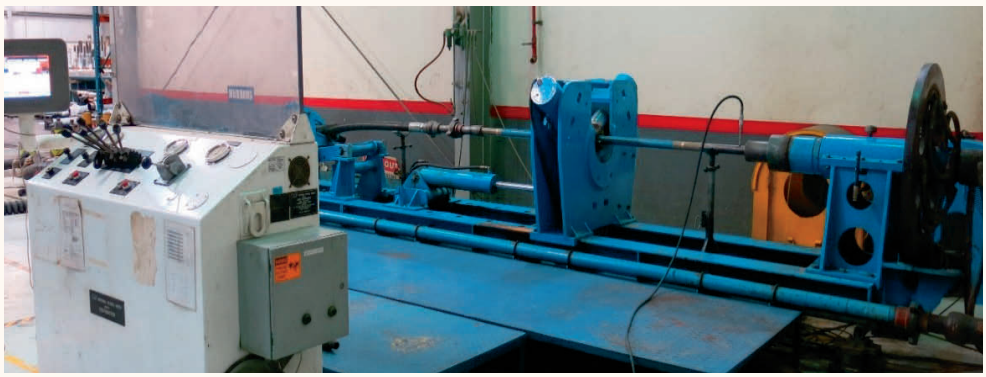

Fig. 8 *Upstream and downstream pressure pulses generated by the FAPT.*

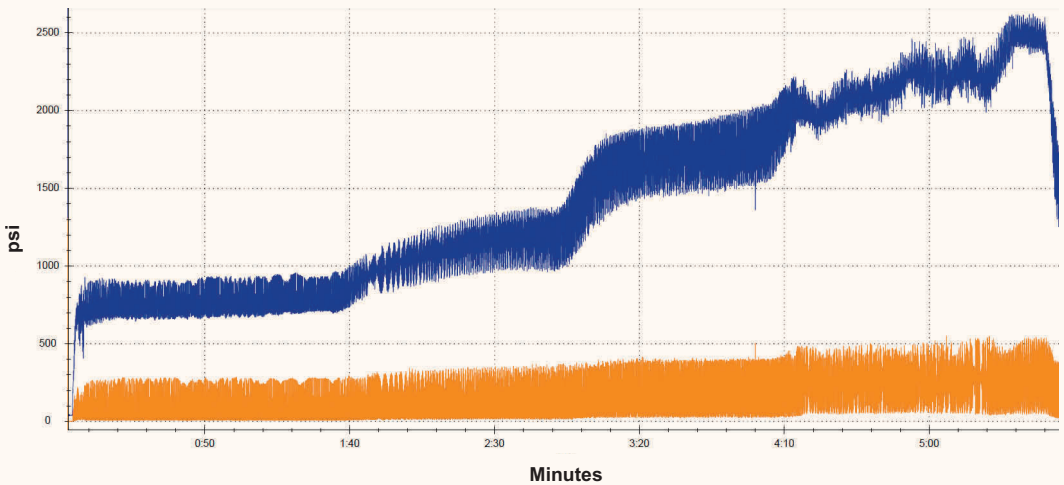

Fig. 9 *Pulse magnitudes of different valve configurations.*

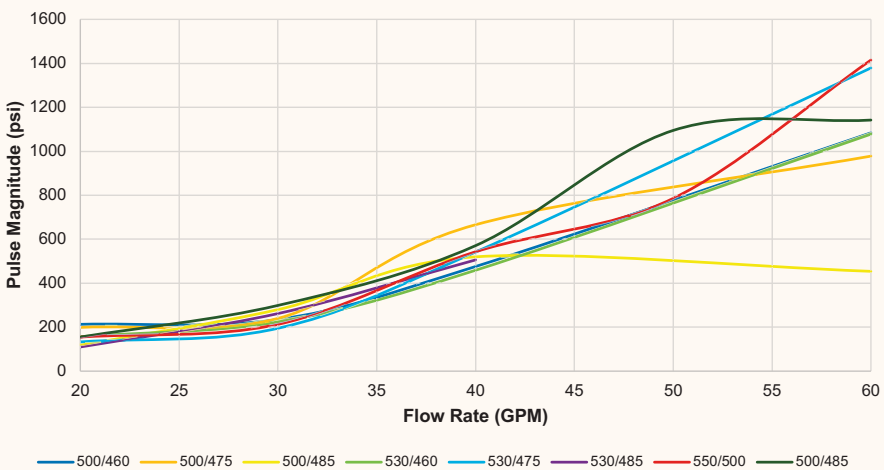

shows a comparison between different kinds of waveforms generated and evaluated as part of the design process.

Trial Results

After the newly designed FAPT was introduced, two challenging extended reach wells were selected to test the new tools' performance — Well-9 and Well-10. Simulations were prepared prior to the runs for both wells using force modeling software, Figs. 11 and 12. The software calculates the forces that act on the CT and study the effect of the well geometry taking into account additional friction and drag forces that result from changes in the well profile and trajectory. The simulation also applies the benefits of friction reducers and any mechanical aid fitted to the BHA to calculate the maximum string reach and lockup depth.

Table 1 shows the expected string reach and lockup depth as per the simulation results.

In these trial wells, the newly designed FAPT surpassed the legacy FAPT's simulated reach to deliver superior results, Fig. 13. In Well-9, the CT reached to a TD covering 3,876 ft of the open hole length, while reaching 18,999 ft MD and adding around 1,460 ft of the open hole coverage to the simulated result using the legacy FAPT.

In Well-10, with more than 5,700 ft open hole length, the new tool achieved its target, covering 95% of the

Fig. 10 *Different wave signatures generated.*

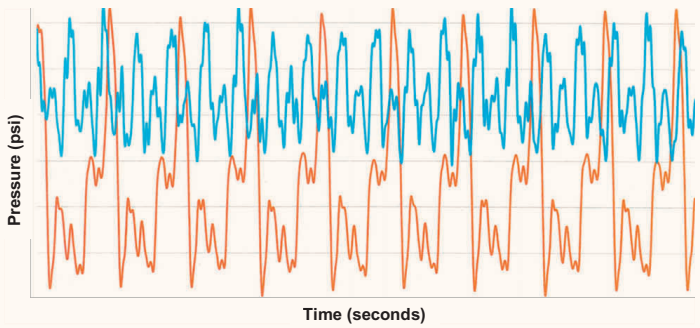

Fig. 11 *Well-9 simulation result lockup depth without FAPT.*

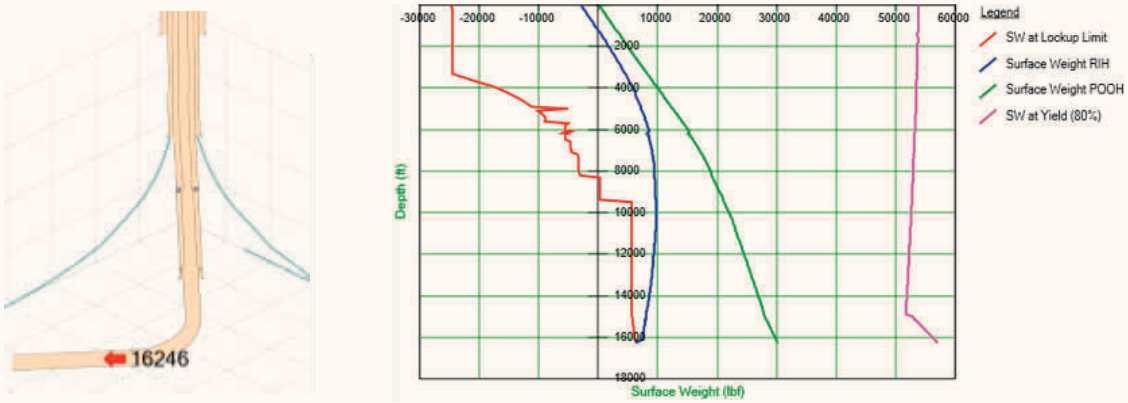

Fig. 12 *Well-10 simulation result lockup depth without FAPT.*

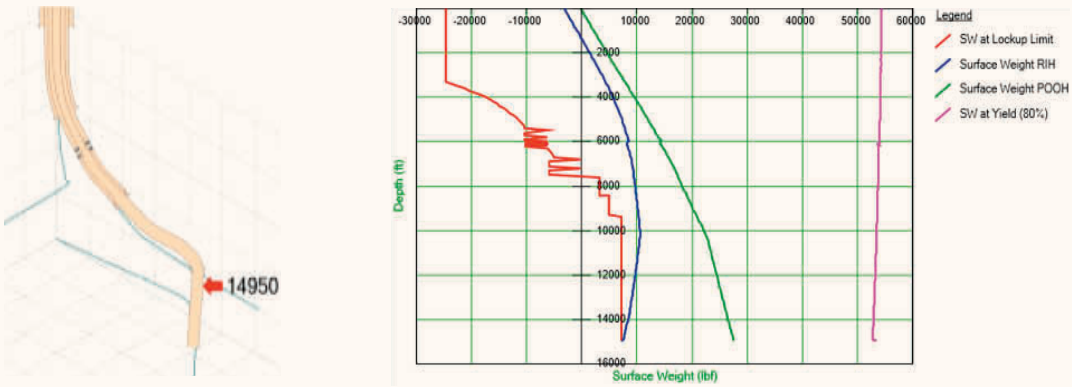

open hole section reaching 19,212 ft MD, while adding around 2,900 ft more of the open hole interval coverage compared to the simulated result using the legacy FAPT. These field trial results have validated the new design enhancements in comparison to the legacy tool delivering a significantly superior performance.

Table 1 *The expected string reach and lockup depth as per the simulation results.*

Well	Lockup Depth without FAPT (ft)	Lockup Depth with Legacy FAPT (ft)
Well-9	16,246	17,535
Well-10	14,950	16,296

Fig. 13 *FAPT field runs.*

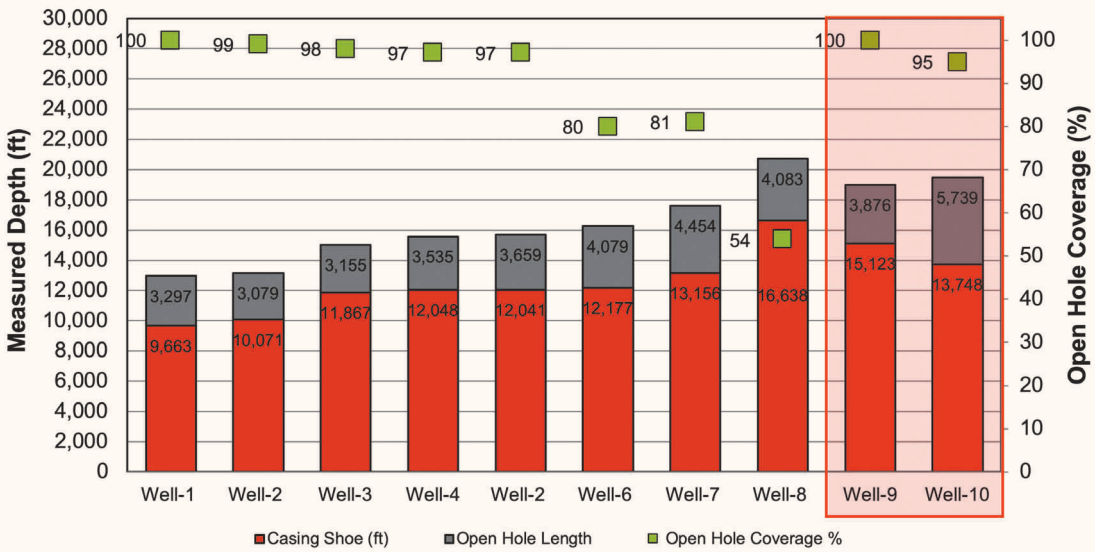

Fig. 14 *Well-9 downhole parameters during the run showing the lockup point before FAPT activation.*

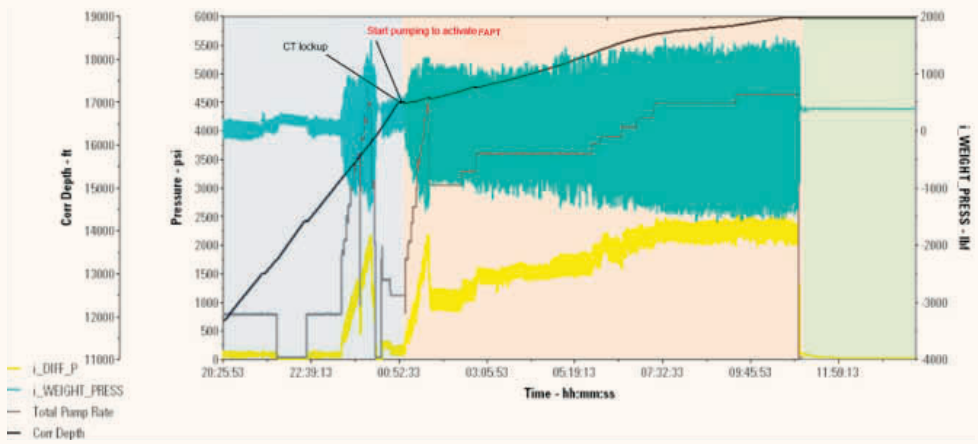

Fig. 15 *Well-10 downhole parameters during the run showing the lockup point before FAPT activation.*

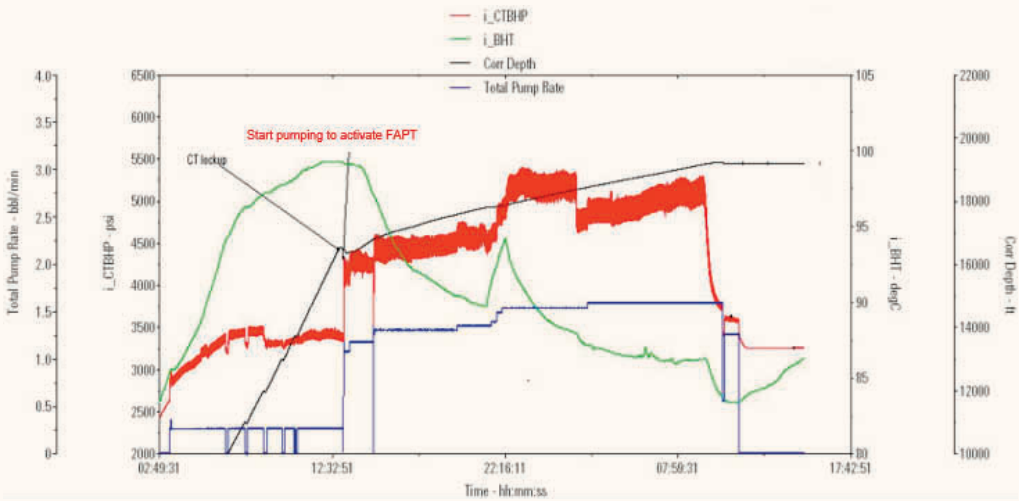

Fig. 16 *Open hole actual coverage with and without FAPT in percentage (%).*

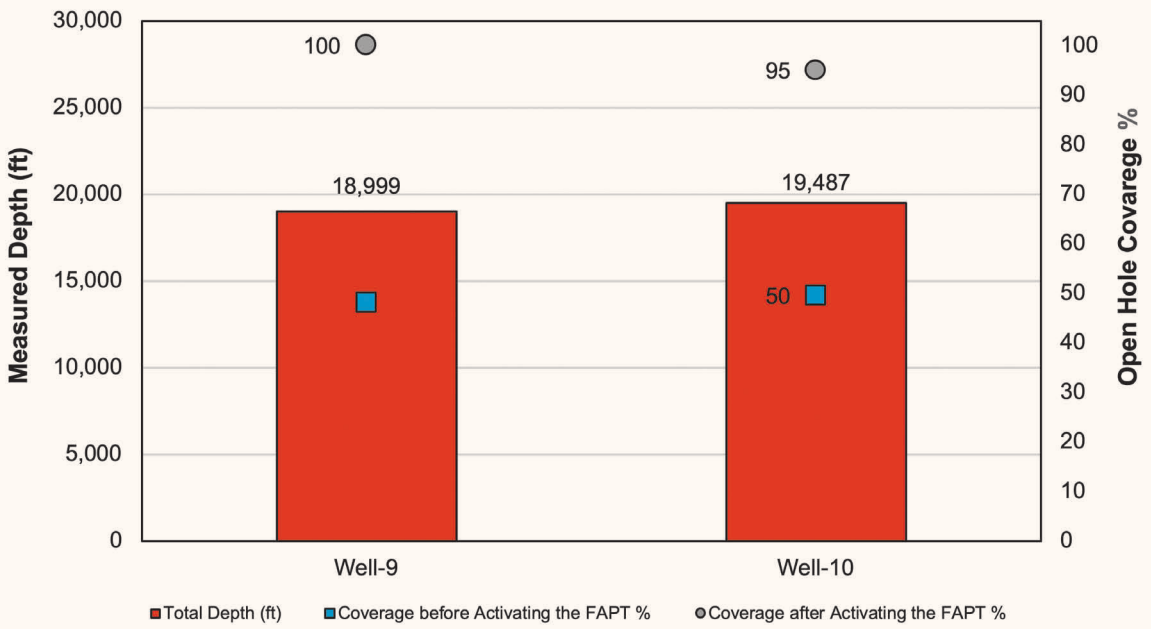

Performance Impact

In both the Well-9 and Well-10 runs, the CT had lockup depth before activation of the tool, Figs. 14 and 15. In Well-9 and Well-10, the coil — without activating the tool — locked up and only reached 16,750 ft MD and 16,541 ft MD, respectively, covering around 49% of the open hole interval for each run. After tool activation, the tool assisted the CT in adding 2,249 ft and 2,671 ft, respectively, or an average of around 98% of the open hole coverage, Fig. 16.

The results of the two trial runs demonstrate a significant performance improvement in the new generation of FAPTs. The newly designed tool also improved on the efficiency performance while being operated at a lower activation flow rate, 0.9 barrel per minute (bpm) to 1.5 bpm compared to the old design flow rate range, 1 bpm to 2 bpm.

Conclusions

The development of the FAPT to perform in challenging

conditions was accomplished in terms of both design intents:

- The effective activation flow rate was reduced to less than 1 bpm, therefore, the tool would be active in the early stages of the intervention operation delaying the onset of the helically buckled state. The added benefits in reducing the volume of pumped fluids to activate the FAPT result in reduced costs, logistics, transportation, storage space, and safety.
- A higher energy FAPT was designed with a new valve assembly that went through an extended series of shop testing to achieve the optimum pulse magnitude with the performance validated in the trial wells.

Acknowledgments

The authors would like to thank the management of Saudi Aramco and National Oilwell Varco for their support and permission to publish this article.

This article was presented at the Abu Dhabi International Petroleum Exhibition and Conference, Abu Dhabi, UAE, November 12-15, 2018.

References

1. Elsherif, T., Dhufairi, M., Bal, M., Krueger Jr., R.E., et al.: "Well Intervention Challenges in Mega-Reach Wells with Coiled Tubing and the Application of the Latest Technologies in Tackling These Challenges, Saudi Arabia," SPE paper 163908, presented at the SPE/ICoTA Coiled Tubing and Well Intervention Conference and Exhibition, The Woodlands, Texas, March 26-27, 2013.
2. Rae, P. and di Lullo, G.: "Matrix Acid Stimulation — A Review of the State-of-the-Art," SPE paper 82260, presented at the SPE European Formation Damage Conference, The Hague, the Netherlands, May 13-14, 2003.
3. Nasr-El-Din, H.A., Shedd, D., Germack, D. and Penny, G.: "Evaluation of Methods to Improve Matrix Stimulation of Horizontal Carbonate Wellbores," SPE paper 177934, presented at the Abu Dhabi International Petroleum Exhibition and Conference, Abu Dhabi, UAE, November 9-12, 2015.
4. Al-Buali, M.H., Dashash, A.A., El Gammal, T., Arevalo, F., et al.: "Intelligent Sensors for Evaluating Reservoir and Well Profiles in Horizontal Wells: Saudi Arabia Case Histories," SPE paper 137202, presented at the Canadian Unconventional Resources and International Petroleum Conference, Calgary, Alberta, Canada, October 19-21, 2010.
5. Blikra, H., Drevdal, K.E. and Aarrestad, T.V.: "Extended Reach, Horizontal and Complex Design Wells: Challenges, Achievements, and Cost Benefits," SPE paper 28005, presented at the 14th World Petroleum Congress, Stavanger, Norway, May 29-June 1, 1994.
6. Afghoul, A.C., Amaravadi, S., Boumali, A., Neves Calmeto, J.C., et al.: "Coiled Tubing: The Next Generation," *Oilfield Review*, Vol. 16, Issue 1, March 2004, pp. 38-57.
7. Noui-Mehidi, M.N., Saeed, A. and Badeghaish, W.: "Analytical Approach of Tractoring Strategies in Coiled Tubing Applications in Horizontal Wells," SPE paper 188943, presented at the Abu Dhabi International Petroleum Exhibition and Conference, Abu Dhabi, UAE, November 13-16, 2017.

About the Authors

Hussain A. Al-Saiood

B.S. in Petroleum Engineering, University of Oklahoma

Hussain A. Al-Saiood is a Production Engineer working in the Manifa Production Engineering Division of Saudi Aramco's Northern Area Production Engineering and Well Services Department. Joining Saudi Aramco as a Petroleum Engineer, he has also held several drilling and reservoir engineering positions, covering several onshore and offshore fields. Hussain's areas of interest include rigless intervention with coiled tubing (CT), wireline, and hydraulic workover operations.

Throughout his career, he has worked in multiple projects, including the change out of electric submersible pumps utilizing the hydraulic workover unit, and developing downhole equipment to enhance the CT reach, i.e., CT tractors and pulsation tools, in extended reach wells for stimulation and logging applications.

Hussain received his B.S. degree in Petroleum Engineering from the University of Oklahoma, Norman, OK.

Laurie S. Duthie

M.S. in Petroleum Engineering, University of New South Wales

Laurie S. Duthie joined Saudi Aramco in 2011 as a Petroleum Engineer focused on the development and production of a large offshore field in the Northern Area. He started his career in 1986 on offshore installations in the U.K. North Sea as a Field Engineer in well testing and wireline operations. Laurie has a strong background in reservoir surveillance, well intervention, acid stimulation, well testing, completions, and cased hole logging. He has gained extensive operational experience in diverse remote onshore and offshore locations — across Africa, Central Asia, the former Soviet Union, Asia Pacific and in the Middle East region since 2009.

Laurie received his M.S. degree in Petroleum Engineering in 2005 from the University of New South Wales, Sydney, Australia.

Ahmed H. Albaqshi

B.S. in Applied Mechanical Engineering, King Fahd University of Petroleum Materials

Ahmed H. Albaqshi joined National Oilwell Varco in Dhahran, Saudi Arabia in 2014 as a Drilling Solutions Engineer and joined the International Development Training Program with an intensive focus on drilling and intervention operations (fishing and coiled tubing (CT)). During his training, Ahmed worked with product design engineering, operations technical support and manufacturing teams in Dubai, Aberdeen, and Houston.

He is currently in charge of the planning for, and the execution of CT buckling and stress simulations for extended reach wells in Saudi Arabia.

Ahmed received his B.S. degree in Applied Mechanical Engineering from King Fahd University of Petroleum and Minerals (KFUPM), Dhahran, Saudi Arabia.

Moumien Ali

B.S. in Mechanical Engineering, University of Khartoum

Moumien Ali is a Drilling Solutions Engineering Supervisor at National Oilwell Varco's Engineering Research & Development Center in Dhahran, Saudi Arabia. He has more than 8 years of professional experience in drilling engineering and product development. Moumien's interests are in drilling, fishing and coiled tubing tools and accessories design and optimization in the oil and gas industry.

He is a member of the Society of Petroleum Engineers (SPE) and actively participates in different workshops and conferences.

Moumien received his B.S. degree in Mechanical Engineering from University of Khartoum, Khartoum, Sudan.

Permanent Removal of Condensate Banking in Tight Gas Reservoirs Using Thermochemicals

Amjed M. Hassan, Dr. Mohamed A. Mahmoud, Dr. Abdulaziz A. Al-Majed, Ayman R. Al-Nakhli, and Dr. Mohammed A. Bataweel

Abstract /

Condensate banking is a common problem in tight gas reservoirs because it diminishes the relative permeability of gas, and significantly reduces the gas production rate. Carbon dioxide (CO_2) injection is a common and very effective solution for condensate removal in tight gas reservoirs. The problem with CO_2 injection is that it is a temporary solution and has to be repeated frequently in the field, in addition to the supply limitations of CO_2 in some areas. Also, the infrastructure required at the surface to handle CO_2 injection makes it expensive to apply CO_2 injection for condensate removal.

In this article, a new permanent technique is introduced to remove the condensate by using a thermochemical technique. Two chemicals will be used to generate in situ CO_2, nitrogen, steam, heat, and pressure. The reaction of the two chemicals downhole can be triggered either by the reservoir temperature or a chemical activator. Two chemicals will start reacting and produce all the mentioned reaction products after 24 hours of mixing and injection. Also, the reaction can be triggered by a chemical activator and this will shorten the time of reaction. Coreflooding experiments were carried out using actual condensate samples from one of the gas fields. Tight sandstone cores with a permeability of 0.9 millidarcies (mD) were used.

The results of this study showed that the thermochemical reaction products removed the condensate and reduced its viscosity due to the high temperature and the generated gases. The novelty in this article is the creation of microfractures in the tight rock sample, due to the in situ generation of heat and pressure from the thermochemical reaction. These microfractures reduced the capillary forces that hold the condensate and enhanced its relative permeability. The creation of microfractures, and in turn the reduction of the capillary forces, can be considered permanent condensate removal.

Introduction

Natural gas is one of the main hydrocarbon resources due to its abundance, low emission of greenhouse gases, and low price compared to the crude oil. Gas reservoirs contain dry gas, wet gas, retrograde gas, or condensate gas based on the reservoir conditions, the hydrocarbon composition, and reservoir temperature and pressure.

During hydrocarbon production, the reservoir pressure declines due to depletion until it reaches a pressure lower than the dew point pressure. Therefore, the gas starts to condensate and create a liquid bank around the borehole; and this phenomenon is defined as condensate banking. The accumulation of condensate liquid reduces the effective permeability for gas, and consequently, results in significant reduction in the total gas production. Figure 1 shows the reduction of relative permeability for gas (K_{rg}) due to condensate accumulation[1]. As the distance from the borehole decreases, the condensate saturation (green curve) increases, and then the relative permeability for gas (red curve) decreases. Usually, the saturation of condensate liquid is lower than critical saturation; therefore, the mobility and relative permeability of condensate liquid is very low and the condensate will be immobile[2, 3].

Several treatments are reported to mitigate the condensate damage and enhance the relative permeability of the gas. Well treatments, such as chemical injection or hydraulic fracturing operations, are extensively applied to remove the accumulated condensate and improve the reservoir deliverability[4]. The ultimate objective of these treatments is to create more favorable flow conditions by either reducing the condensate viscosity or decreasing the drawdown pressure that is required to flow the hydrocarbon into the wellbore.

Solvents are injected into reservoirs to reduce the condensate viscosity by dissolving the condensate back into the gas phase[5]. Methanol is the most common solvent used in field applications. Methanol displacement of liquid accumulations is attributed to the multiple contact miscible technique[6]. Methanol injection improves the effective permeability of the gas in both sandstone and carbonate reservoirs[7, 8]. The problem with solvent injection is that the production enhancement will fade away after a few months — 3 to 6 months — which is attributed to the depletion of solvents during well production, leading to significantly decreased effects. Therefore, injection of solvents is considered as a temporary method for condensate removal, and the treatment has to be conducted frequently — every 3 to 6 months — based on the reservoir situation.

Fig. 1 *Condensate blockage schematic with reflection to relative permeability curves[1].*

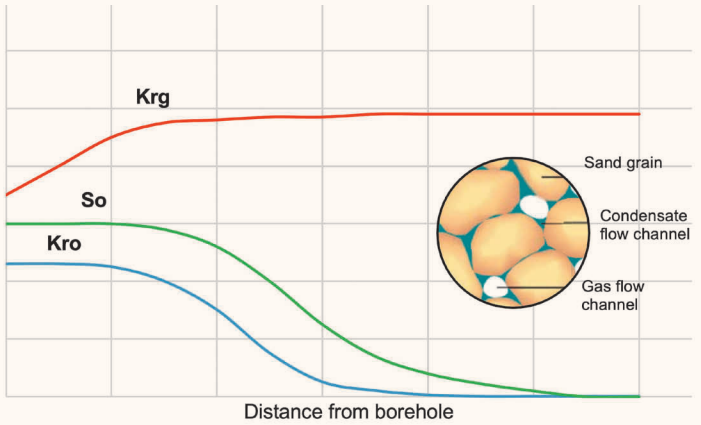

Hydraulic fracturing is applied to generate conductive paths between the reservoir and the treated well. The generated fractures reduce the pressure drop significantly, which leads to a delay of the condensate accumulation. Also, these conductive paths contribute to the condensate production and reduce its saturation around the wellbore[9]. In some cases, the fracture treatment resulted in enhancing the total gas production from tight carbonate reservoirs threefold[10]. The effectiveness of the fracturing treatment depends on several parameters, including formation permeability, injected fluids, and fracture cleanup. Hydraulic fracturing provides an effective tool for delaying the condensate accumulation around the wellbore. These fractures will only delay the condensation phenomenon from occurring as they do not present a permanent mitigation technique. After a period of time, liquids will accumulate in the created fractures and reduce the mobility of the gas.

Gas injection into hydrocarbon reservoirs helps sustain the pressure above dew point[11], and therefore, prevent the generation of condensate banking[12]. Carbon dioxide (CO_2) injection is a common and very effective solution for recovering the condensate liquid from tight gas reservoirs[13]. Su et al. (2017)[14] investigated the condensate removal using CO_2 injection. Several experiments were conducted, including pressure-volume-temperature analysis and coreflooding tests. They concluded that injection of CO_2 is more recommended than waterflooding for removing the condensate damage and improving the gas deliverability. The problem of CO_2 injection is that it is a temporary solution and has to be repeated frequently in the field, in addition to the supply limitations in some areas. Also, the infrastructure required at the surface to handle CO_2 injection makes it expensive to apply CO_2 injection for condensate removal.

The current methods of condensate removal showed several limitations, such as temporary removal of condensate banking or limited improvements in the gas productivity as well as the expensive operations of some condensate treatments. Therefore, the industry is looking for new and permanent techniques to mitigate the condensate damage. One of the effective techniques is the in situ generation of heat and pressure at reservoir conditions. This treatment is conducted by injecting chemical fluids that react at downhole conditions and generate pressure and temperature. The induced heat and pressure could be designed in such a way as to remove the condensate bank by vaporizing the liquid and converting it to a gaseous phase. Also, the generated pressure could be maximized to create microfractures, which will reduce the capillary forces and improve the relative permeability of the gas.

This article introduces a new method for removing the condensate banking from tight formations, by utilizing chemical injection. Tight sandstone samples were flooded with two thermochemical fluids to remove the condensate and improve the flow conditions. The used chemicals are able to generate in situ nitrogen, steam, heat, and pressure at reservoir conditions. The two chemicals are stable at surface conditions, and they start the reaction at downhole conditions. Reaction products are produced only when the reaction is triggered. The thermochemical reaction can be triggered by either the reservoir temperature, or chemical activator. In this work, an activator was utilized to trigger the reaction, which led to shortening the time of reaction. The generated temperature and pressure were able to remove condensate and significantly reduce its viscosity. Also, tiny fractures were observed in all core samples after the treatment operations. The generated fractures showed significant improvements on the effective permeability and capillary forces of the gas.

Experimental Approach

Materials

Tight core samples were prepared for coreflooding tests, to evaluate the effectiveness of the thermochemical treatment on removing the condensate liquid. Table 1 lists the mineralogical composition of the Scioto sandstone samples used. The samples showed high percentages of quartz (70%), a medium quantity of illite (18%), and traces of feldspar (2%) and kaolinite (1%). Also, chlorite and plagioclase minerals were detected with weight percentages of 4% and 5%, respectively. The used core

Table 1 *Mineral composition of the core samples.*

Minerals	wt%
Quartz	70
Feldspar	2
Kaolinite	1
Illite	18
Chlorite	4
Plagioclase	5

Table 2 *Core sample properties used in the flooding tests.*

Sample ID	Diameter (cm)	Length (cm)	Bulk Volume (cc)	Pore Volume (cc)	Porosity (%)	Absolute Permeability (mD)
1	3.81	7.34	83.72	14.29	17.07	0.898
2	3.81	2.54	28.95	4.61	15.93	0.900

samples were characterized by measuring the porosity and absolute permeability.

Table 2 lists the properties of the core samples used in flooding tests. The average permeability and porosity are 0.9 millidarcies (mD) and 16.5%, respectively. Actual condensate liquid was utilized in the flooding experiments; the condensate had an API gravity of 48° and viscosity of 1.8 centipoise (cP) at standard conditions. Two thermochemical fluids were injected at a ratio of one-to-one molar ratio, and an activator was used to trigger the reaction to shorten the time required for the thermochemical treatment.

Coreflooding Setup

Coreflooding setup was built to run the thermochemical flooding experiments. The system consists of a core holder, a transfer cell, an injection pump, pressure gauges, a nitrogen cylinder, and pressure transducer. Figure 2 is a schematic of the coreflooding setup used in this work. A back pressure of 400 psi and an overburden pressure of 1,000 psi were applied. Two injection methods were used; continuous flooding and the Huff and Puff technique. The thermochemical fluids were injected at rate of 0.5 cc/minute, and the activator was injected every 10 minutes. The produced effluents were collected, and the inlet and outlet pressures were recorded.

Fig. 2 *Coreflooding setup.*

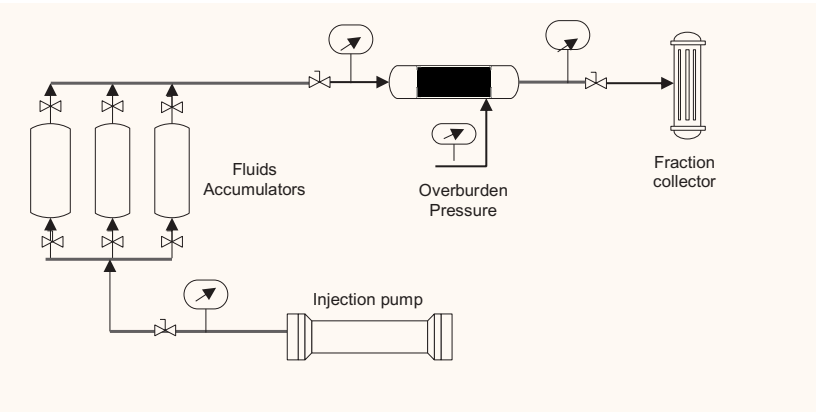

Results and Discussion

Condensate Removal

Coreflooding tests were carried out to study the condensate removal using the thermochemical treatment. Tight core samples and actual condensate liquid were used. Thermochemical fluids were injected, and an activator was used to trigger the reaction. Figure 3 shows the profile of condensate recovery and the inlet and outlet pressures for continuous injection of the thermochemical fluids. A total of 63% of the original condensate in place was recovered by injecting 2.1 pore volume of thermochemical fluids. The inlet pressure increased significantly due to thermochemical reaction, a pressure of 2,300 psi was achieved at the core inlet. A pressure regulator was utilized to maintain the outlet pressure at 400 psi.

The condensate recovery could be attributed to several mechanisms such as viscosity reduction, immiscible displacement, and alteration of rock properties. The generated pressure due to chemicals reaction reached 2,300 psi, which leads to significant changes in the condensate behavior. Based on the two-phase diagram, Fig. 4, the condensated liquid could be turned into a gas phase by pressurizing the condensate region, which results in a significant reduction in the hydrocarbon viscosity and solubility of the liquid condensate in the gaseous phase. Also, the pressure pulses alter the rock properties, especially the permeability and capillary forces.

Tiny fractures were observed in all core samples after flooding operations. The generated factures would contribute in reducing the saturation of condensate liquid around the wellbore, by decreasing the capillary forces that hold the condensate. Those fractures were developed due to a rapid increase in the pore pressure when the thermochemical reaction was activated. As previously seen in Fig. 3, the pressure at the core's inlet (orange curve) increased dramatically from 200 psi to 2,100 psi. The thermochemical reaction generated a significant amount of gases, such as nitrogen and steam. A considerable volume of gases was observed in the produced effluent. The generated gases contributed in the condensate recovery by improving the condensate mobility.

The Huff and Puff technique was used to mitigate the condensate damage. The thermochemical fluids were injected, then the samples were soaked for 40 minutes to allow the chemical reaction to take place. After that, the condensate was produced for 25 minutes. The soaking and production periods were determined based on pressure and recovery stabilization. Figure 5 illustrates the profiles of condensate recovery and pressures at the core's inlet and outlet. Four cycles of the Huff and Puff technique were applied; 56% of the condensate was recovered in the first cycle, recovery of 5% was obtained in the second cycle,

Fig. 3 *Profiles of condensate recovery, inlet and outlet pressures for continuous injection of thermochemical fluids.*

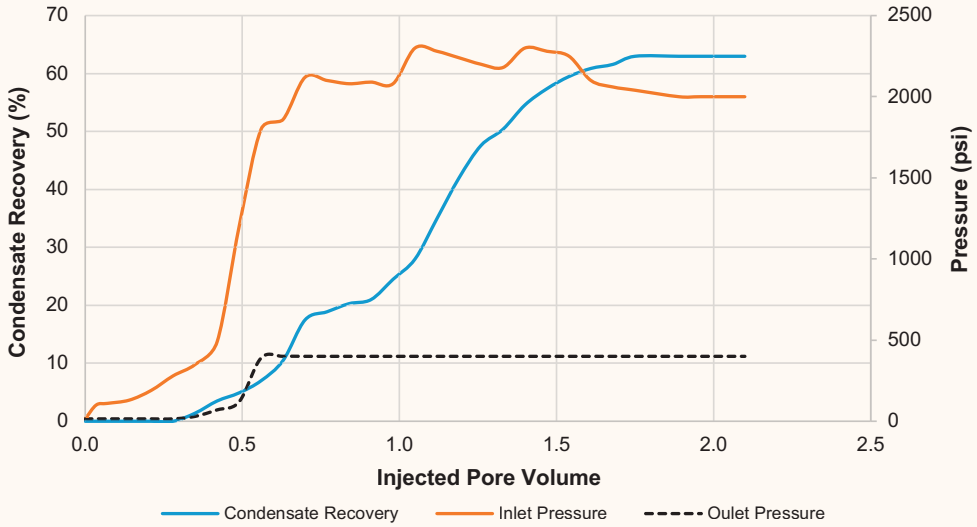

Fig. 4 *Alterations of condensate behavior due to the thermochemical treatment.*

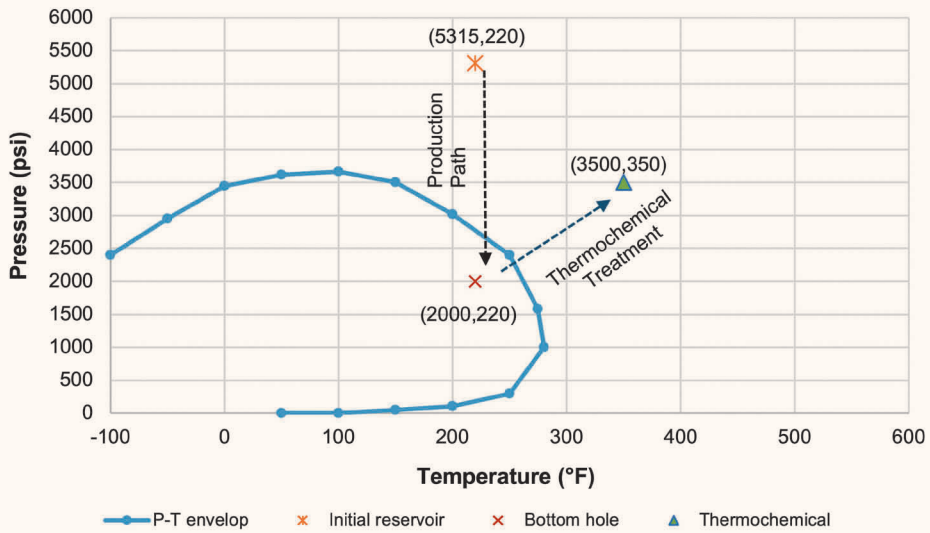

while the third and fourth cycles resulted in 1.8% and 1.5%, respectively. During the soaking periods, the pore pressure increased significantly due to thermochemical reaction, and a pressure of 1,900 psi was obtained. The generated pressure showed significant impact on the core properties; microfractures were observed in the sample after the flooding operation.

The Huff and Puff treatment resulted in 35% remaining condensate saturation, which could be considered as irreducible saturation and at which the condensate liquid is immobile. Also, the Huff and Puff operation indicates that two cycles of thermochemical injection and production is sufficient for removing the condensate banking, since the third and fourth cycles showed limited improvement in the condensate removal, as less than 2% was recovered.

Comparing the two flooding modes, the continuous injection of thermochemical fluids and the Huff and Puff operations, showed that the Huff and Puff technique is more recommended for condensate treatment. The soaking period during the Huff and Puff operations provide more time for the chemicals to react, which improves the performance of thermochemical treatment. The continuous injection of thermochemical fluids showed lower effectiveness in removing the condensate banking. Because the volume of chemicals used during

Fig. 5 *Profiles of condensate recovery, inlet and outlet pressures for the Huff and Puff treatment.*

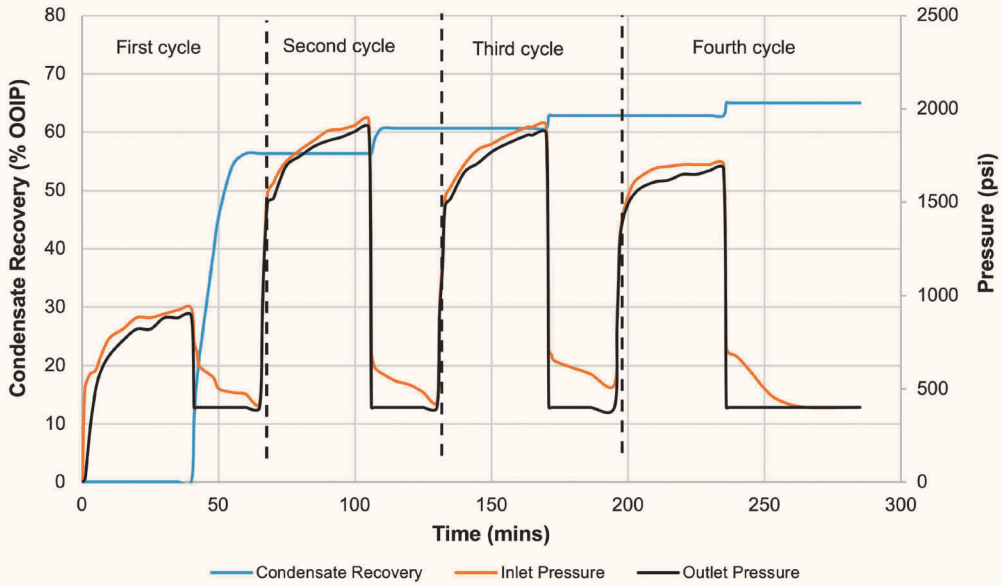

the Huff and Puff technique was less, the operational cost of the Huff and Puff treatment was reduced. Further optimization of the Huff and Puff process is required to optimize the duration of each cycle and the amount of injected chemicals.

Gas Relative Permeability

Condensate banking significantly reduces the relative permeability of the gas; a reduction up to 80% was reported[6]. Injecting thermochemical fluids will lead to enhance the effective gas permeability by reducing the condensate saturation around the wellbore. The improvement of the relative permeability of the gas is due to the thermochemical treatment being estimated using mathematical models. Several models are reported to predict the relative permeability[15-18]. Equations 1, 2, and 3 were used to determine the fluid's relative permeability before and after chemical treatment[19].

$$k_{row} = 0.76067\left[\frac{\left(\frac{S_o}{1-S_{iw}}\right)- S_{or}}{1-S_{orw}}\right]^{1.8}$$

$$\left[\frac{S_o-S_{orw}}{1-S_{orw}- S_{orw}}\right]^2 + 2.6318\emptyset(1 - S_{orw})$$

$$(S_o - S_{orw}) \quad 1$$

Fig. 6 *Relative permeability curves for gas (K_{rg}) and condensate (K_{ro}).*

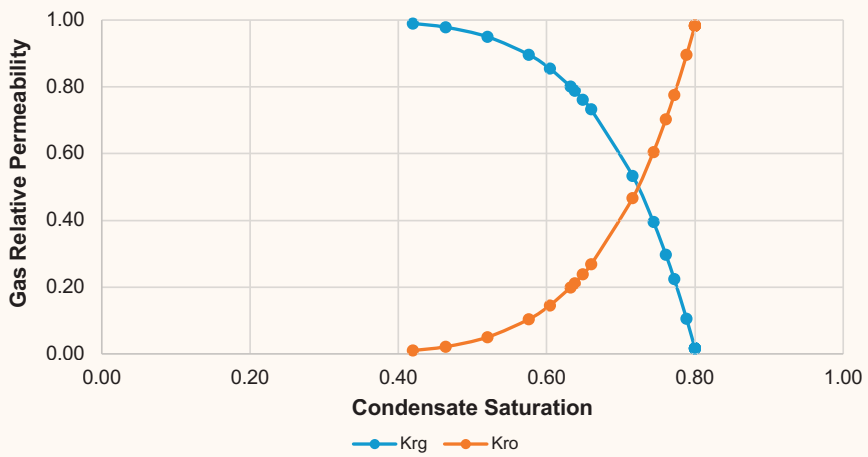

$$k_{rog} = 0.98372\left[\frac{S_o}{1-S_{iw}}\right]^4\left[\frac{S_o-S_{org}}{1-S_{iw}-S_{org}}\right]^2 \quad 2$$

$$k_{rg} = 1.1072\left[\frac{S_g-S_{gc}}{1-S_{iw}}\right]^2 K_{rgo} + 2.7794S_{org}\left[\frac{S_g-S_{gc}}{1-S_{iw}}\right]K_{rgro} \quad 3$$

Figure 6 shows the relative permeability of the gas (blue), and the condensate relative permeability (orange) against the saturation of the condensate liquid. Considerable reduction in the relative permeability for gas was observed due to the condensate banking, relative permeability of less than 0.05 was obtained. Injecting thermochemical fluids results in enhancing the relative permeability for gas by decreasing the condensate saturation. The relative permeability of the gas was improved by a factor of 1.98, due to the thermochemical treatment.

Enhancement of Gas Mobility

The fluid mobility plays a significant role in the well productivity, usually higher mobility means better flow conditions. The fluid mobility is determined based on the ratio of effective permeability to fluid viscosity. The fluid mobility can be maximized by increasing the effective permeability or reducing the fluid viscosity. Injecting thermochemical fluids into gas reservoirs leads to enhancing the gas mobility by reducing the hydrocarbon viscosity and enhancing the effective permeability of the gas.

Thermochemical treatment increases the reservoir pressure and temperature, around the borehole, and beyond the dew point curve as previously seen in Fig. 4. The condensate liquid will be converted into a gaseous phase due to the in situ generation of heat and pressure. Converting the liquid condensate into a gas phase will result in significantly reducing the fluid viscosity. The viscosities of gas and condensate are 0.02 cP and 0.34 cP, respectively. Therefore, the hydrocarbon viscosity can be reduced 17 times using thermochemical treatment.

Microfractures will be generated during thermochemical treatment due to the pressure pulses. The developed fractures will result in reducing the capillary forces that hold the condensate, then, more condensate will be recovered. The reduction in capillary forces can be predicted using Eqn. 4[16]:

$$P_c = P_d S_e^{-\frac{1}{\lambda}} \quad 4$$

where S_e is the effective fluid saturation and can be determined using Eqn. 5[16]:

$$S_e = \frac{S_{con}-S_{conr}}{1-S_{conr}} \quad 5$$

where P_c is the capillary pressure, P_d is the displacement or threshold pressure, Se is the effective fluid saturation and λ is the pore size distribution parameter; for sandstone lambda is 4.17. The improvement in capillary conditions due to thermochemical treatment was determined by utilizing the coreflooding results and mathematical models. Figure 7 shows the capillary pressure against the injected volume of thermochemical fluids. A reduction of 90% in the capillary forces was achieved using the thermochemical flooding, the values of capillary pressure before and after treatment are 90.4 psi and 1.36 psi, respectively. Combining the improvement in capillary forces with the reduction of fluid viscosity, the ultimate enhancement in hydrocarbon mobility will reach 94%.

Conclusions

A new technique for removing the condensate banking by using thermochemical fluids is presented. The influence of thermochemical treatment on reducing the condensate saturation and improving the gas mobility was investigated. The following conclusions could be drawn from this work:

- Thermochemical treatment removes more than 65% of the condensate banking, utilizing viscosity reduction and immiscible mechanisms.
- The Huff and Puff mode showed better performance than continuous chemical injection in mitigating the condensate damage and minimizing the injected chemicals.
- Removing the condensate banking improves the effective permeability of the gas. The relative permeability to gas was improved by a factor of 1.98 using the thermochemical treatment.
- The pressure pulse generated due to the reaction and the high temperature created microfractures in the tight sandstone. Tiny fractures were observed in all samples after the chemical treatment.
- Injecting thermochemical fluids improved the gas mobility by reducing the condensate viscosity and enhancing the effective permeability of the gas. The hydrocarbon viscosity was reduced 17 times using thermochemical treatment.

Fig. 7 *Variation of capillary pressure against the injected pore volume of thermochemical fluids.*

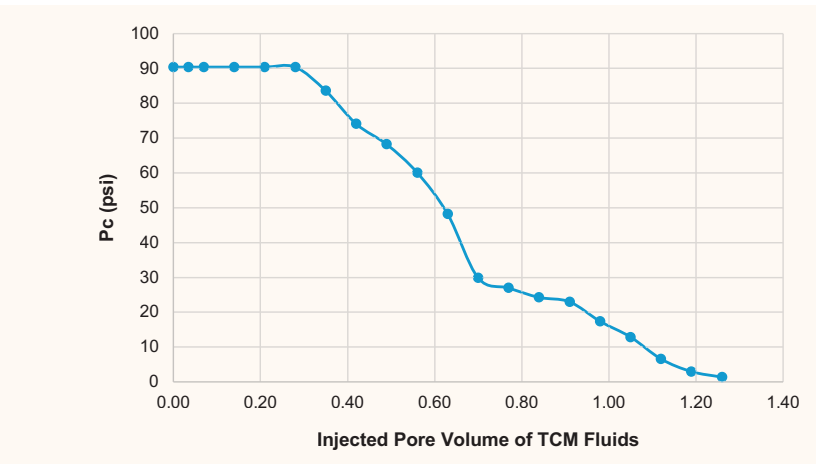

- The reduction in capillary pressure due to thermochemical treatment was determined, a reduction of 90% in the capillary forces was achieved. The values of capillary pressure before and after treatment are 90.4 psi and 1.36 psi, respectively.
- Combining the improvement in capillary forces with the reduction of fluid viscosity revealed that the ultimate enhancement in hydrocarbon mobility would reach to 94%.

Acknowledgments

The authors would like to thank the management of Saudi Aramco and the College of Petroleum and Geoscience at King Fahd University of Petroleum and Minerals for their support and permission to publish this article. Saudi Aramco is also acknowledged for funding this research under project number CIPR2317.

This article was presented at the SPE International Conference on Oil Field Chemistry, Galveston, TX, April 8-9, 2019.

References

1. Sayed, M.A. and Al-Muntasheri, G.A.: "Mitigation of the Effects of Condensate Banking: A Critical Review," *SPE Production & Operations*, Vol. 31, Issue 2, May 2016, pp. 85-102.
2. Fevang, O. and Whitson, C.H.: "Modeling Gas-Condensate Well Deliverability," *SPE Reservoir Engineering*, Vol. 11, Issue 4, November 1996, pp. 221-230.
3. Marokane, D., Logmo-Ngog, A.B. and Sarkar, R.: "Applicability of Timely Gas Injection in Gas Condensate Fields to Improve Well Productivity," SPE paper 75147, presented at the SPE/DOE Improved Oil Recovery Symposium, Tulsa, Oklahoma, April 13-17, 2002.
4. Al-Anazi, H.A., Xiao, J.J., Al-Eidan, A.A., Buhidma, I.M., et al.: "Gas Productivity Enhancement by Wettability Alteration of Gas-Condensate Reservoirs," SPE paper 107493, presented at the European Formation Damage Conference, Scheveningen, the Netherlands, May 30-June 1, 2007.
5. Du, L., Walker, J.G., Pope, G.A., Sharma, M.M., et al.: "Use of Solvents to Improve the Productivity of Gas Condensate Wells," SPE paper 62935, presented at the SPE Annual Technical Conference and Exhibition, Dallas, Texas, October 1-4, 2000.
6. Al-Anazi, H.A., Walker, J.G., Pope, G.A., Sharma, M.M., et al.: "A Successful Methanol Treatment in a Gas/Condensate Reservoir: Field Application," *SPE Production & Facilities*, Vol. 20, Issue 1, February 2005, pp. 60-69.
7. Al-Anazi, H.A., Pope, G.A., Sharma, M.M. and Metcalfe, R.S.: "Laboratory Measurements of Condensate Blocking and Treatment for Both Low and High Permeability Rocks," SPE paper 77546, presented at the SPE Annual Technical Conference and Exhibition, San Antonio, Texas, September 29-October 2, 2002.
8. Asgari, A., Dianatirad, M., Ranjbaran, M., Sadeghi, A.R., et al.: "Methanol Treatment in Gas Condensate Reservoirs: A Modeling and Experimental Study," *Chemical Engineering Research and Design*, Vol. 92, Issue 5, January 2013, pp. 876-890.
9. Khan, M.N., Siddiqui, F.I., Mansur, S. and Ali, S.D.: "Hydraulic Fracturing in Gas Condensate Reservoirs: Successes, Setbacks and Lessons Learnt," SPE paper 142848, presented at the SPE/PAPG Annual Technical Conference, Islamabad, Pakistan, November 10-11, 2010.
10. Franco, C.A., Solares, J.R., Asiri, K.S., Shammari, N., et al.: "Optimization of Conventional Acid Jobs and the Historical Trend Leading to Multistage Acid Fracturing Stimulation to Increase Gas-Condensate Productivity in Carbonate Reservoirs in Saudi Arabia," SPE paper 141339, presented at the SPE Middle East Oil and Gas Show and Conference, Manama, Kingdom of Bahrain, September 25-28, 2011.
11. Sänger, P.J. and Hagoort, J.: "Recovery of Gas Condensate by Nitrogen Injection Compared with Methane Injection," *SPE Journal*, Vol. 3, Issue 1, March 1998, pp. 26-33.
12. Hoier, L., Cheng, N. and Whitson, C.H.: "Miscible Gas Injection in Undersaturated Gas-Oil Systems," SPE paper 90379, presented at the SPE Annual Technical Conference and Exhibition, Houston, Texas, September 26-29, 2004.
13. Odi, U.: "Analysis and Potential of CO_2 Huff-n-Puff for Near Wellbore Condensate Removal and Enhanced Gas Recovery," SPE paper 160917, presented at the SPE Annual Technical Conference and Exhibition, San Antonio, Texas, October 8-10, 2012.
14. Su, Z., Tang, Y., Ruan, H., Wang, Y., et al.: "Experimental and Modeling Study of CO_2 — Improved Gas Recovery in Gas Condensate Reservoir," *Petroleum*, Vol. 3, Issue 1, March 2017, pp. 87-95.
15. Corey, A.T.: "The Interrelation between Gas and Oil Relative Permeabilities," *Producers Monthly*, Vol. 19, November 1954, pp. 38-41.
16. Brooks, R.H. and Corey, A.T.: "Hydraulic Properties of Porous Media," *Hydrology Papers*, No. 3, Colorado State University, Fort Collins, Colorado, March 1964, 27 p.
17. Henderson, G.D., Danesh, A., Tehrani, D.H., Al-Shaidi, S., et al.: "Measurement and Correlation of Gas Condensate Relative Permeability by the Steady-State Method," *SPE Journal*, Vol. 1, Issue 2, June 1996, pp. 191-202.
18. Ibrahim, M.N.M.: "Two-Phase Relative Permeability Prediction Using a Linear Regression Model," Ph.D. thesis, University of Missouri-Rolla, Missouri, 1999, 182 p.
19. Honarpour, M.M., Koederitz, L. and Harvey, A.H.: *Relative Permeability of Petroleum Reservoirs*, Boca Raton, Florida: CRC Press, 1986, 152 p.

About the Authors

Amjed M. Hassan

M.S. in Petroleum Engineering, King Fahd University of Petroleum and Minerals

Amjed M. Hassan is a Ph.D. Researcher at King Fahd University of Petroleum and Minerals (KFUPM) in Dhahran, and a Lecturer at the Khartoum University, in Khartoum, Sudan. His research interests are varied and includes condensate removal processes, enhanced oil recovery methods, well testing, and artificial intelligence applications in the petroleum industry.

Amjed has participated in many workshops, conferences, and regional contests. He has authored more than 15 scientific articles and Society of Petroleum Engineers (SPE) papers.

Amjed has received several awards. The most recent are the Society of Petrophysicists and Well Log Analysts (SPWLA) prize for the best research in petrophysics, and a Schlumberger award for the best academic performance in petroleum engineering.

He received his M.S. degree in Petroleum Engineering from KFUPM.

Dr. Mohamed A. Mahmoud

Ph.D. in Petroleum Engineering, Texas A&M University

Dr. Mohamed A. Mahmoud is an Associate Professor working in the Petroleum Engineering Department with King Fahd University of Petroleum and Minerals (KFUPM), Dhahran, Saudi Arabia. Prior to assuming this position in 2016, he had been a Research Assistant in the same department since 2008.

From 2004 to 2008, Mohamed worked as a Petroleum Engineer at Belayim Petroleum Co. in Egypt. During the period from 2001 to 2004, he was a Drilling Engineer at Magawish Petroleum Co., Egypt.

Mohamed's research interests are varied and cover several subjects, including well simulation, enhanced oil recovery, and multiphase flow in vertical and horizontal wells.

He received his Ph.D. degree in Petroleum Engineering from Texas A&M University, College Station, TX, in 2011.

Dr. Abdulaziz A. Al-Majed

Ph.D. in Petroleum Engineering, University of Southern California

Dr. Abdulaziz A. Al-Majed is an Adjunct Professor working in the Department of Petroleum Engineering at King Fahd University of Petroleum and Minerals (KFUPM) in Dhahran, Saudi Arabia. Prior to that he was Chairman of the Department and Director of the Center for Petroleum and Minerals at the Research Institute in KFUPM.

Abdulaziz has taught courses in drilling engineering, reservoir engineering, and petroleum engineering economics, supervised numerous M.S. Thesis and Ph.D. Dissertation committees, and managed many client funded research projects in the Research Institute. He has published over 60 journal and conference papers, and obtained five patents. Abdulaziz has won several educational and research awards.

He was a member of the committee that prepared the "Strategic Plan for Innovation, Localization and Development of Oil and Gas Exploration and Production Technologies in Saudi Arabia." Abdulaziz was also the Team Leader of the team charged to prepare "The Improved Drilling Operations; Quality and Efficiency Technology Target Area" as part of the Strategic Plan.

He is a member of the Society of Petroleum Engineers (SPE) and the American Institute of Mining Engineers (AIME), and a previous member of the Board of Directors of the SPE-Saudi Arabia Section.

In 1978, Abdulaziz received his B.S. degree from KFUPM, in 1981 he received his M.S. degree from Stanford University, Stanford, CA, and in 1988, Abdulaziz received his Ph.D. degree from the University of Southern California, Los Angeles, CA, all in Petroleum Engineering.

Ayman R. Al-Nakhli

M.S. in Entrepreneurship for New Business Development, Open University Malaysia

Ayman R. Al-Nakhli is a Petroleum Scientist in Saudi Aramco's Exploration and Petroleum Engineering Center – Advanced Research Center (EXPEC ARC), where he leads the research program on thermochemicals and develops technologies related to conventional and unconventional reservoirs such as pulse fracturing, stimulation, water shutoff, diverting agents, and heavy oil.

Ayman has developed several novel technologies, and received the World Oil Award for Best Production Chemical in 2015. He has also been awarded for his innovative work within Saudi Aramco.

Ayman has filed more than 20 patents and published several papers.

He received his B.S. degree in Industrial Chemistry from King Fahd University of Petroleum and Minerals (KFUPM), Dhahran, Saudi Arabia, and an M.S. degree in Entrepreneurship for New Business Development from Open University Malaysia, Bahrain.

Dr. Mohammed A. Bataweel

Ph.D. in Petroleum Engineering, Texas A&M University

Dr. Mohammed A. Bataweel is a Champion for the Smart Fluid focus area in the Production Technology Division of Saudi Aramco's Exploration and Petroleum Engineering Center – Advanced Research Center (EXPEC ARC). He has led his team in the development and deployment of several in-house technologies in Saudi Aramco fields. Throughout his career, Mohammed has represented his department on several field development, asset, and multidisciplinary teams. His research interests include formation damage due to drilling and completion fluids, investigation and mitigation of injectivity decline, conformance control, sand production prediction, special core analysis, chemical enhanced oil recovery, productivity enhancement technologies, visualization of fluid flow in porous media, and oil field chemicals.

Mohammed is an active member of the Society of Petroleum Engineers (SPE) where he has served on several conferences. He initiated and co-chaired several SPE advanced technical workshop series in the region. Mohammed has published more than 40 SPE papers in local and international conferences and refereed journals.

He received his B.S. degree in Mechanical Engineering from King Fahd University of Petroleum and Minerals (KFUPM), Dhahran, Saudi Arabia, and his M.S. degree in Petroleum Engineering from Heriot-Watt University, Edinburgh, U.K. Mohammed received his Ph.D. degree in Petroleum Engineering from Texas A&M University, College Station, TX.

Novel Plant-based Particulate and Fibrous LCM Products for Loss Control while Drilling

Dr. Md. Amanullah, Dr. Mohammed K. Al-Arfaj, and Dr. Raed A. Alouhali

Abstract /

Novel fibrous and particulate loss circulation material (LCM) products of variable mechanical characteristics and chemical composition were developed using physio-mechanical treatment and processing of various waste components of date palm trees, which are available each year as pruning waste, post-crop harvesting waste, waste generated after making cookies and confectioneries, and also the waste arising from the removal of deceased and nonproductive date trees.

Experimental tests were conducted using a pore plugging test (PPT) apparatus at a pressure of 500 psi and 1,500 psi, and at a temperature of 250 °F, with a 2 mm slotted disc, demonstrated the efficient sealing and blocking for all of the particulate and fibrous LCM products, either immediately after the application (0 to 10 seconds) of the overbalance pressure or after a period of 5 to 10 minutes, depending on the pressure and composition. Some of the LCM products showed an instantaneous sealing capacity after the application of overbalance pressure.

Several commercial LCM products were also tested and evaluated using the same concentration and test conditions for comparative assessment of the performance of the newly developed LCM products. Interestingly, all of the new LCM products showed similar or better performance than the equivalent commercial products. Engineered fiber blends developed using the date palm industry waste also showed similar or better performance than the commercial or currently used LCM blends.

Experimental results also indicated the suitability of date palm industry waste in replacing some of the synthetic fibers used by the industry in a commercial LCM blend design. All of these experimental results indicate that the date palm industry wastes are potential sources of raw materials for various product development for oil and gas field applications.

Introduction

Analyses of various drilling challenges encountered while drilling to explore and exploit oil and gas resources indicate loss of circulation as one of the major challenges faced by the industry. It can have serious technical, economical and environmental impacts if not prevented or controlled to an acceptable level by treating the drilling mud using suitable loss circulation material (LCM) products and/or designing an LCM pill or slurry that suits particular loss zone characteristics.

Economic analyses of the total drilling cost of wells that encountered moderate-to-severe loss of circulation indicate a significant increase in the total drilling cost due to an exponential growth of nonproductive time, especially in extreme drilling environments. It is also one of the major problems that increase mud and mud management cost significantly. In addition to creating problems by itself, it can also trigger other drilling problems such as borehole instability, severe formation damage, cross-flows, kick and blowout, pipe sticking, etc., and so can increase the nonproductive time dramatically[1-4]. Therefore, it could be a very costly drilling problem if not controlled immediately after its occurrence. Even a single loss circulation event can lead to a huge monetary loss by triggering a series of other drilling problems that could cost up to a million dollars or more[5]. Therefore, preventing loss circulation is a better strategy than the cure after the occurrence of the loss circulation event.

Review of various drilling challenges encountered while drilling in the Middle Eastern region indicate that moderate and severe loss of circulation is one of the major drilling challenges in this region due to the complex subsurface geology and unique geomechanical and geophysical characteristics of the formations. Amanullah et al. (2018)[6] highlighted the role of various geological, geophysical, and geomechanical controls such as the karstified solution cavities, open, closed, and cemented fractures, formations with interconnected vugular zones, communicably connected cavernous regions and faulted neighborhoods, etc. Van Oort et al. (2009)[7] and Song and Rojas (2006)[8] highlighted the significance of rock mechanical properties along with the importance of strengthening the near wellbore formation to prevent loss of circulation while drilling. These unseen or poorly known subsurface geological and geophysical features, their physical sizes, areal extend, spatial distribution patterns, near-field and far-field interconnectivity, volumetric size of solution cavities, vugs, and the caves have a tremendous effect on successful

treatment of loss zones. Inadequate knowledge of the huge number of uncertain and unknown factors make it difficult to prevent loss of circulation in the first place in many cases. Therefore, the drilling program always include the corrective/curative approaches of loss control to eliminate or minimize the scope of losses while drilling or cementing a wellbore.

In both preventive and curative approaches of loss control, various types of loss circulation materials such as conventional, unconventional, or a combination of them are used to combat loss circulation problems. Traditional particulate, fibrous and flaky LCMs or their blends typically belongs to conventional LCM products. Specially designed gel-based, cross-linked, thermally set, etc., LCM products or their blends typically belong to unconventional LCMs. Sometimes, a combination of conventional and unconventional LCM products that incorporate both the traditional and the especially designed LCM products are used to prevent or control loss of circulation. Historical analyses of past and present LCM treatment jobs indicate that the conventional particulate, fibrous and flaky LCMs still play an important role in controlling seepage, moderate, and severe loss of circulation[9, 10], both for preventive and curative approaches of loss control.

In the case of a preventive approach of loss control, the LCM products or their blends are incorporated into an active mud system to take action immediately after the appearance of a loss circulation event. The main objectives of this type of loss control strategy are to strengthen the near wellbore formation and increase the fracture gradient of the formation. This will widen the mud weight window and reduce the scope of induced loss of circulation[11]. Traditionally, sized particulate LCMs or a combination of particulate and fibrous LCM products are frequently used to widen the mud weight window of weak and critical formations that have a low fracture gradient. Several experts have described various models to predict the strengthening effect of a near wellbore formation and widen the mud weight window to prevent induced loss of circulation while drilling[12-14]. These models also highlighted the use of appropriate sized particulate and fibrous LCM products for adequate and efficient strengthening of the near wellbore formations to prevent induced loss of circulation. These particulate, fibrous and flaky LCM products are also used to control natural loss of circulation of drilling mud, both for preventive and corrective approaches of loss control.

In the corrective or curative approach of loss control, an appropriate amount of various loss circulation materials are added continuously to an active mud system to control the loss to an acceptable level or cure it totally, if possible. Alternatively, the LCMs are used to design a pill to spot at the loss zone to control or prevent the mud losses. This type of loss control approach requires special design strategy, mixing procedure and placement techniques for successful completion of a LCM treatment job. Sometimes, a rapidly dehydrating loss control slurry is designed to combat loss of circulation in depleted, poorly consolidated, highly permeable, super-K, fractured and vugular formations by creating a solid plug in the flow path. According to Wang et al. (2005)[15], LCMs that are capable of forming deformable, viscous and cohesive plugs are likely to be more effective in taking a corrective approach to loss circulation.

The date palm industry in the Kingdom and the Middle East produces various waste products and byproducts such as date seeds, deceased palm trees, yearly pruning wastes, empty fruit bearing panicles and fruit caps, etc., in huge quantities each year. These waste products are potential sources of raw materials for manufacturing various conventional LCM products locally[1]. Due to the organic nature of the materials, products and additives derived from these raw materials would be eco-friendly, nontoxic and biodegradable. As the industry is constantly shifting toward green products/additives for oil and gas field applications, due to the enactment of increasingly strict environmental laws and regulations by the regional and the global environmental protection agencies, the date palm waste-based LCM products could play an important role in complying with environmental norms. The industry push for more eco-friendly and green products is reflected in increasing research activities in developing virtually nontoxic, readily biodegradable and environmentally benign green chemicals and polymers for current and future drilling operations[16-18]. This article describes the experimental results of several green LCM products developed using the date palm industry wastes as the raw materials.

Date Palm Industry

Published information indicates that there are more than 120 million date palm trees cultivated by various countries across the world. According to Ghori et al. (2018)[19] date palm trees are one of the major agricultural crops that are found abundantly in Saudi Arabia, Northern Africa, Pakistan, India, and the U.S. state of California. More than two-thirds of the global date palm trees are cultivated in the Middle East region. The Kingdom of Saudi Arabia alone has more than 23 million registered date palm trees.

These trees in general survive for a long time to produce date fruits and date palm wastes, if proper attention is given to protect and maintain the growth of the trees. Relatively small revenues are generated from the huge volume of date seeds and date palm wastes generated each year. Therefore, additional revenue can be generated by recycling and reusing the date palm industry wastes for various industrial applications, including the vibrant oil and gas industry of the region. This will solve several industry problems simultaneously, such as the disposal problem of the date palm industry, and the date fruit-based product manufacturing industries. In addition, the creation of a local supply source of conventional LCM products for the regional oil and gas industry will ensure an uninterrupted supply of LCM products in any geopolitical situation.

The utilization of date palm industry wastes will also help in the growth of local industries and enterprises to create new job opportunities for the public to uplift the social and economic condition of the public and the

date farming communities. The additional economic contribution of utilization and commercialization of date palm waste-based products can make the date palm industry one of the most attractive industrial sectors of the Middle East.

Source of Fibrous LCMs

Usually 10-20 leaves of date palm tree are worn out or aged each year and are removed as pruning waste. Only the yearly pruning waste of a single date tree of the date palm industry can generate 6 kg to 10 kg of dry leaves/annum to supply as raw materials for fibrous LCM products. The industry also produces thousands of deceased and old date trees, which are additional sources of raw material for fibrous LCMs. After a fruit harvesting period, large quantities of date palm empty fruit bunches, or panicles, along with the empty fruit bearing spikelets are generated each year, which also provide a potential source of raw material for fibrous LCM production.

In the current study, several grades of fibrous LCM products were developed using the pruning and the deceased date tree wastes. These fibers are virtually nontoxic, and ultimately biodegradable, and so are highly environmentally friendly like other natural fibers. These natural fibers also have other technical advantages over synthetic fibers. According to Jawaid and Khalil (2011)[20] natural fibers are getting increasing attention as they offer considerable advantages such as low cost, are low-density, and cause minimum wear on tools and equipment compared to synthetic fibers. The authors further emphasized that due to a renewable source of supply, non-carcinogenic nature and highly favorable biodegradable characteristics compared to synthetic fibers, they are getting increasing attention for various industrial applications. The favorable technical, physical and environmental properties of date tree-based bio-fibers also made them an ideal candidate for the oil and gas field application.

Source of Particulate LCM Products

Saudi Arabia is the second largest date producing country in the Middle East with a yearly date seed waste production capacity of more than 150,000 tons. These dates are produced by a variety of date trees that are cultivated in different regions of the Kingdom. There is a large variety of date seeds available as the waste product from various date farming communities and date fruit-based product manufacturing industries.

According to Amanullah (2017)[21], all the date seeds have a similar material toughness that is comparable to the toughness of calcium carbonate based sized particulate material currently used by the oil and gas industry. All of them, either alone or together, can be used as the potential source of raw materials for localization of particulate LCM development for partial fulfillment of the goals and objectives of Saudi Vision 2030.

The authors further showed that the date seed-based particulate LCM also has similar mechanical properties like the commercially available and widely used walnut-based particulate LCMs. The waste date seeds generated by the date palm industry is a highly potential local source of renewable raw materials for localization of sized particulate LCM products. Due to the low cost of the raw materials and the manufacturing process, it can provide equivalent or better products at a lower cost. The eco-friendly and physio-mechanical manufacturing process that can be used to manufacture various grades of particulate LCM products will incur no waste disposal cost as the process generates no chemical or other harmful waste products or byproducts.

Preparation of Fibrous LCM "ARC Eco-Fibers"

Several grades of fibrous LCM products, coined "ARC Eco-fibers" — coarse (C), medium (M), and fine (F) — were prepared using deceased date tree trunks collected from various date farms. Figure 1 shows the photos of some collected date trees, the chopped date tree trunk, and final fibrous LCM product.

To improve the product quality, the collected deceased trees and waste materials are washed using high power water jet to remove all soil debris and other contaminants. To improve the handing and process ability of the deceased date tree trunk, it was chopped into 1.5 m to 2 m logs before transferring to the grinder. The block diagram shown in Fig. 2 indicates the process adopted in producing the fibrous LCM products. Before conducting the sieve analyses, the fibers were dried to reduce the moisture content to less than 4%. Various grades of the fiber products were defined by conducting

Fig. 1 *Images of the (a) deceased date tree trunk, (b) chopped date tree trunk, and (c) the fibers produced by grinding.*

Fig. 2 *Flow diagram of date tree trunk-based fibrous LCM preparation.*

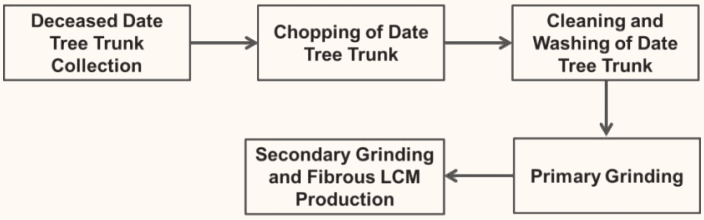

sieve analyses. Figure 3 shows a photographic view of the coarse, medium, and the fine grade fibrous LCM products developed using date palm industry wastes.

Preparation of Sized Particulate LCM "ARC Plug"

The block diagram in Fig. 4 shows the manufacturing process of various grades of a date seed-based particulate LCM product called "ARC plug." After collection of the seeds, they are dynamically washed using water in a mechanized washing system to remove all leftover flesh

Fig. 3 *ARC Eco-fibers prepared using deceased date trees available as date palm industry waste: (a) ARC Eco-fiber C, (b) ARC Eco-fiber M, and (c) ARC Eco-fiber F.*

Fig. 4 *Block diagram showing the ARC plug manufacturing process, a sized particulate LCM.*

Fig. 5 *The various grades and types of the ARC plug product.*

Table 1 *Mud system and sized particulate LCM concentrations used.*

Mud Systems	Date Seed-based Particulate LCM ARC Plug (ppb)		Walnut Shell-based Particulate LCM (ppb)	
65 pcf Bentonite Mud	10	30	10	30
73 pcf KCl Polymer Mud	10	30	10	30
80 pcf NaCl Polymer Mud	10	30	10	30
90 pcf $CaCl_2$ Polymer Mud	10	30	10	30

and debris from the main seed to improve product quality.

After washing, the seeds are adequately dried to a moisture content of less than 3% to improve the grinding ability. After grinding, sieve analyses are performed to define various grades of ARC plug. Finally, the ARC plug admixture was prepared by mixing an appropriate proportion of all grades. Figure 5 shows the various grades of ARC plug along with the ARC plug admixture.

Mud Systems Used as Carrier Fluids

Four different water-based muds, commonly used in drilling operations, were selected to evaluate the performance of the ARC plug using the standard pore plugging test (PPT) apparatus. Table 1 shows the mud systems along with the concentration of ARC plug and the commercially equivalent walnut shell-based particulate LCM product. For evaluation of the performance of the fibrous LCM products, only bentonite and KCl polymer muds were used.

Laboratory Testing and Evaluation

The standard PPT apparatus shown in Fig. 6 was used to evaluate the performance of the newly developed date seed-based particulate LCMs — ARC plug and the date palm waste-based fibrous LCMs — ARC Eco-fibers. The apparatus consists of a 500 ml cell that has a movable piston at the bottom to pressurize the LCM containing mud system. The tests were conducted by incorporating 10 ppb and 30 ppb date seed-based sized particulate LCMs and date palm waste-based fibrous LCMs. Four different mud systems, such as a 65 pcf bentonite mud, 80 pcf sodium chloride (NaCl) polymer mud, 73 pcf KCl polymer mud, and 90 pcf calcium chloride ($CaCl_2$) polymer muds were used to test the ARC plug and the equivalent commercial products. Two different mud systems such as a 65 pcf bentonite mud and 73 pcf KCl polymer mud were used to test the ARC Eco-fibers, equivalent commercial products and two commercially available LCM blends.

For testing and evaluation, all LCM products were mixed properly into the mud system for homogeneous distribution of LCMs into the mud system and then introduced into the test cell. After introducing the LCM containing mud system, a 2 mm slotted disc was fixed at the appropriate position of the test cell. Then, a top cap with a slightly greater aperture (> 2 mm) was fixed above

Fig. 6 *PPT apparatus and the 2-mm slotted disc used for testing the ARC plug.*

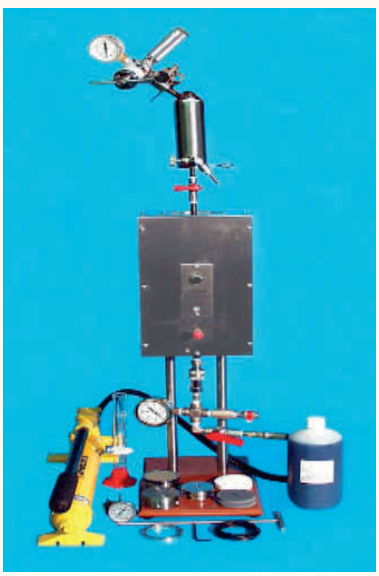

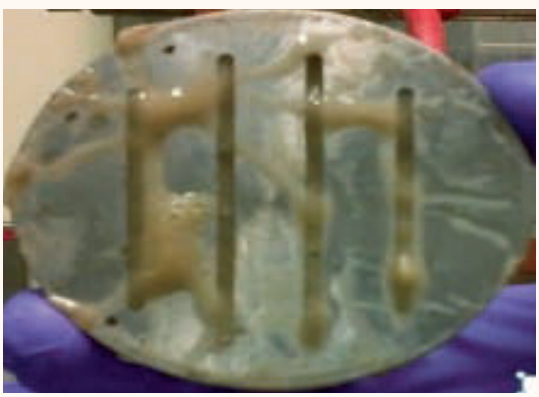

the slotted disc for collecting any drilling fluid lost during the test interval. During the test, the cell was heated to 250 °F and a pressure of 1,500 psi was applied for testing the ARC plug and equivalent commercial products. For ARC Eco-fibers and equivalent commercial products, a pressure of 500 psi instead of 1,500 psi was used. Pressure was applied at the bottom of the test cell using a hand pump. A built-in heating jacket surrounding the test cell allowed the heating of the LCM containing drilling mud to 250 °F before the application of pressure.

Results and Discussion

The experimental results of sized particulate LCM ARC plug and the commercially available and widely used equivalent walnut-based particulate LCM are given in Tables 2, 3, 4, and 5. The experimental results of various grades of fibrous LCM products — ARC Eco-fibers and the commercially available equivalent fibrous LCM products are given in Tables 6 and 7. A comparison of sealing and blocking performance of ARC Eco-fibers and two commercial LCM blends is shown in Table 8. A detailed discussion of the test results are given next.

Sized Particulate LCM ARC Plug

Table 2 shows the plugging efficiency test results conducted by incorporating 10 ppb and 30 ppb date seed and walnut-based LCMs into a 65 pcf bentonite mud. The results clearly show the effective sealing and blocking capacity of the date seed-based LCM ARC plug both at 10 ppb and 30 ppb concentrations.

The commercial walnut-based LCM showed poor plugging potential at a concentration of 10 ppb, which is indicated by a loss of a significant volume of the fluid. It showed effective plugging at a concentration of 30 ppb. As the newly developed date seed-based particulate LCM passed the plugging test, both at 10 ppb and 30 ppb concentrations, it has a somewhat better performance than the commercial walnut-based sized particulate LCMs. It is a better and superior alternative to combat loss of circulation while drilling compared to the currently used walnut-based particulate LCMs.

Table 3 shows the plugging efficiency test conducted by incorporating 10 ppb and 30 ppb date seed and walnut-based LCMs into a 73 pcf KCl polymer mud, which is another common mud system that is frequently used by

Table 2 *Comparison blocking efficiency of date seed and walnut-based LCMs (bentonite mud).*

Bentonite Mud LCM Test Results with 2 mm Slot, 250 °F and 1,500 psi							
Mud System	**LCM**	**Concentration**	**Spurt Loss (cc)**	**Fluid Loss (cc)**	**Total Leakoff (cc)**	**Cake Thickness (mm)**	**PPT Value (cc)**
65 pcf	Date Seed-based LCM Admixture	10 ppb	0	0.2	0.2	N/A	0.4
65 pcf	Walnut-based LCM Admixture	10 ppb	1.2	133	134.2	N/A	268.4
65 pcf	Date Seed-based LCM Admixture	30 ppb	0	0	0	N/A	0
65 pcf	Walnut-based LCM Admixture	30 ppb	0	0	0	N/A	0

Table 3 *Comparison blocking efficiency of date seed and walnut-based LCMs (KCl polymer mud).*

KCl Polymer Mud LCM Test Results with 2 mm Slot, 250 °F and 1,500 psi							
Mud System	**LCM**	**Concentration**	**Spurt Loss (cc)**	**Fluid Loss (cc)**	**Total Leakoff (cc)**	**Cake Thickness (mm)**	**PPT Value (cc)**
73 pcf	Date Seed-based LCM Admixture	10 ppb	0	0	0	N/A	0.4
73 pcf*	Walnut-based LCM Admixture	10 ppb	6.8	92	98.8	N/A	197.6
73 pcf	Date Seed-based LCM Admixture	30 ppb	0	0	0	N/A	0
73 pcf	Walnut-based LCM Admixture	30 ppb	0	0	0	N/A	0
*Blocked after loss of a significant volume of fluid							

Table 4 *Comparison of blocking efficiency of date seed and walnut-based LCMs (NaCl polymer mud).*

NaCl Polymer Mud LCM Test Results with 2 mm Slot, 250 °F and 1,500 psi							
Mud System	**LCM**	**Concentration**	**Spurt Loss (cc)**	**Fluid Loss (cc)**	**Total Leakoff (cc)**	**Cake Thickness (mm)**	**PPT Value (cc)**
80 pcf	Date Seed-based LCM Admixture	10 ppb	0	0	0	N/A	0
80 pcf	Walnut-based LCM Admixture	10 ppb	0	0	0	N/A	0
80 pcf	Date Seed-based LCM Admixture	30 ppb	0	0	0	N/A	0
80 pcf	Walnut-based LCM Admixture	30 ppb	0	0	0	N/A	0

the industry. As before, the test was conducted using a 2 mm slotted disc and a PPT apparatus at 250 °F temperature and 1,500 psi differential pressure.

The results again show the effective sealing and blocking capacity of the date seed-based LCM ARC plug both at 10 ppb and 30 ppb concentrations. The commercial walnut-based LCM shows partial plugging potential at a concentration of 10 ppb, which is reflected by the fluid loss character of the fluid during the test. It showed effective plugging at a concentration of 30 ppb. Like the 65 pcf bentonite mud, the newly developed date seed-based particulate LCM passed the plugging test both at 10 ppb and 30 ppb concentrations in the 73 pcf KCl polymer mud with virtually no loss of any fluid. It indicates that the date seed-based LCM ARC plug was able to seal and plug the slots quickly and effectively after the application of the overburden pressure. The data again demonstrates that the newly developed date seed-based LCM has somewhat better performance than the commercial walnut-based sized particulate LCMs.

Table 4 shows the plugging efficiency test conducted by incorporating 10 ppb and 30 ppb date seed and walnut-based LCMs into an 80 pcf NaCl polymer mud. Tests were conducted using the same test condition as described before. The data clearly shows the effective sealing and blocking capacity for the date seed-based LCM ARC plug, both at 10 ppb and 30 ppb concentrations. The commercial walnut-based LCM was also able to plug at a concentration of 10 ppb and 30 ppb. In the presence of this mud system, the newly developed date seed-based sized LCM ARC plug and the commercial walnut-based LCM showed similar performance. The results again confirm that the date seed-based particulate LCM ARC plug is a viable alternative to replace the equivalent commercial products used by the industry.

Table 5 shows the plugging efficiency test conducted by incorporating 10 ppb and 30 ppb date seed and walnut-based LCMs into a 90 pcf $CaCl_2$ polymer mud. The same test conditions were used for this study also. The results clearly show the effective sealing and blocking capacity of the date seed-based LCM, both at 10 ppb and 30 ppb concentrations. The commercial walnut-based LCM also showed effective plugging potential, both at concentrations of 10 ppb and 30 ppb in this mud system. The EXPEC ARC developed date seed-based LCM ARC plug has a very similar performance rating with respect to the commercially available walnut-based sized particulate LCM. Based on the experimental results, it

Table 5 *Comparison of blocking efficiency of date seed and walnut-based LCMs ($CaCl_2$ polymer mud).*

$CaCl_2$ Polymer Mud LCM Test Results with 2 mm Slot, 250 °F and 1,500 psi							
Mud System	**LCM**	**Concentration**	**Spurt Loss (cc)**	**Fluid Loss (cc)**	**Total Leakoff (cc)**	**Cake Thickness (mm)**	**PPT Value (cc)**
90 pcf	Date Seed-based LCM Admixture	10 ppb	0	0	0	N/A	0
90 pcf	Walnut-based LCM Admixture	10 ppb	0.1	2.8	2.9	N/A	5.8
90 pcf	Date Seed-based LCM Admixture	30 ppb	0	0	0	N/A	0
90 pcf	Walnut-based LCM Admixture	30 ppb	0	0	0	N/A	0

Table 6 *Comparison of sealing and blocking efficiency of ARC Eco-fiber and a conventional fibrous LCM (bentonite mud).*

LCM Products	Spurt Loss (cc)	Fluid Loss (cc)	Total Leakoff (cc)	Cake Thickness (mm)	PPT Value (cc)
ARC Eco-fiber C	0	0	0	29	0
ARC Eco-fiber M	0	0	0	12.7	0
ARC Eco-fiber F	2	23	25	6.4	50
Conventional Fibrous LCM C	0	0	0	11.1	0
Conventional Fibrous LCM M	0	0	0	9.2	0
Conventional Fibrous LCM F	3	21	24	9	48

can be concluded that the date seed-based ARC plug is either similar or better in performance compared to equivalent commercial products.

In conclusion, it can be said that the experimental results demonstrated the potential of using the date seed-based LCM ARC plug as a befitting alternative to commercial sized particulate LCM products imported from overseas countries each year to save the money associated with the importation of these LCM products. The application of the locally available date seed waste as the raw material will also act as a powerful catalyst for the growth of local industries and enterprises. It will also create new job opportunities for the needy and low income public and the date farming communities to uplift their social and economic status.

Fibrous LCM ARC Eco-Fibers

Table 6 shows the experimental results of PPTs conducted using the various grades of date tree waste-based fibrous LCMs using bentonite mud, and a 2 mm slotted disc to represent a fractured loss zone at 250 °F and 500 psi overbalance pressure to simulate the bottom-hole temperature and pressure effect on the LCM products. The results clearly show that the newly developed date tree waste-based fibrous LCMs have the ability to seal loss zones containing up to 2 mm fractures. Comparison of the performance of various grades of ARC Eco-fibers with the performance of various grades of a commercial fibrous LCM products indicate better or similar performance for the newly developed date tree waste-based fibrous LCMs. This demonstrates that the date tree waste-based fibrous LCMs are viable alternatives to imported fibrous LCM products, and therefore, can replace them in controlling the loss circulation problems of the region.

Table 7 shows the experimental results of PPTs conducted using the various grades of date tree waste-based fibrous LCMs using KCl polymer mud, and a 2 mm slotted disc at 250 °F, but at 500 psi overbalance pressure. The results clearly show that the newly developed date tree waste-based fibrous LCMs have the ability to seal loss zones containing up to 2 mm fractures. Comparison of the performance of various grades of ARC Eco-fibers with the performance of various grades of commercial fibrous LCM products indicate nearly similar performance for the newly developed date tree waste-based fibrous LCMs and the commercially available equivalent fibrous LCM products. This demonstrates that the date tree waste-based fibrous LCMs are viable alternatives to imported fibrous LCM products, and so can replace them in controlling the loss circulation problems of the region.

Table 8 shows a comparison of test results of various grades of ARC Eco-fibers with respect to two specially

Table 7 *Comparison of blocking efficiency of ARC Eco-fiber and a conventional fibrous LCM (KCl polymer mud).*

LCM Products	Spurt Loss (cc)	Fluid Loss (cc)	Total Leakoff (cc)	Cake Thickness (mm)	PPT Value (cc)
ARC Eco-fiber C	2	3	5	24	10
ARC Eco-fiber M	1	3	4	12.7	8
ARC Eco-fiber F	2	15	18	6.4	36
Conventional Fibrous LCM C	3	5	8	11.1	16
Conventional Fibrous LCM M	2	6	8	9.2	16
Conventional Fibrous LCM F	3	16	19	9	38

Table 8 *Comparison of blocking efficiency of ARC Eco-fiber and commercial LCM blends (bentonite mud).*

LCM Products	Spurt Loss (cc)	Fluid Loss (cc)	Total Leakoff (cc)	Cake Thickness (mm)	PPT Value (cc)
ARC Eco-fiber C	0	0	0	29	0
ARC Eco-fiber M	0	0	0	12.7	0
ARC Eco-fiber F	2	23	25	6.4	50
Commercial LCM Blend 1	0.7	16	16.7	3.97	33.4
Commercial LCM Blend 1	0	2	2	6.4	4

designed LCM blends that have a proven success rate in the field. The results clearly indicate that the date palm waste-based fibrous LCMs have similar or better performance with respect to these specially designed LCM blends. It indicates that the use of date tree waste-based fibrous LCMs in an engineered LCM blend design will improve the blend performance significantly, and so can play a highly positive role in combating moderate and severe loss circulation problems of the region.

Conclusions

1. The Kingdom of Saudi Arabia has a huge supply source of date palm industry wastes for localization of the production of sized particulate and fibrous LCMs to meet the national and regional demand.
2. The date seed-based sized particulate LCM ARC plug has similar or better physical and mechanical properties like the conventional sized LCMs available commercially.
3. As date seeds available from various types of date palm trees have nearly similar mechanical characteristics, all of them can be used either alone or in combination to manufacture sized particulate LCM products.
4. Due to low-density of date seed-based sized particulate LCM compared to natural sized particulate products such as sized calcium carbonate, these particles can easily remain suspended in the carrier fluid, and therefore can show no/negligible settlement problems.
5. The low-density of the date seed particles will allow the incorporation of a much higher concentration of LCMs in the mud system without any detrimental impact on the mud density.
6. The huge volume of date tree wastes such as deceased date trees, old and discarded trees, yearly pruning wastes, empty fruit bunches, etc., provides a potential and sustainable source of raw materials for fibrous LCM production.
7. Experimental results demonstrated similar or better performance in sealing and blocking 2 mm slots for the date tree waste-based fibrous LCMs compared to the equivalent commercial fibrous LCM products.
8. Even the 10 ppb date tree waste-based fibrous and particulate LCMs showed effective sealing and blocking capacity in the presence of a 2 mm slotted disc that was used to simulate a fractured loss zone.
9. Comparison of the date tree waste-based fibrous LCM performance to two commercial LCM blends containing various types of LCM products indicate a very similar performance for the date tree waste-based fibers.
10. The renewable source of waste date seeds and the date palm industry wastes ensures a perpetual source of supply of locally available raw materials for uninterrupted production of particulate and fibrous LCM products.
11. Standard PPT results indicate similar or better performance for the date seed-based particulate LCM ARC plug compared to the commercial equivalent walnut-based particulate LCMs.
12. Due to the eco-friendly, nontoxic and biodegradable nature of date palm industry wastes, these raw materials are highly suitable for various green product development for oil and gas field applications.
13. The transformation of date palm industry wastes into valuable commercial products will act as a powerful catalyst for the growth of local industries and the creation of new job opportunities.
14. The additional economic contribution of utilization and commercialization of date palm waste-based industrial products can make the date farming industry an attractive industrial sector for the Middle East.

Acknowledgments

The authors would like to thank the management of Saudi Aramco for their support and permission to publish this article.

This article was presented at the International Petroleum Technology Conference, Beijing, China, March 26-28, 2019.

References

1. Amanullah, M.: "Characteristics, Behavior and Performance of ARC Plug — A Date Seed-based Sized Particulate LCM," SPE paper 182840, presented at the SPE Kingdom of Saudi Arabia Annual Technical Symposium and Exhibition, Dammam, Saudi Arabia, April 25-28, 2016.
2. Friedheim, J., Sanders, M. and Roberts, N.: "Unique Drilling Fluids Additives for Improved Wellbore Stability

and Reduced Losses," paper presented at the SEFLU Conference, Margarita Island, Venezuela, May 19-23, 2008.

3. Reid, P. and Santos, H.: "Novel Drilling, Completion and Workover Fluids for Depleted Zones: Avoid Losses, Formation Damage and Stuck Pipe," SPE paper 85326, presented at the SPE/IADC Middle East Drilling Technology Conference and Exhibition, Abu Dhabi, UAE, October 20-22, 2003.

4. Sweatman, R.E., Kessler, C.K. and Hillier, J.M.: "New Solutions to Remedy Lost Circulation, Crossflows, and Underground Blowouts," SPE paper 37671, presented at the SPE/IADC Drilling Conference, Amsterdam, the Netherlands, March 4-6, 1997.

5. Kumar, A. and Savari, S.: "Loss Circulation Control and Wellbore Strengthening: Looking beyond Particle Size Distribution," paper AADE-11-NTCE-21, presented at the AADE National Technical Conference and Exhibition, Houston, Texas, April 12-14, 2011.

6. Amanullah, M., Alouhali, R.A. and Arfaj, M.K.: "Impact of Geological and Geomechanical Controls in Creating Various Drilling Problems," AAPG/Datapages Inc., Search & Discovery Article 42199, April 23, 2018.

7. Van Oort, E., Friedheim, J.E., Pierce, T. and Lee, J.: "Avoiding Losses in Depleted and Weak Zones by Constantly Strengthening Wellbores," SPE paper 125093, presented at the SPE Annual Technical Conference and Exhibition, New Orleans, Louisiana, October 4-7, 2009.

8. Song, J.H. and Rojas, J.C.: "Preventing Mud Losses by Wellbore Strengthening," SPE paper 101593, presented at the SPE Russian Oil and Gas Technical Conference and Exhibition, Moscow, Russia, October 3-6, 2006.

9. White, R.J.: "Lost Circulation Materials and Their Evaluations," paper API-56-352, presented at the Drilling and Production Practice Conference, New York, New York, January 1, 1956.

10. Whitfill, D.L.: "Lost Circulation Material Selection, Particle Size Distribution, and Fracture Modeling with Fracture Simulation Software," SPE paper 115039, presented at the IADC/SPE Asia Pacific Drilling Technology Conference and Exhibition, Jakarta, Indonesia, August 25-27, 2008.

11. Salehi, S. and Nygaad, R.: "Numerical Modeling of Induced Fracture Propagation: A Novel Approach for Lost Circulation Materials (LCM) Design in Borehole Strengthening Applications of Deep Offshore Drilling," SPE paper 135155, presented at the SPE Annual Technical Conference and Exhibition, San Antonio, Texas, October 8-10, 2012.

12. Alberty, M.W. and McLean, M.R.: "A Physical Model for Stress Cages," SPE paper 90493, presented at the SPE Annual Technical Conference and Exhibition, Houston, Texas, September 26-29, 2004.

13. Dupriest, F.E.: "Fracture Closure Stress (FCS) and Loss Return Practices," SPE/IADC paper 92192, presented at the SPE/IADC Drilling Conference, Amsterdam, the Netherlands, February 23-25, 2005.

14. Aadnoy, B.S. and Belayneh, M.: "Elasto-plastic Fracturing Model for Wellbore Stability Using non-Penetrating Fluids," *Journal of Petroleum Science and Engineering*, Vol. 45, Issues 3-4, December 2004, pp. 179-192.

15. Wang, H., Sweatman, R.E., Engelman, R.E., Deeg, W.F.J., et al.: "The Key to Successfully Applying Today's Lost Circulation Solutions," SPE paper 95895, presented at the SPE Annual Technical Conference and Exhibition, Dallas, Texas, October 9-12, 2005.

16. Amanullah, M. and Yu, L.: "Environment Friendly Fluid Loss Additives to Protect the Marine Environment from the Detrimental Effect of Mud Additives," *Journal of Petroleum Science and Engineering*, Vol. 48, Issues 3-4, September 2005, pp. 199-208.

17. Tehrani, A., Yong, S., Gerrard, D. and Fernandez, J.: "Environmentally Friendly Water-based Fluid for HPHT Drilling," SPE paper 121783, presented at the SPE International Symposium on Oil Field Chemistry, The Woodlands, Texas, April 20-22, 2009.

18. Rae, P., Di Lullo, G. and Ahmad, A.: "Toward Environmentally Friendly Additives for Well Completion and Stimulation Operations," SPE paper 68651, presented at the SPE Asia Pacific Oil and Gas Conference and Exhibition, Jakarta, Indonesia, April 17-19, 2001.

19. Ghori, W., Saba, N., Jawaid, M. and Asim, M.: "A Review of Date Palm (Phoenix Dactylifera) Fibers and Its Polymer Composites," *IOP Conference Series: Material Science and Engineering*, Vol. 368, June 2018.

20. Jawaid, M. and Abdul Khalil, H.P.S.: "Cellulosic/Synthetic Fiber Reinforced Polymer Hybrid Composites: A Review," *Carbohydrate Polymers*, Vol. 86, Issue 1, August 2011, pp. 1-18.

21. Amanullah, M., Arfaj, M.K., Gadalla, A., Saleh, R., et al.: "Date Seed-based Particulate LCM "ARC Plug" — Its Development, Laboratory Testing and Trial Test Results," SPE paper 187988, presented at the SPE Kingdom of Saudi Arabia Annual Technical Symposium and Exhibition, Dammam, Saudi Arabia, April 24-27, 2017.

About the Authors

Dr. Md. Amanullah

Ph.D. in Petroleum Engineering, Imperial College

Dr. Md. Amanullah is a Senior Petroleum Engineering Consultant working at Saudi Aramco's Exploration and Petroleum Engineering Center – Advanced Research Center (EXPEC ARC). Prior to joining Saudi Aramco, he worked as a Principal Research Scientist at CSIRO in Australia.

Aman is the lead inventor of a vegetable oil-based dielectric fluid (patented) that led to the formation of a spinoff company in Australia for commercialization of the product.

He has published more than 100 technical papers and filed more than 75 patents, with 30 already granted. Two of Aman's patents were highlighted in scholarly editions of two books published in the U.S.

He is one of the recipients of the 2005 Green Chemistry Challenge Award from the Royal Australian Chemical Institute. Aman also received the CSIRO Performance Cash Reward in 2006, the Saudi Aramco Mentorship Award in 2008 and 2010, the World Oil Certificate Award for nano-based drilling fluid development in 2009, the Intellectual Asset Recognition Award in 2014, and the Award of Recognition for Outstanding Contribution to the success of agricultural waste and environmental protection in 2014. His date tree waste-based product development was highlighted in *The Arabian Sun*, the *Arab News* and also in the *Al Riyadh* newspaper.

Aman is a member of the Society of Petroleum Engineers (SPE). He received the SPE Regional Service Award in 2014 and also the SPE Middle East Drilling Engineering Award in 2016 for his contribution to the industry. In 2018, Aman received the Middle East Oil and Gas Technical Innovation of the Year Award, and he also received the Board of Engineers Recognition Certificate for Date Seed-based ARC Plug development.

In early 2019, Aman received the 2018 Technology Deployment Award (EXPEC ARC Annual Awards) for high-impact and high-profile technology deployment of the year.

Aman received his M.S. degree (First Class) in Mechanical Engineering from the Moscow Oil and Gas Institute, Moscow, Russia, and his Ph.D. degree in Petroleum Engineering from Imperial College, London, U.K.

Dr. Mohammed K. Al-Arfaj

Ph.D. in Petroleum Engineering, King Fahd University of Petroleum and Minerals

Dr. Mohammed K. Al-Arfaj joined Saudi Aramco in 2006 as a Petroleum Engineer, working with the Drilling Technology Team in the Exploration and Petroleum Engineering Center – Advanced Research Center (EXPEC ARC). He works in the area of drilling and completion, and has conducted several projects in the areas of shale inhibition, drilling nano-fluids, loss circulation materials, spotting fluids, swellable packers, completion fluids, and oil well cementing.

Mohammed received his B.S. degree in Chemical Engineering from King Fahd University of Petroleum and Minerals (KFUPM), Dhahran, Saudi Arabia, in 2006. In 2009, he received his M.S. degree in Petroleum Engineering from Heriot-Watt University, Edinburgh, Scotland. In 2017, Mohammed received his Ph.D. degree in Petroleum Engineering specializing in molecular modeling and experimental studies of shale fluid interactions from KFUPM.

Dr. Raed A. Alouhali

Ph.D. in Petroleum Engineering, Texas Tech University

Dr. Raed A. Alouhali is a Petroleum Engineer working with the Drilling Technology Team in Saudi Aramco's Exploration and Petroleum Engineering Center – Advanced Research Center (EXPEC ARC). He conducts research projects related to drilling fluids, lost circulation, and shale inhibition to find solutions to current drilling and workover challenges by utilizing the latest advancement in technology, such as 3D printing, data mining, and artificial intelligence.

Raed has 10 patent applications and seven published papers in journals.

He received his B.S. degree in Petroleum Engineering from University of Louisiana at Lafayette, Lafayette, LA, and his M.S. degree with a Smart Oil Field certificate from the University of Southern California, Los Angeles, CA. Raed received his Ph.D. degree in Petroleum Engineering from Texas Tech University, Lubbock, TX.

A Novel Machine Learning Model for Early Operational Anomaly Detection Using LWD/MWD Data

Mohammed A. Al-Ghazal and Viranchi Vedpathak

Abstract /

Drilling and workover operations represent a crucial part of a well's life cycle in terms of deliverability and economics. Understanding the underlying phenomena that cause operational anomalies is the stepping stone into early detection and control of undesired events, such as a kick.

The evolution of artificial intelligence and machine learning applications lend itself to well operations, to gain new efficiencies and unveil hidden insightful observations about downhole and surface operating conditions. Incorporating the mechanisms of natural phenomena and big data, retrieved from sources such as logging while drilling (LWD) and measurement while drilling (MWD) logs, and placed into machine learning models, boost capabilities for early detection of operational anomalies, and mitigation of potential negative consequences, while eliminating human bias.

This article highlights a novel machine learning model developed to streamline early detection for the operational anomaly of uncontrolled hydrocarbon flow during well operations, such as drilling. The proposed technique detects and classifies the risk level of a kick before it reaches the surface, to extend the safe response time limit. When this method is integrated with LWD data in real-time mode by means of software, an alarm system can be embedded to alert field hands about downhole conditions. This does not only promote safer operations, but also significantly improves the availability and reliability of critical information.

To further fine-tune the accuracy of the predictive model, multiple rounds of cross-validation were executed on the training data. It is evident that training machine learning models allow for more learning through practice. The technique presented shows that big data and machine learning algorithms are powerful tools to uncover hidden information, and enable improvement in operational leadership.

Introduction

The daily flow of vast, fast, and varied data represents vast opportunities for the oil and gas industry as this data is processed and refined into meaningful information[1]. Accordingly, machine learning models are used to analyze the collected data to generate insights that would describe, predict and prescribe operating trends. Other advantages of machine learning are the elimination of human bias and streamlining error prone repetitive tasks. Machine learning models are categorized into four major categories: unsupervised learning, supervised learning, semi-supervised learning, and reinforcement learning[2].

One machine learning application that is gaining wider applicability is anomaly detection during drilling, workover and completion operations. Many companies find it appealing to use machine learning algorithms to identify undesired outcomes, such as kicks and blowout, in real-time mode[3]. According to Unrau and Torrione (2017)[4], anomaly detection machine learning algorithms offer new capabilities, such as reduction in false alarm reports, higher anomaly detection rating, and reduction in detection time lag.

The influx of fluids into a wellbore is an operational anomaly encountered during a drilling operation, even though the flow of fluids at surface is controlled using methods, including changes in mud weight and shutting wells. A severe case of fluid influx is an uncontrolled flow of hydrocarbons from a high-pressure subsurface structure, and is known as a blowout. The Foundation for Scientific and Industrial Research at the Norwegian Institute of Technology (SINTEF) conducted a study and found that about 117 well control incidents occurred in the period from 2000 through 2014. Given the importance of safety while drilling a well, a relatively limited volume of literature is published in the area of kick detection and management, using data-driven models and machine learning algorithms.

Fraser et al. (2014)[5] suggests a method to early detection of influx flow rate for offshore wells. Installing a Coriolos flow meter outside of the riser on the seabed provides the ability to measure the flow rate even before the fluids reach the surface, reducing kick detection volume by a factor of 2. Unrau et al. (2017)[6] developed a machine

learning algorithm to prevent false alarms of fluid influx. Accounting for fluctuations in flow rate and mud levels due to operations, including changing mud pump rates, making connections and transferring mud; the system was trained to accurately detect fluid influx or mud loss.

Predictive Model Development

In this study, the operational anomaly of hydrocarbon kick was detected using parameters recorded through logging while drilling (LWD), and measurement while drilling (MWD). At the most fundamental level, for a well to experience a kick, this novel approach considers the following conditions:

1. Subsurface rock is porous enough to hold any fluid.
2. Subsurface rock pores contains fluid.
3. The actual subsurface pressure is higher than the expected pressure (calculated based on pressure gradient data).

Using LWD tool data, it is possible to determine if the above three conditions are met in real-time. Kicks are conventionally identified by a rise in fluid level at the mud pits. The proposed method will detect a kick before it reaches the surface, and alarm the crew ahead of time to be prepared for necessary well control measures, to eliminate or abate any potential negative consequences. LWD tool assembly parameters required for this study are as follows: resistivity log, neutron porosity log, bulk density log, and pressure measurement[7].

Considering each of the three stated conditions separately — and expanding on how it can be achieved using LWD data — is useful in developing the proposed predictive machine learning model. First, subsurface rock should be porous enough to hold any fluid. The combination of bulk density and neutron porosity logs can determine the porosity of the subsurface formation. Figure 1 illustrates typical bulk density and neutron porosity logs. The positive separation of the two logs indicates a porous formation with fluids. Second, subsurface rock pores should have a presence of fluids. Resistivity logs can investigate the presence of fluids in the shallow, near the wellbore, and deep regions of the hole. In this study, we consider any spike (in case of hydrocarbons) or drop (in case of brine) in resistivity measurement for an extended depth interval with a minimum 15 ft. This is to compensate for noise in measurements attributed to the presence of fluid.

Fig. 1 *Typical bulk density and neutron porosity logs used for detecting the presence of hydrocarbons and type of fluid.*

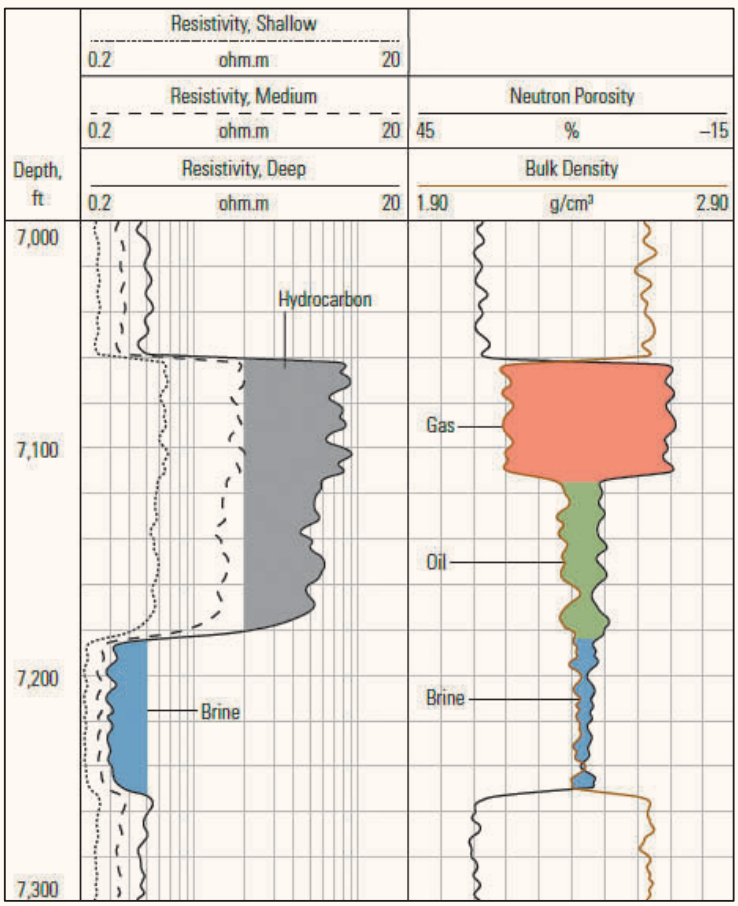

Fig. 2 *Pressure and pressure gradient vs. depth (Appendix).*

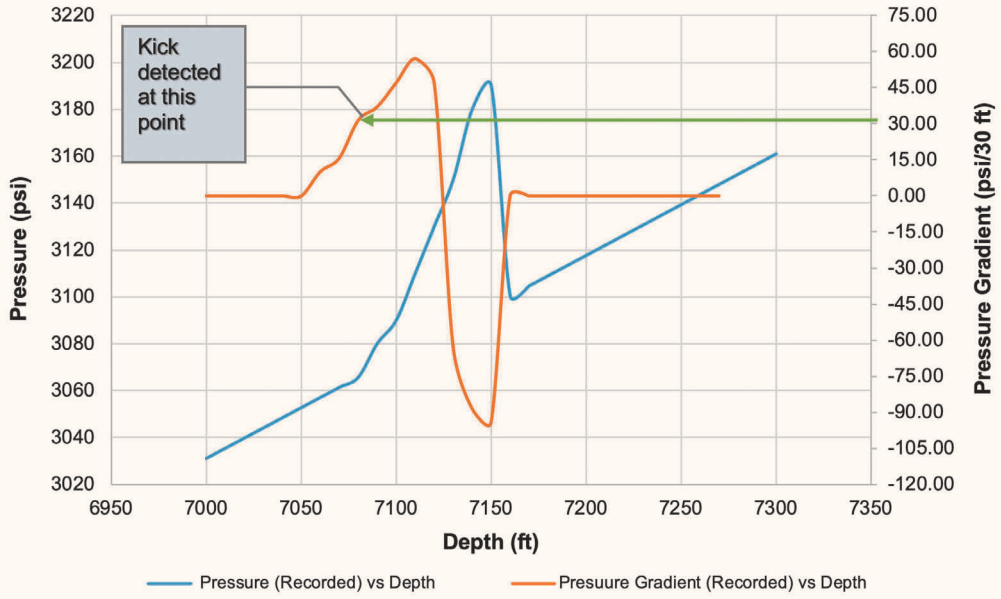

Third, the actual subsurface pressure should be higher than the expected pressure. Assuming the downhole pressure measurement tool is part of the LWD and MWD assembly, the instrument measures downhole pressure every 10 ft and the pressure gradient is calculated (Δ psi/10 ft) and recorded every 10 ft. Any unexpected rise in pressure gradient can be attributed to the influx of fluids. The noise in the data could indicate a false kick. To mitigate such false indications, the pressure gradient is calculated over 30 ft intervals (Δ psi/30 ft), even though the tool may measure pressure every 10 ft. If the recorded pressure gradient is higher than the expected pressure gradient by 30 psi/30 ft (green line in Fig. 2), fluid influx is assumed. The expected pressure gradient can be calculated knowing the depth of the well, hole geometry, mud properties and volume of annular hydrostatic column, Appendix 1.

This method can identify a kick just 30 ft after the pressure measurement tool records the pressure at a given depth. Unlike traditional detection methods that rely on surface flow parameters and visual inspection of the volume of mud pits for kick identification, the proposed predictive method identifies a kick much before the downhole influx reaches the surface. When this method is integrated with LWD data in real-time by means of a software, an alarm system can be developed to notify the rig crew about the possibility of fluid influx. This ensures safer drilling operations and assists the crew to be prepared for any well control activities. This kick identification method requires minimal cost of installation — only the cost of the alarm system — when a comprehensive LWD assembly is already installed.

A decision matrix, Table 1, is designed to indicate the risk of kick, based on the data recorded. Knowledge of the typical measurements of different logs and pressure gradients for a particular oil field is helpful to assign risk classifications of high, medium, or low, based on the recorded parameters' value range.

Model Optimization

The novel machine learning technique, introduced in this article, eliminates the time lag, often encountered to detect and classify undesired events, utilizing big data retrieved in real-time mode from LWD and MWD. A pattern recognition logic, which is fit to existing operating workflow frames, is used to analyze the LWD and MWD data, and identify symptoms of downhole formation fluid kick, and its corresponding risk level.

The input parameters for the data-driven machine learning model are LWD and MWD data, including resistivity, neutron porosity, bulk density and pressure gradient. These inputs — represented as vector matrices — are the features and observations used to understand the fluid kick. The target variable of the model is fluid influx classification (Yes or No influx), which is a discrete data set. The data science classification decision tree method was selected to categorize the target variable, because it is suitable for a discrete set of values, which is the case in this application. The ultimate purpose of the classification decision tree method is to split the data set into a class of either influx or no influx.

As far as model training to fine-tune accuracy and reliability, LWD and MWD data was used from multiple wells to feed and calibrate the model. The trained model was further tested using a multifold cross validation test method. Additionally, multiple rounds of cross-validation were executed to streamline the predictive data analytics model.

Table 1 *A decision matrix for risk classification of high, medium, or low.*

Water/Oil	Pressure Gradient	Neutron Porosity	Risk
Yes	H	H	High
Yes	H	M	High
Yes	H	L	Med
Yes	M	H	High
Yes	M	M	Med
Yes	M	L	Med
Yes	L	H	Low
Yes	L	M	Low
Yes	L	L	Low

It is evident that machine learning model training allows the algorithm model to learn through repetitive practices. This work is a testimony to the power of big data and machine learning algorithms, to unveil insights about drilling and completion operations that would enhance decision making, to safeguard human lives and valuable assets.

Conclusions

Digitalization, in the form of artificial intelligence, machine learning and big data analytics, continues to progress in the oil and gas industry, spanning upstream, midstream, and downstream applications. In the specific case of this article, a novel machine learning model for early detection of the operational anomaly of kick has been outlined. The machine learning model was developed to streamline early detection of a kick to enable new control capabilities toward operational robustness, which is the need of the hour to add nonexisting efficiencies.

The model uses a decision matrix to categorize the risk of kick based on the data recorded from the LWD and MWD data. The input parameters for the predictive machine learning model are the LWD and MWD data, including resistivity, neutron porosity, bulk density and pressure gradient. These inputs are the features and observations used to describe the downhole conditions. The target variable of the model is fluid influx identification and classification. The data science classification decision tree method was selected to categorize the target variable because it is suitable for a discrete set of values, which is the case in this application. The ultimate purpose of the classification decision tree method is to split the data set into a class of either influx or no influx, based on predetermined value ranges. Finally, multiple rounds of cross-validation were executed to verify the predictive data analytics model and its accuracy.

Acknowledgments

The authors would like to thank the management of Saudi Aramco and Stratagraph for their support and permission to publish this article.

References

1. Baaziz, A. and Quoniam, L.: "How to Use Big Data Technologies to Optimize Operations in Upstream Petroleum Industry," paper presented at the 21st World Petroleum Congress, Moscow, Russia, June 15-19, 2014.
2. Noshi, C.I. and Schubert, J.J.: "The Role of Machine Learning in Drilling Operations: A Review," SPE paper 191823, presented at the SPE/AAPG Eastern Regional Meeting, Pittsburgh, Pennsylvania, October 7-11, 2018.
3. Al-Ghazal, M.A.: "The Value of Digital Data Analytics," *Oil & Gas Vision*, Vol. 14, 2018, pp. 10-11.
4. Unrau, S. and Torrione, P.: "Adaptive Real-Time Machine Learning-based Alarm System for Influx and Loss Detection," SPE paper 187155, presented at the SPE Annual Technical Conference and Exhibition, San Antonio, Texas, October 9-11, 2017.
5. Fraser, D., Lindley, R., Moore, D.D. and Vander Staak, M.: "Early Kick Detection Methods and Technologies," SPE paper 170756, presented at the SPE Annual Technical Conference and Exhibition, Amsterdam, the Netherlands, October 27-29, 2014.
6. Unrau, S., Torrione, P., Hibbard, M., Smith, R., et al.: "Machine Learning Algorithms Applied to Detection of Well Control Events," SPE paper 188104, presented at the SPE Kingdom of Saudi Arabia Annual Technical Symposium and Exhibition, Dammam, Saudi Arabia, April 24-27, 2017.
7. Dowell, I., Mills, A., Ridgway, M. and Lora, M.: *Petroleum Engineering Handbook, Volume II: Drilling Engineering*, Chapter 15, Society of Petroleum Engineers, 2006, pp. 647-685.

Appendix 1 *Pressure gradient calculation example data set.*

Depth (ft)	Pressure (Expected) (psi)	Pressure (Recorded) (psi)	Pressure (Difference) (psi)	Pressure Gradient (Expected) (psi/30 ft)	Pressure Gradient (Recorded) (psi/30 ft)	Pressure Gradient (Difference) (psi/30 ft)
7,000	3,031	3,031	0	—	—	—
7,010	3,035.33	3,035.33	0	—	—	—
7,020	3,039.66	3,039.66	0	—	—	—
7,030	3,043.99	3,043.99	0	12.99	12.99	0.00
7,040	3,048.32	3,048.32	0	12.99	12.99	0.00
7,050	3,052.65	3,052.65	0	12.99	12.99	0.00
7,060	3,056.98	3,056.98	0	12.99	12.99	0.00
7,070	3,061.31	3,061.31	0	12.99	12.99	0.00
7,080	3,065.64	3,065.64	0	12.99	12.99	0.00
7,090	3,069.97	3,080	10.03	12.99	23.02	10.03
7,100	3,074.3	3,090	15.7	12.99	28.69	15.70
7,110	3,078.63	3,110	31.37	12.99	44.36	31.37
7,120	3,082.96	3,130	47.04	12.99	50	37.01
7,130	3,087.29	3,150	62.71	12.99	60	47.01
7,140	3,091.62	3,180	88.38	12.99	70	57.01
7,150	3,095.95	3,190	94.05	12.99	60	47.01
7,160	3,100.28	3,100.28	0	12.99	-49.72	-62.71
7,170	3,104.61	3,104.61	0	12.99	-75.39	-88.38
7,180	3,108.94	3,108.94	0	12.99	-81.06	-94.05
7,190	3,113.27	3,113.27	0	12.99	12.99	0.00
7,200	3,117.6	3,117.6	0	12.99	12.99	0.00
7,210	3,121.93	3,121.93	0	12.99	12.99	0.00
7,220	3,126.26	3,126.26	0	12.99	12.99	0.00
7,230	3,130.59	3,130.59	0	12.99	12.99	0.00
7,240	3,134.92	3,134.92	0	12.99	12.99	0.00
7,250	3,139.25	3,139.25	0	12.99	12.99	0.00
7,260	3,143.58	3,143.58	0	12.99	12.99	0.00
7,270	3,147.91	3,147.91	0	12.99	12.99	0.00
7,280	3,152.24	3,152.24	0	12.99	12.99	0.00
7,290	3,156.57	3,156.57	0	12.99	12.99	0.00
7,300	3,160.9	3,160.9	0	12.99	12.99	0.00

About the Authors

Mohammed A. Al-Ghazal

M.S. in Engineering, University of Southern California

Mohammed A. Al-Ghazal is a Petroleum Engineer, working with a team responsible for upstream operations at Saudi Aramco. His expertise covers upstream exploration and production, modern information control models, value chain, energy outlook, artificial intelligence, machine learning and health, safety, security and environment (HSSE).

Mohammed has been involved with several projects, including those addressing machine learning models, real-time downhole monitoring, digital data analytics, integrated cyber and physical security, logical information control modeling, environment friendly fluids, safety instrumented systems and big data quality.

He has published numerous Society of Petroleum Engineers (SPE) papers and peer-reviewed technical journal articles as well as multiple in-house technical reports and guidelines. In recognition of Mohammed's contributions, he is the recipient of several regional and international awards and honors. Recently, Mohammed was selected as the recipient of the 2018 Young Oil and Gas Professional of the Year Award by Oil & Gas and Refining & Petrochemicals Middle East.

In 2010, Mohammed received his B.S. degree with honors in Petroleum Engineering from King Fahd University of Petroleum and Minerals (KFUPM), Dhahran, Saudi Arabia. In 2015, he received an M.S. degree with honors in Engineering from the University of Southern California, Los Angeles, CA.

Viranchi Vedpathak

M.S. in Petroleum Engineering, University of Southern California

Viranchi Vedpathak is a Wellsite Geologist at Stratagraph Inc., working in the oil fields of the Permian Basin in Texas. Research is one of his favorite activities, and he is interested in finding innovative ways to use oil field data.

Viranchi served as the President of the Society of Petroleum Engineers (SPE) chapter at his university for the term 2016-2017.

He received his M.S. degree in Petroleum Engineering with a specialization in Smart Oil Field Technologies from the University of Southern California, Los Angeles, CA.

Nanoparticles Stabilized CO_2/Brine Emulsions at Reservoir Conditions: A New Way of Mitigating Gravity Override in CO_2 Floods

Dr. Zuhair A. Al-Yousif, Dr. Mohammed Al-Mobarky, and Dr. David S. Schechter

Abstract /

Carbon dioxide (CO_2) injection is an effective method for enhanced oil recovery (EOR); however, the efficiency of CO_2 is hindered by mobility problems. The high mobility of CO_2, compared with the reservoir fluids, may lead to early breakthrough of CO_2, resulting in an incomplete sweep. The use of surface modified nanoparticles has provided an excellent alternative to generate a stable CO_2/brine emulsion for CO_2 mobility control. The objective of this work is to investigate the effect of: emulsion quality, shear rates, salinity, pressure, nanoparticle concentration and nanoparticle size on the strength of the emulsion.

Glass beads — as a porous medium — and a capillary tube to measure the apparent viscosity were used to perform the tests at reservoir conditions. Three types of coated silica particles were used to conduct this study. Three qualities were tested: 50%, 70%, and 90%. Also, five shear rates were used to assess the strength of emulsions. Solutions with 1 wt%, 3 wt%, and 8 wt% of sodium chloride (NaCl) were used. The role of the nanoparticle size was also tested for one type of silica particles. The effect of these parameters was evaluated at high pressures of 800 psi and 1,800 psi, and temperature, 50 °C.

For all tested materials, the quality of the emulsion was found to be an important parameter for emulsion strength. Emulsion viscosity increases as quality decreases, which indicates that the strongest emulsion was achieved at 50% quality. For silica partially modified with methyl silyl, the results showed that the change of salinity has no effect on emulsion viscosity. Subsequently, the increase of salinity produced emulsions with higher viscosities for silica modified with polyethylene glycol (PEG), and silica modified with an appropriate material. The shear rate has a significant impact on the behavior of the emulsion for silica modified partially with methyl silyl and PEG. Also, the study showed that the change of nanoparticle size has no effect on the emulsion strength. The change in pressure, however, has a significant impact on the emulsion viscosity.

The use of nanoparticles to stabilize CO_2/brine emulsion has the potential to mitigate the gravity override challenge in a CO_2 flood. Long-term stability of nanoparticle stabilized emulsion is a critical factor in selecting the appropriate emulsifying agent. This work improves our understanding of the effect of different parameters on the strength of emulsions, which can be used to control CO_2 mobility, and therefore, improve sweep efficiency.

Introduction

To mitigate gas mobility issues in enhanced oil recovery (EOR), foams are being generated using surfactants as the main emulsifying agents. Although, there are a handful of challenges associated with foam generation and stabilization at reservoir conditions. Reservoir temperature, high salinity and surfactant adsorption to the rock are considered harsh conditions that may result in weaker generation of foam, and therefore, poor sweep efficiency[1-7]. Moreover, there are challenges associated with the use of supercritical carbon dioxide (CO_2) in foam generation, and these drawbacks make it difficult to generate a stable emulsion with water, therefore, limiting its applicability. Due to the fact that CO_2 has a zero permanent dipole moment and weak van der Waals forces, it exhibits low polarizability. Consequently, a CO_2 philic tail is considered a poor solvent for both polar and high molecular weight solutes. As a result, instability of the emulsion can occur in the form of flocculation or coalescence[8-10].

The use of solid nanoparticle are considered an innovative technique to stabilize gas-liquid foam and/or emulsion. Nanoparticles provide an excellent alternative to the use of surfactants to stabilize foams and control gas mobility in a petroleum reservoir. In comparison with surfactant molecules, the nanoparticles exhibit strong adsorption ability at the gas-brine interface and form stable CO_2 foams/emulsions. Furthermore, using nanoparticles as an alternative option for surfactant or mixed with surfactants[5-6, 11-16] to stabilize foam/emulsion may offer a solution to the long-term instability and adsorption issues associated with surfactant foams. In addition, they are showing excellent chemical stability and low retention on rock surfaces[5, 17-19].

Table 1 *Experimental parameters and conditions.*

Parameter	Silica 1	Silica 2	Silica 3	Unit
Pressure	1,800	800-1,800	1,800-2,500	psi
Temperature	50	50	50	°C
Concentration	1	1	1-1.5	wt%
Quality	50-70-90	50-70-90	90	%
Salinity	1-3-8	1-3-8	1-3	wt%
Shear Rate	910-1,365-1,820	1,365-2,090-2,730	1,365-1,820	s^{-1}
NPs Surface Area	120-250	—	—	m^2/g

There have been a wide variety of particles used to stabilize foams/emulsions, e.g., silica, iron oxide, hydroxides, metal sulfates, clays, and carbon. Silica nanoparticles have been mostly addressed for EOR applications[20]. As studied[21], nanoparticles potentially have a better CO_2 solvation capability. Surface modified silica nanoparticles using polyethylene glycol (PEG) and dichlorodimethylsilane were successful in stabilizing CO_2 water emulsions at harsh reservoir conditions[17-19]. It was found that the hydrophilic CO_2 philic balance (particle wetting) of the solid particles to have a significant effect on the emulsion type and stability. Depending on the degree of the hydrophilicity, either CO_2 in a water emulsion, or water in a CO_2 emulsion is going to be formed. This behavior is understood through the concept of contact angles and the resulting energies of attachment for the different particles at the CO_2 water interface[19, 22].

This work improves our understanding of the effect of different parameters on the strength of emulsions. The main objective of this work is to investigate the effect of: emulsion quality, shear rates, salinity, pressure, nanoparticle concentration and nanoparticle size on the strength of the emulsion.

Materials

Chemicals

Three different types of silica nanoparticles were used in this study: silica 1, silica 2, and silica 3. Coated fumed silica (silica 1) with two different sizes (H-15 and H-30) were received from Wacker Chemie AG. These fumed silica are partially modified with methyl silyl. These materials were received as powder. Also, silica nanoparticles modified with an appropriate chemical (silica 2) was purchased from NYACOL Nano Technologies Inc. It was received as dispersed particles in deionized water with a total solid concentration of 30.5 wt%. The average particle size of these particles was measured using dynamic light scattering and found to be 30 nm +/- 1. Moreover, a silica coated with PEG (silica 3) was received from a local vendor with a concentration of 5 g in 125 ml and the average size of the particles is 10 nm.

Brine

Deionized water, ASTM type II, obtained from LabChem was used to prepare all solutions. Brine was prepared using deionized water and sodium chloride (NaCl, 99% Cole-Parmer).

Fig. 1 *A schematic of the viscosity measurement system.*

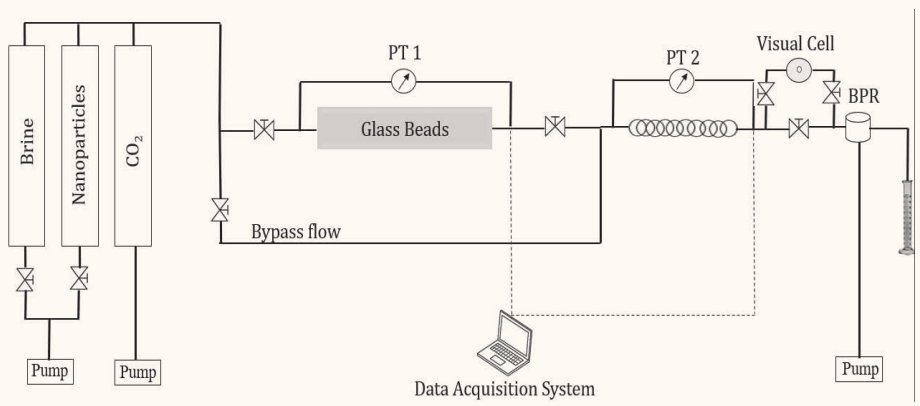

Fig. 2 *The effect of quality on the viscosity measurement of silica 1 at 1,365 s^{-1} and 1,820 s^{-1}.*

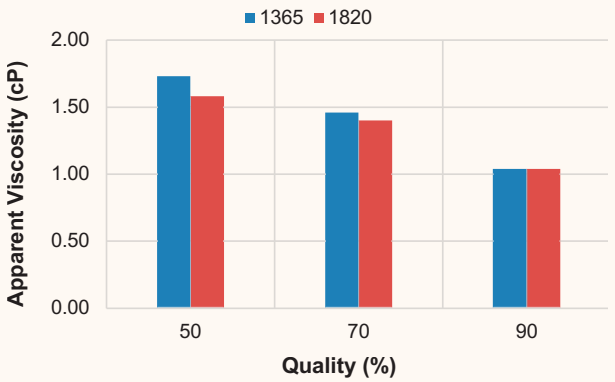

Fig. 3 *The effect of quality on the viscosity measurement for silica 2 at 3 wt% and 8 wt% salinity.*

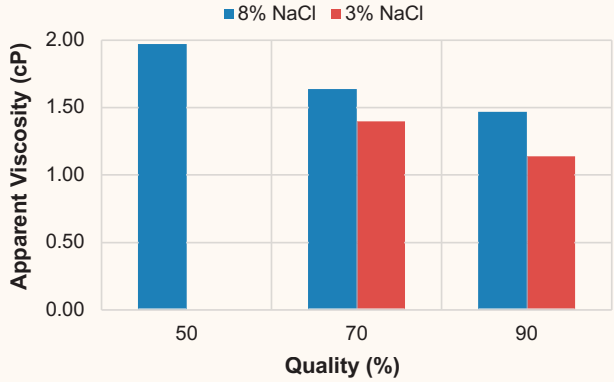

Gas

An industrial grade CO_2 was used to generate foams/emulsions. It was used in gaseous form (800 psi, 50 °C), and supercritical phases (1,800 psi and 2,500 psi, and 50 °C).

Methodology

The efficiency of each nanoparticle to generate and stabilize emulsion was evaluated by measuring the emulsion apparent viscosity at various conditions: emulsion quality (gas volume/the total injected volume), shear rates, salinity, pressure, nanoparticle concentration, and size. The experimental parameters and conditions used to conduct this study are summarized in Table 1. Figure 1 is a schematic of the setup used for conducting viscosity measurements. It consists mainly of an injection system, porous media, a visualization system, a capillary tube, and a production system. The purpose of using porous media — glass beads — is to act as a foam/emulsion generator. To measure emulsion viscosity, the system was first fully saturated with brine. The experimental pressure and temperature were then set. After that, one pore volume of tested solution was injected into the system, followed by a co-injection of CO_2 and nanoparticle solution at different conditions.

The emulsion was generated by a co-injection of gas and liquid that contains the nanoparticles, and the pressure drop across the capillary tube was then measured. The fluid's apparent viscosity is calculated using the Hagen-Poiseuille equation:

$$\mu_{apparent} = \frac{\pi \Delta P R^4}{8 L Q} \quad (1)$$

where R is the radius of the capillary tube (m), ΔP is the pressure drop across the capillary tube (Pa), L is the length of the capillary tube (m), and Q is the total injection flow rate (m^3/s).

Fig. 4 *The effect of salinity on the viscosity measurement for silica 1 at 1,365 s^{-1} and 1,820 s^{-1}.*

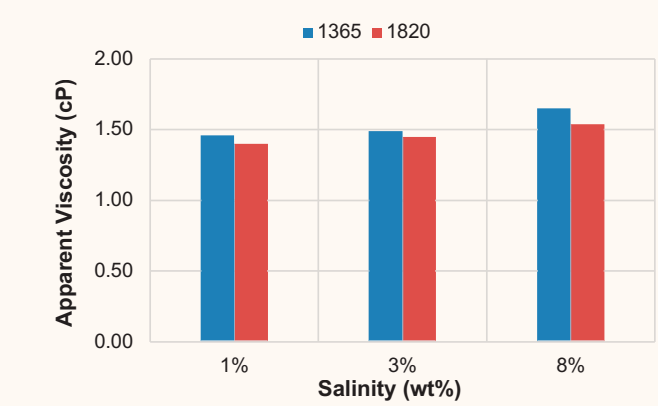

Fig. 5 *The effect of salinity on the viscosity measurement for silica 2 at 70% and 90% quality.*

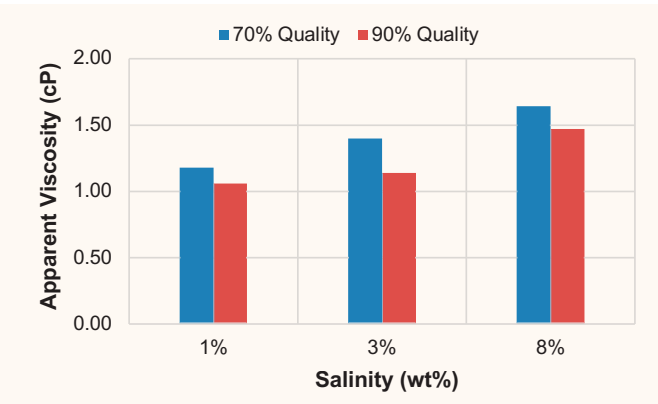

Fig. 6 *The effect of salinity on the viscosity measurement for silica 3 at 1,365 s^{-1} and 1,820 s^{-1}.*

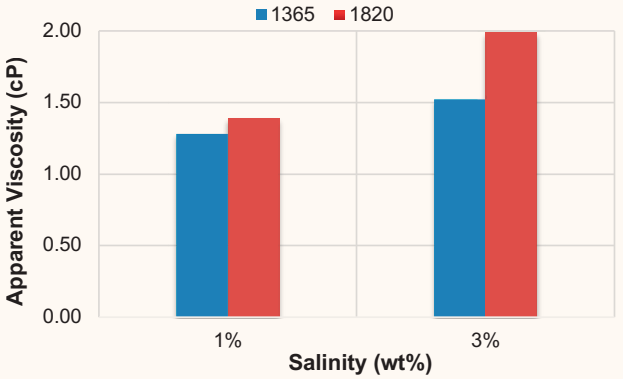

Fig. 7 *The effect of shear rate on the emulsion viscosity measurement for silica 1 at 3 wt% and 8 wt% salinity.*

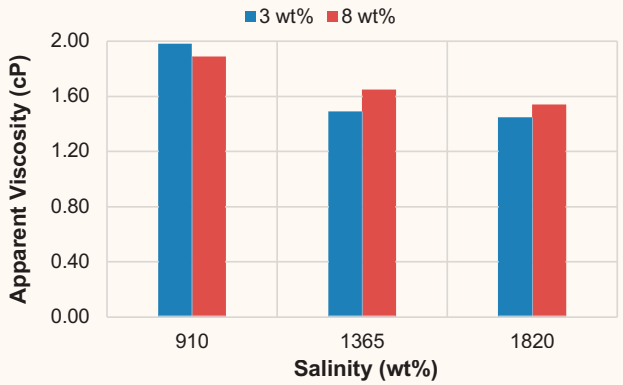

Fig. 8 *The effect of the nanoparticle concentration on the emulsion viscosity measurement for silica 3 at 1 wt% and 1.5 wt%.*

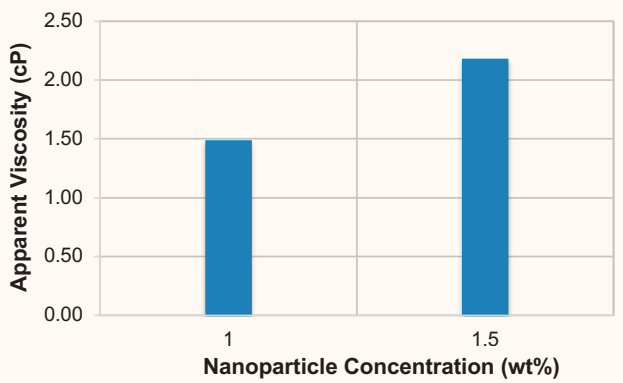

The ratio of the apparent viscosity of the generated emulsion to a baseline viscosity ($\mu_{baseline}$), and CO_2 viscosity at experimental conditions, can be used to estimate the gas flow resistance factor (RF).

$$RF = \frac{\mu_{apparent}}{\mu_{baseline}} \quad (2)$$

The Hagen-Poiseuille equation assumes a laminar flow regimen so it is necessary to ensure that the flow regimen of the generated emulsion fulfills this condition. Calculating the Reynolds number (Re) determines the type of flow regimen as *Re* less than 2,300 represents laminar flow.

Results and Discussion

The results of each material will be presented and discussed for each parameter at the conditions previously shown in Table 1. For silica 1, even though this material has been reported previously in the literature as a CO_2 water emulsion stabilizer, this study examines the effect of several parameters on the strength of generated emulsions and compares the results of this material with other tested materials, silica 2 and silica 3.

Effect of Quality

For silica 1 and silica 2, the results showed that quality is a critical parameter on emulsion generation and rheological properties. Emulsion viscosity increases as quality decreases, with the strongest emulsion reported at 50% quality. Figure 2 shows the effect of quality for silica 1 at two different shear rates, and Fig. 3 depicts the effect of quality for silica 2 at two different salinities. The lowest quality, 50%, had a high volume of liquid containing nanoparticles compared to the other tested qualities. Consequently, the probability that a large number of particles will be adsorbed at the CO_2 water interface is very high. As a result, the emulsion generation process is enhanced.

Effect of Salinity

The effect of salinity on the ability of silica 1, silica 2, and silica 3 to generate and stabilize CO_2 water emulsion at high-pressure and temperature was assessed at three salinities: 10,000 ppm, 30,000 ppm, and 80,000 ppm of NaCl, corresponding to 1 wt%, 3 wt%, and 8 wt%, respectively. For silica 3, the effect of salinity was evaluated at 1 wt% and 3 wt% of NaCl. The results, Fig. 4, indicates that salinity has no significant effect on the emulsion viscosity for silica 1. Almost the same viscosity values were reported. The test was conducted at two different shear rates to confirm this conclusion.

Consequently, the salinity showed a significant impact on emulsion viscosity for silica 2 and silica 3. As the salinity increases, the emulsion becomes more viscous. An increase in salinity

makes the particles less hydrophilic, thereby increasing the affinity of the particles to be adsorbed by CO_2 at the interface, and therefore, enhancing CO_2 brine emulsion generation and stability. Figures 5 and 6 depict the effect of salinity on the emulsion apparent viscosity for silica 2 and silica 3, respectively, at different test conditions.

Effect of Shear Rate

The impact of the shear rate on the emulsion generation and stability was evaluated by measuring emulsion viscosity at different shear rates: silica 1 (910 s^{-1}, 1,365 s^{-1}, and 1,820 s^{-1}), silica 2 (1,365 s^{-1}, 2,090 s^{-1}, and 2,730 s^{-1}), and silica 3 (1,365 s^{-1} and 1,820 s^{-1}).

The results showed a proportional relationship between the shear rates and emulsion viscosity for silica 3. This means the emulsions generated exhibit shear thickening behavior since their viscosity values increase as shear rates increase. Figure 6 depicts the viscosity values for silica 3 at 1,365 s^{-1} and 1,820 s^{-1} shear rates, and at 1 wt% and 3 wt% salinity.

For silica 1, the shear rate had an inverse relationship with emulsion viscosity. This behavior was most noticeable for the change of shear rates from 910 s^{-1} to 1,365 s^{-1}. The change of shear rates from 1,365 s^{-1} to 1,820 s^{-1} showed no significant impact on emulsion viscosity, Fig. 7. In general, emulsions are classified as non-Newtonian fluids whose viscosity is shear rate dependent. Based on the shear rates' behavior, emulsions can have a shear thickening or a shear thinning behavior. The produced emulsions here exhibit shear thinning behavior since their viscosity values decrease as shear rates increase.

For silica 2 — at different conditions — the results showed no significant influence of shear rates on the emulsion's stability and viscosity.

Effect of Nanoparticle Concentration

The impact of nanoparticle concentration on the emulsion viscosity was evaluated for silica 3 at two concentrations: 1 wt% and 1.5 wt%. The reported results showed that the emulsion viscosity increases with nanoparticle concentration. Figure 8 presents the emulsion viscosity calculated at 1 wt% and 1.5 wt% of the nanoparticles. This result was expected since the addition of more particles in solutions increases the number of particles being adsorbed by the CO_2 and water at the interface, thereby improving the emulsion generation process.

Effect of Nanoparticle Size

Two sizes of nanoparticles were selected to evaluate the effect of nanoparticle size of silica 1 on the emulsion's stability and viscosity. Two particles, H15 and H30, with 120 m^2/g and 250 m^2/g, respectively, were used in this study.

Fig. 9 *The effect of the nanoparticle's size on the emulsion viscosity measurement for silica 1 at different shear rates.*

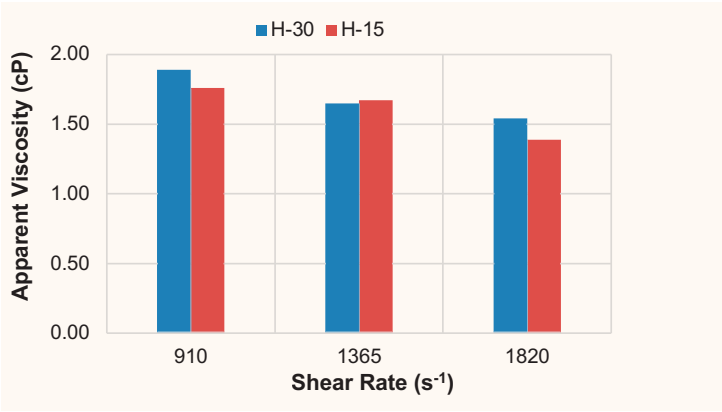

Fig. 10 *The effect of experimental pressure on the emulsion viscosity measurement for silica 2 at 70% and 90% quality.*

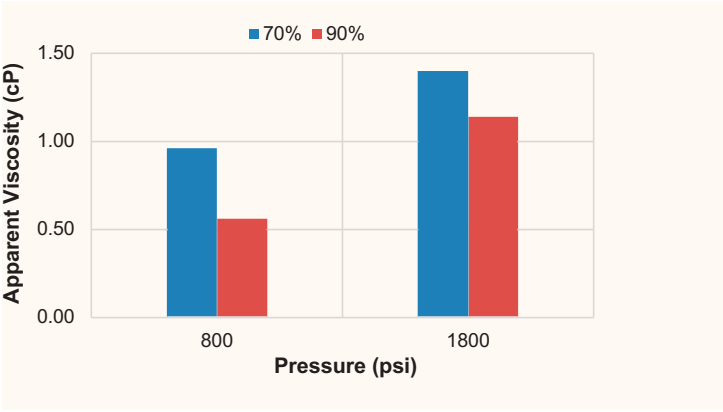

Fig. 11 *The effect of experimental pressure on the emulsion viscosity measurement for silica 3 at a shear rate of 1,365 s^{-1} and 1,820 s^{-1}.*

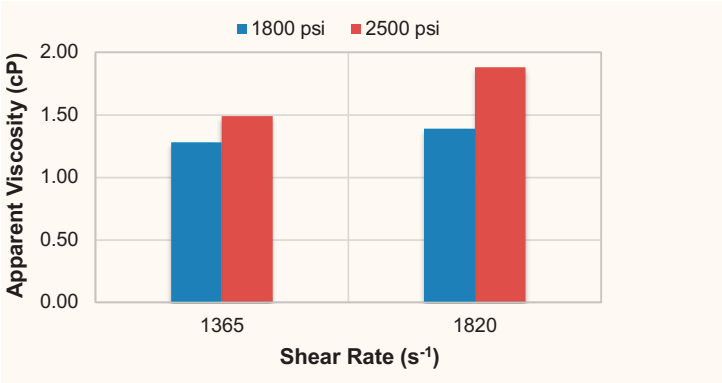

The results showed that the size has no influence on emulsion viscosity. The change of the nanoparticle's size and at different experimental conditions, Fig. 9, has produced almost the same

Table 2 *The overall results summary of all tests conducted.*

Test #	Material	Pressure (psi)	Nanoparticle Concentration (wt%)	Salinity (wt%)	Quality (%)	Shear Rate (s^{-1})	Re	μ (emulsion) (cP)	RF
1	H-30	1,800	1	1	50	1,365	25	1.73	43
2	H-30	1,800	1	1	50	1,820	36	1.58	40
3	H-30	1,800	1	1	70	1,365	26	1.46	37
4	H-30	1,800	1	1	70	1,820	36	1.4	35
5	H-30	1,800	1	1	90	1,365	31	1.04	26
6	H-30	1,800	1	1	90	1,820	42	1.04	26
7	H-30	1,800	1	3	70	910	13	1.98	50
8	H-30	1,800	1	3	70	1,365	25	1.49	37
9	H-30	1,800	1	3	70	1,820	34	1.45	36
10	H-30	1,800	1	8	70	910	13	1.89	47
11	H-30	1,800	1	8	70	1,365	23	1.65	41
12	H-30	1,800	1	8	70	1,820	32	1.54	39
13	H-15	1,800	1	8	70	910	14	1.76	44
14	H-15	1,800	1	8	70	1,365	22	1.67	42
15	H-15	1,800	1	8	70	1,820	36	1.39	35
16	Silica 2	1,800	1	8	50	2,090	33	1.97	47
17	Silica 2	1,800	1	1	70	2,090	49	1.18	28
18	Silica 2	1,800	1	3	70	2,090	41	1.4	33
19	Silica 2	1,800	1	8	70	2,090	35	1.64	39
20	Silica 2	1,800	1	1	90	2,090	47	1.06	25
21	Silica 2	1,800	1	3	90	2,090	44	1.14	27
22	Silica 2	1,800	1	8	90	2,090	34	1.47	35
23	Silica 2	800	1	3	70	2,090	34	0.96	53
24	Silica 2	800	1	3	90	2,090	31	0.56	31
25	Silica 3	1,800	1	1	90	1,365	25	1.28	31
26	Silica 3	1,800	1	1	90	1,820	31	1.39	34
27	Silica 3	1,800	1	3	90	1,365	21	1.52	37
28	Silica 3	1,800	1	3	90	1,820	22	1.99	49
29	Silica 3	2,500	1	1	90	1,365	29	1.49	24
30	Silica 3	2,500	1	1	90	1,820	30	1.88	30
31	Silica 3	2,500	1.5	1	90	1,365	19	2.18	35

value of viscosity. This finding is similar to that reported by Al Otaibi et al. (2013)[18].

Effect of Pressure

The role of pressure on the emulsion stability and viscosity was evaluated by measuring the viscosity at different pressures: silica 2 (800 psi and 1,800 psi), and silica 3 (1,800 psi and 2,500 psi). At 800 psi, CO_2 is at gaseous phase, whereas at 1,800 psi and 2,500 psi, it is at the supercritical phase. The results showed that as the pressure increases, the emulsion viscosity increases, too. This is attributed to the small difference in density, between the brine and CO_2, at higher pressure compared to that at lower pressure. This should enhance the emulsion generation process, creating an emulsion with a higher viscosity. Figures 10 and 11 depict the effect of experimental pressure on the emulsion viscosity for silica 2 and silica 3, respectively, at different conditions.

The results of all tests conducted at different conditions are summarized in Table 2. This table presents all experimental conditions, measured viscosity, Reynolds number, and flow resistance factor at reservoir conditions.

Conclusions

Silica nanoparticles with three different surface coatings were studied to investigate the effect of: emulsion quality, shear rates, salinity, pressure, nanoparticle concentration and nanoparticle size on the viscosity of emulsion. Based on these tests:

- All three surface modified nanoparticles were able to stabilize the gas-liquid emulsion and generate viscous emulsions compared to CO_2 at a high-pressure and temperature.
- All three tested silica were successful in increasing the CO_2 viscosity 24-53 fold.
- The results showed that as the quality increased, the emulsion viscosity decreased.
- In most scenarios, salinity was found to have a significant impact on the emulsion's strength. As the salinity increased, the emulsion viscosity did also.
- The concentration of nanoparticles showed analogous behavior, with the nanoparticle's concentration and viscosity being directly proportional.
- The shear rate was found to be a crucial variable for emulsion stability and viscosity.
- The nanoparticle's size provided no significance on emulsion stability and viscosity.
- More viscous emulsions could be achieved with increased pressure.

Acknowledgments

The authors would like to thank the management of Saudi Aramco, King Saud University, and Texas A&M University for their support and permission to publish this article.

This article was previously presented at the SPE Kingdom of Saudi Arabia Annual Technical Symposium and Exhibition, Dammam, Saudi Arabia, April 23-26, 2018.

References

1. Figdore, P.E.: "Adsorption of Surfactants on Kaolinite: NaCl vs. $CaCl_2$ Salt Effects," *Journal of Colloid and Interface Science*, Vol. 87, Issue 2, June 1982, pp. 500-517.
2. Al-Hashim, H.S., Celik, M.S., Oskay, M.M. and Al-Yousef, H.Y.: "Adsorption and Precipitation Behavior of Petroleum Sulfonates from Saudi Arabian Limestone," *Journal of Petroleum Science and Engineering*, Vol. 1, Issue 4, October 1988, pp. 335-344.
3. Mannhardt, K., Schramm, L.L. and Novosad, J.J.: "Effect of Rock Type and Brine Composition on Adsorption of Two Foam-Forming Surfactants," *SPE Advanced Technology Series*, Vol. 1, Issue 1, April 1993, pp. 212-218.
4. Grigg, R.B. and Bai, B.: "Sorption of Surfactant Used in CO_2 Flooding onto Five Minerals and Three Porous Media," SPE paper 93100, presented at the SPE International Symposium on Oil Field Chemistry, The Woodlands, Texas, February 2-4, 2005.
5. AlYousef, Z.A., Almobarky, M.A. and Schechter, D.S.: "Enhancing the Stability of Foam by the Use of Nanoparticles," *Energy & Fuels*, Vol. 31, Issue 10, August 2017, pp. 10620-10627.
6. AlYousef, Z.A., Almobarky, M.A. and Schechter, D.S.: "Surfactant and a Mixture of Surfactant and Nanoparticles Stabilized CO_2/Brine Foam for Gas Mobility Control and Enhanced Oil Recovery," CMTC paper 486622, presented at the Carbon Management Technology Conference, Houston, Texas, July 17-20, 2017.
7. Almobarky, M.A., AlYousef, Z.A. and Schechter, D.S.: "A Comparison between Two Anionic Surfactants for Mobility Control of Supercritical CO_2 in Foam Assisted Miscible EOR," CMTC paper 486486, presented at the Carbon Management Technology Conference, Houston, Texas, July 17-20, 2017.
8. Bartscherer, K.A., Minier, M. and Renon, H.: "Microemulsions in Compressible Fluids — A Review," *Fluid Phase Equilibria*, Vol. 107, Issue 1, May 1995, pp. 93-150.
9. Eastoe, J., Dupont, A., Paul, A., Steytler, D.C., et al.: "Design and Performance of Surfactants for Carbon Dioxide," *ACS Symposium Series*, Vol. 860, Chapter 19, August 2003, pp. 285-308.
10. Johnston, K.P. and da Rocha, S.R.P.: "Colloids in Supercritical Fluids over the Last 20 Years and Future Directions," *The Journal of Supercritical Fluids*, Vol. 47, Issue 3, January 2009, pp. 523-530.
11. Zhang, S., Sun, D., Dong, X., Li, C., et al.: "Aqueous Foams Stabilized with Particles and Nonionic Surfactants," *Colloids and Surfaces A: Physicochemical and Engineering Aspects*, Vol. 324, Issues 1-3, July 2008, pp. 1-8.
12. Cui, Z-G., Cui, Y-Z., Cui, C-F., Chen, Z., et al.: "Aqueous Foams Stabilized by in Situ Surface Activation of $CaCO_3$ Nanoparticles via Adsorption of Anionic Surfactant," *Langmuir*, Vol. 26, Issue 15, July 2010, pp. 12567-12574.
13. Worthen, A.J., Bryant, S.L., Huh, C. and Johnson, K.P.: "Carbon Dioxide-in-Water Foams Stabilized with Nanoparticles and Surfactant Acting in Synergy," *AIChE Journal*, Vol. 59, Issue 9, September 2013, pp. 3490-3501.
14. Carn, F., Colin, A., Pitois, O., Vignes-Adler, M., et al.: "Foam Drainage in the Presence of Nanoparticle-Surfactant Mixtures," *Langmuir*, Vol. 25, Issue 14, June 2009, pp. 7847-7856.
15. Xue, Z., Worthen, A., Qajar, A., Robert, I., et al.: "Viscosity

and Stability of Ultra-High Internal Phase CO_2-in-Water Foams Stabilized with Surfactants and Nanoparticles with or without Polyelectrolytes," *Journal of Colloid and Interface Science*, Vol. 461, January 2016, pp. 383-395.

16. AlYousef, Z.A., Almobarky, M.A. and Schechter, D.S.: "The Effect of Nanoparticles Aggregation on Surfactant Foam Stability," *Journal of Colloid and Interface Science*, Vol. 511, February 2018, pp. 365-373.
17. Espinoza, D.A., Caldelas, F.M., Johnston, K.P., Bryant, S.L., et al.: "Nanoparticle-Stabilized Supercritical CO_2 Foams for Potential Mobility Control Applications," SPE paper 129925, presented at the SPE Improved Oil Recovery Symposium, Tulsa, Oklahoma, April 24-28, 2010.
18. Al Otaibi, F.M., Kokal, S.L., Chang, Y., AlQahtani, J.F., et al.: "Gelled Emulsion of CO_2-Water-Nanoparticles," SPE paper 166072, presented at the SPE Annual Technical Conference and Exhibition, New Orleans, Louisiana, September 30-October 2, 2013.
19. Worthen, A.J., Bagaria, H.G., Chen, Y., Bryant, S.L., et al.: "Nanoparticle-Stabilized Carbon Dioxide-in-Water Foams with Fine Texture," *Journal of Colloid and Interface Science*, Vol. 391, February 2013, pp. 142-151.
20. Li, S., Hendraningrat, L. and Torsaeter, O.: "Improved Oil Recovery by Hydrophilic Silica Nanoparticles Suspension: 2-Phase Flow Experimental Studies," IPTC paper 16707, presented at the International Petroleum Technology Conference, Beijing, China, March 26-28, 2013.
21. Dickson, J.L., Binks, B.P. and Johnston, K.P.: "Stabilization of Carbon Dioxide-in-Water Emulsions with Silica Nanoparticles," *Langmuir*, Vol. 20, Issue 19, August 2004, pp. 7976-7983.
22. Binks, B.P. and Lumsdon, S.O.: "Influence of Particle Wettability on the Type and Stability of Surfactant-Free Emulsions," *Langmuir*, Vol. 16, Issue 23, June 2000, pp. 8622-8631.

About the Authors

Dr. Zuhair A. Al-Yousif

Ph.D. in Petroleum Engineering, Texas A&M University

Dr. Zuhair A. Al-Yousif joined Saudi Aramco as a Petroleum Engineer in August 2008. Since that time, he has worked in a variety of departments within Saudi Aramco. The emphasis of Zuhair's work has been on enhanced oil recovery (EOR) projects. He is currently leading the gravity override mitigation and the gas mobility control research, and contributing to high-impact projects within the area of carbon dioxide EOR, which has received international recognition.

Zuhair is a member of the Society of Petroleum Engineers (SPE). He has authored and coauthored numerous technical papers, including peer-reviewed articles, and filed several patent applications.

In 2008, Zuhair received his B.S. degree in Petroleum Engineering from King Fahd University of Petroleum and Minerals (KFUPM), Dhahran, Saudi Arabia. He then received his M.S. degree in 2012 and his Ph.D. degree in 2017, both in Petroleum Engineering from Texas A&M University, College Station, TX.

Dr. Mohammed Al-Mobarky

Ph.D. in Petroleum Engineering, Texas A&M University

Dr. Mohammed Al-Mobarky has been working in the Petroleum and Natural Gas Engineering Department in King Saud University (KSU) since October 2004. He has taught many courses in petroleum engineering and contributed in a variety of research projects.

Currently, Mohammed is an Assistant Professor in the department. His work includes teaching, contributing in projects related to enhanced oil recovery (EOR), particularly carbon dioxide EOR and mobility control, and leading the unit of safety and risk management in the College of Engineering. Mohammed's research interests also include visualizing fluid flow in porous media using micromodels and produced water management.

He is a member of the Society of Petroleum Engineers (SPE) and has authored and coauthored numerous technical papers, including peer-reviewed articles.

Mohammed received his B.S. degree in 2003 and M.S. degree in 2007, both from King Saud University, Riyadh, Saudi Arabia, and in 2017, he received his Ph.D. degree from Texas A&M University, College Station, TX, all in Petroleum Engineering.

Dr. David S. Schechter

Ph.D. in Physical Chemistry, Bristol University

Dr. David S. Schechter is Professor of Petroleum Engineering at Texas A&M University. His area of interest includes reservoir characterization, and modeling and simulation in naturally fractured reservoirs. David also manages a research program in enhanced oil recovery (EOR), both with aqueous phase chemical additives in completion fluids for wettability alteration and EOR via gas injection, including hybrid use of both aqueous phase chemicals and gas injection.

He specializes in EOR with carbon dioxide (CO_2) and is Director of the Chaparral-Fischer CO_2 EOR Laboratory and Manager of the Chevron Imaging Laboratory at Texas A&M. David has 30 years of direct experience in EOR with surface active agents and gas/CO_2, including everything from basic laboratory studies to the development of full field projects.

Recently, he has been specializing in EOR by surfactants in a variety of important domestic basins, such as the Bakken, Niobrara, Wolfcamp, Eagle Ford, and the SCOOPS-STACK in Oklahoma. The work has focused on surfactant assisted spontaneous imbibition (SASI), gas huff n' puff, and hybrid techniques utilizing soaks with alternating miscible gas and SASI.

David has published over 200 manuscripts in various journals and conferences.

In 1984, he received his B.S. degree in Chemical Engineering from the University of Texas at Austin, Austin, TX, and in 1988, he received his Ph.D. degree in Physical Chemistry from Bristol University, Bristol, U.K. David then taught and performed research at Stanford University (1989-1993), and New Mexico Tech (1993-2000), prior to joining Texas A&M.

Engineered Vesicles for the Controlled Release of Chemical Additives and Application for Enhanced Oil Well Cement Integrity

Dr. Elizabeth Q. Contreras, Kenneth Dejuan Johnson, Diana Rasner, and Carl J. Thaemlitz

Abstract /

Encapsulation-based systems are of interest in the oil and gas industry in applications such as chemical additive preservation, small molecule release, particle delivery, and self-sealing materials. Many methods are used to encapsulate relevant chemical additives for the controlled release of contents like polymeric vesicles, inorganic shells, and mesoporous materials. Here, a novel system for the controlled release of encapsulated cargo that utilizes engineered features of permeable polymeric shell walls is shown.

When placing cement, a multitude of additives in large quantities are needed to meet a variety of functional needs that are suitable for the many diverse wellbore conditions. Although, using large amounts of certain additives could have adverse effects, which can destabilize the slurry at surface conditions. Using vesicles, cement additives are delivered without requiring modification. In this way, the possibilities of formulations comprised of a number of vesicles with various encapsulants lends to significant advancements in cementing. Applications in cement design is demonstrated from measurements obtained using the consistometer as well as testing from oil field equipment.

Experimental results show that a basic cement slurry design responds to the release of an encapsulant by the measure of change in viscosity and thickening times at two different temperatures at 3,000 psi. For example, the thickening time of a slurry can be controlled with the delayed release of an accelerant, at ambient pressure. With an increase in temperature up to 100 °F and 300 °F, the encapsulated additive is squeezed at a higher diffusion rate, resulting in a faster thickening time. In all cases, the vesicles are observed to remain intact within the set cement and contribute significantly to the mechanical properties of the set cement. Vesicle dual performance stems from unique characteristics, such as an aqueous core, wall thickness and permeability, chemical composition, and mechanical integrity of the shell wall. Here, the shell walls are engineered with high molecular weight polymeric material that upon release of the encapsulated chemical additives, the emptied vesicles continue to impart beneficial mechanical properties to the set cement, such as compression strength.

Introduction

During the construction process of a well, cementing serves the purpose of providing a reliable infrastructure during production and for zonal isolation of the casing string from subterranean environments. The placement of cement downhole requires the complete control of a slurry formulation for adequate hydrostatic pressure and set time of the cement[1]. The hydrostatic pressure maintains formation fluids, such as gases and liquids, from permeating through the slurry to the surface. After the placement of cement, the cement is expected to harden at a set time into an impermeable cement sheath that isolates fluids from different formation zones for the lifetime of the well.

The hydration of cement yields an impervious structure that is strong but susceptible to thermomechanical stresses. The durability of cement is derived from various mechanical properties, such as compression strength and elasticity[2]. The isolation of these formation zones in constructing the well is key for the safe and efficient production of a well. Immense efforts toward cement sheath integrity helps to maintain the production of the hydrocarbons cost-efficient and safe. Numerous factors can cause cement to fail; from the inadequate placement of a cement slurry to the loss of cement sheath integrity.

One of those scenarios occurs during the construction of the well. The transition of cement from a slurry into a solid sheath can span over a significant length of time[3]. As cement begins to thicken, the hydrostatic pressure decreases below formation pressures. This can lead to fluids, such as gases to permeate through a gelled slurry, forming channels behind the casing[4]. Subsequently, the channels get cemented permanently, which is indicative of a bad cement job. The ideal scenario is to minimize or eliminate the transition time of the slurry where the cement sets instantaneously, for right-angle set cements.

Competent cement systems are designed to allow the placement of cement behind the casing and at a set time,

by using chemical additives. The function of these chemical additives is extensive and used to control cement properties, such as setting time, rheology, fluid loss, gas migration, density, and enhanced mechanical properties[5]. Challenges arise when a suitable selection of additives are promptly depleted or prematurely manifested before placing the cement behind the casing. Additives, such as accelerants, are used to accelerate the set time of the cement only after properly being placed downhole during the construction of a well.

To ensure cement quality, innovative polymers, based upon a family of polymers known as aromatic polyamides, or aramides, are used here as a single additive in cementing. The vesicular design of the polymer offers unique delivery system features, which provide chemical reagents when needed[6]. In this way, the polymer is designed to produce a vast array of encapsulants for controlling the release of additives downhole during cement operations. The application of using vesicles for the development of "right-angle set" cements is shown here. Thereafter, the spent vesicles remain embedded as an elastomer and the robustness of the shell imparts beneficial mechanical properties to the cement sheath.

Experimental

Figure 1 maps the process of using an emulsion template to form vesicles for the modified release of additives. Briefly, interfacial polymerization comprised of two immiscible solvents, a chloroform ($CHCl_3$) cyclohexane mix and water are stirred to form an emulsion. Droplets are captured by a semipermeable polymer shell[7]. The dispersed phase contains the accelerant calcium chloride ($CaCl_2$) to serve in the design of right angle set cements.

General Procedure for Polyamide Synthesis

Reagents 1,3,5-benzenetricarboxylic acid chloride (BTCAC), 1,3-phenylenediamine (diamine I), 1,6-diaminohexane (co-monomer II), sebacoyl chloride (co-monomer III), Span 85, cyclohexane, and $CHCl_3$, are used as received. To a 2L two-neck round bottom flask is added the organic phase consisting of cyclohexane/$CHCl_3$ (4:1, 750 mL) and Span 85 mixture (2% v/v), and stirred at 600 rpm with an overhead stirrer. An aqueous solution (200 mL), consisting of a diamine, such as 16.2 g of 1,3-phenylenediamine and calcium salt (Ca^{2+}), is added at once and the emulsion is stirred for 30 minutes.

In a separate flask, BTCAC (26.5 g) is dissolved in cyclohexane/$CHCl_3$ (200 mL) and the solution added at 1 mL/min to the stirring solution in the 2L two-neck flask, and allowed to stir for 24 hours. Various aramide polymers are made using diamine monomer and co-monomers to react with BTCAC — in the same way, a second composition of polymer uses an acid dichloride co-monomer with BTCAC to react with a diamine. The resulting polymer is left to settle and is filtered; and then further washed by stirring in a bicarbonate solution, and filtered again. The polymer is laid out to dry in a vacuum oven at 180 °F overnight, or until a constant weight is obtained. Clumps are broken up using a 35-mesh screen to form a free flowing powder. The percent yield is about 65%. The polyaramide vesicles are added as a single additive.

Cement Mixing and Curing Procedure

Cement samples are prepared using Class G cement. A cement slurry consists of six components: water, cement, dispersant, cement retarder, applied polymer at 3% by weight of cement (bwoc), and anti-foamer (1 mL added to mix water), Table 1. The polyaramide vesicles are added as a single additive.

The slurry is mixed at 4,000 rpm for 15 seconds and then increased to 12,000 rpm for 35 seconds. The cement slurry is then poured into an API cement consistometer for measurement of slurry thickening time, using Bearden units of consistency (Bc). After the slurry is brought to the fill line in the slurry cup, the cup is assembled with a paddle and capped, a thermocouple is inserted. Cement

Fig. 1 *Process of encapsulation using interfacial polymerization.*

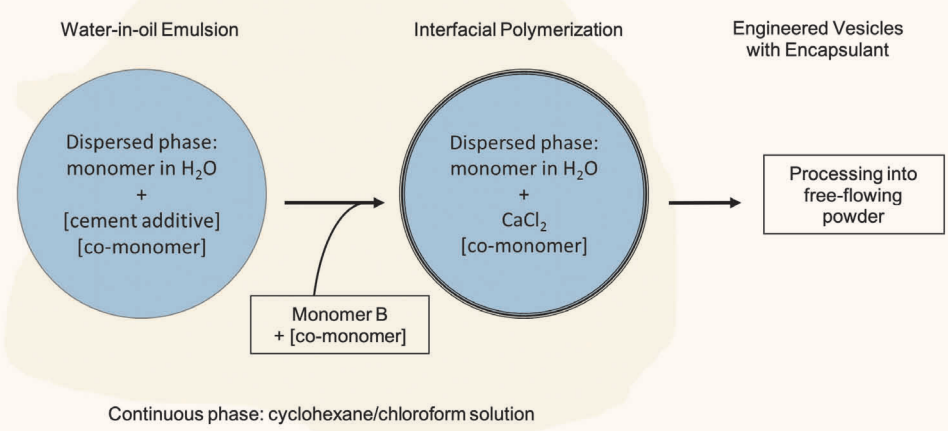

Table 1 *Summary of slurry design for cement samples.*

Neat Cement	Amount	Units
Class G Cement	100	% bwoc
Dispersant	0.8	% bwoc
Retarder	0.5	% bwoc
Polymer	3	% bwoc
Mix Water	43	% bwoc
Slurry Density	15.8	lb/gal
Volume	600	mL

viscosity is recorded up to 100 Bc at both 100 °F and 300 °F at 3,000 psi.

Results and Discussions

Smart Vesicles and Modified Release of Chemical Additives into Cement

Vesicles, aromatically cross-linked, are synthesized using two immiscible solvents, water and oil. Two aliphatic co-monomers with different functional groups (II, III) cause a change in shell permeability and release rate due to different chemical compositions. After synthesizing these aromatic polyamides, the resulting shapes of the polymers are uniquely vesicular in form, and hollow, which allows for the development of a chemical delivery system. With light microscopy, the vesicles are shown to be hollow, Fig. 2. After drying, the vesicles are suspended in water and allowed to swell. The dynamic motion of the shell can be easily observed. This characteristic provides a novel and efficient tool needed to develop the next generation of chemical additives in the oil and gas field. Overall, the flexibility in chemical design for these structurally sound technologies for unconventionals may lead to a plethora of smart cement formulations with control released additives.

Generally, cementing a well consists of pumping cement slurry from the surface down the casing so that it then returns to the surface in the backflow via the annulus between the casings and/or the formation. Because of the hydraulic pressure from the height of the cement column, the injected slurry is also capable of preventing gas migration; and when cement begins to set, it is also impermeable to gas. Subsequently, there is a critical transition time between these two phases, which last several hours, during which the slurry no longer behaves as a liquid with hydrostatic pressure, nor as an impermeable solid[4]. During this transition time, gas migration occurs, which can lead to pressure buildup and loss of zonal isolation. When the cement sets, the channels become permanent. These cement challenges are costly and dangerous to production and safety.

The solution to lengthy transition times are right angle set cements, which are characterized by a 90° set time as measured by a consistometer[3]. In one scenario, a slurry design using cement accelerant, calcium salt (Ca^{2+}), is encapsulated for delayed release into the slurry. Two systems for encapsulation using a different co-monomer are discussed further, based on performance in controlling cement properties. The first system uses gradient concentrations of co-monomer II (diamine hexane), while keeping the 1:1 molar equivalence of the carbonyl and amine for the interfacial polymerization of the membrane shell, Table 2. Diamine hexane is a known

Fig. 2 *Polyaramide vesicles: (Left) Photomicrograph of vesicles (red areas) in cement (gray material) at 20 minutes. Insert: Polyamide vesicle encapsulating polymeric material in the dispersed phase by interfacial polymerization. (Right) Representative particle size distribution of vesicles formed with an average diameter of 252 µm (Polymer 8).*

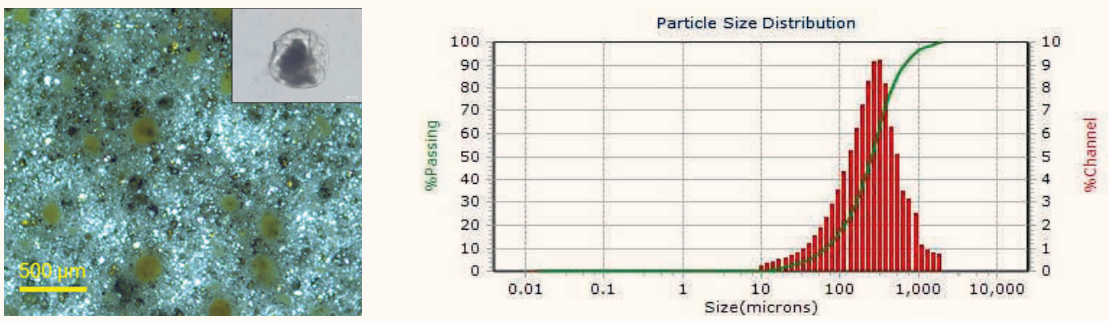

Table 2 *Cement slurry design and thickening times for samples in Fig. 3.*

Polymer Cement	Membrane Composition BTCAC + (diamine I: co-monomer II)	Acid/Amine	Encapsulated $CaCl_2$	Thickening Times at 70 Bc (hh:mm)
20	(4:1)	1:1	2% bwoc	03:50
40	(3:2)	1:1	2% bwoc	04:16
60	(2:3)	1:1	2% bwoc	04:46
80	(1:4)	1:1	2% bwoc	05:22
Vesicle only cement	(1:0)	1:1	None	04:57
Neat cement	None	None	None	14:58

Fig. 3 *Different set times of slurries at 100 °F and 3,000 psi.*

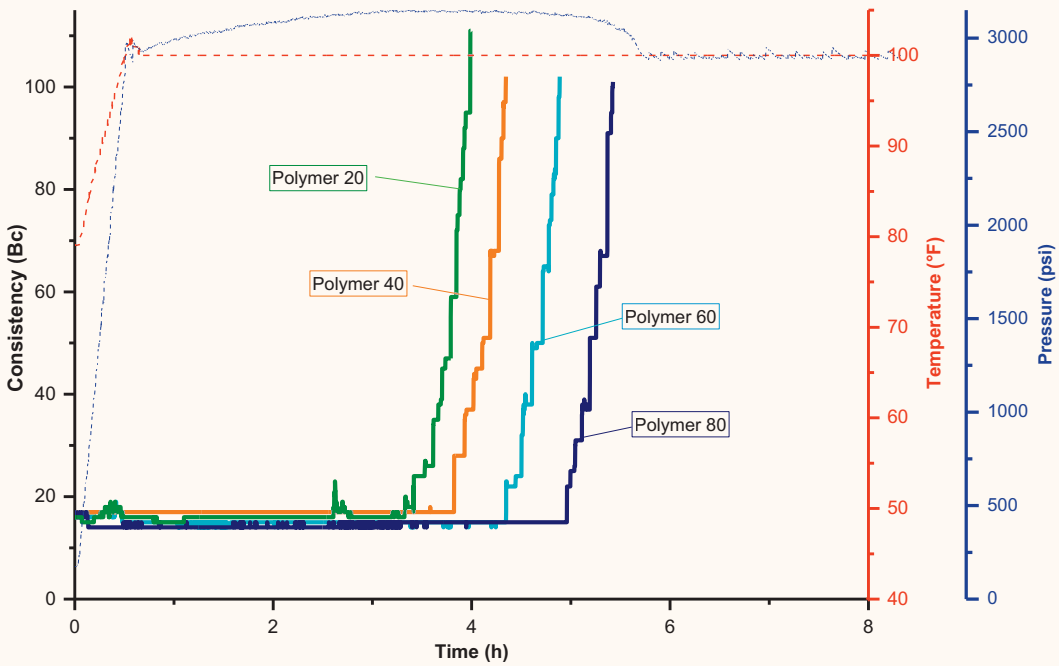

chelator of salts. Here, the addition of co-monomer II causes a significant change in cement properties as seen in the rheological measurements of cement slurries. On a consistometer, the rheological measure near 20 Bc is ideal for cement slurry pumpability. Figure 3 shows up to four different right-angle set times at 100 °F and 3,000 psi. This shows how these polymeric vesicles at 3% bwoc, when used for the delayed release of the accelerant, helped control the rheological property and the set time of cement.

The second delivery system was formulated and measured at two different temperatures using the same slurry design, Fig. 4. The initial consistency measurements were characteristically similar in these two experiments, but an increase in temperature from 100 °F to 300 °F caused the cement to set significantly faster. The data shows that changes in diacyl chloride (co-monomer III) concentrations in designing the vesicles can be used to control the permeability of the shell and the release rate of the encapsulant, Table 3[8]. Here, the addition of co-monomer III causes a decrease in Bc and differences in set times, which is indicative of the engineering design of the encapsulant and vesicles for cement slurries. At 300 °F, efforts toward the optimization of this delivery system

Fig. 4 *Different set times of slurries at (a) 100 °F, and (b) reaching 300 °F at 3,000 psi.*

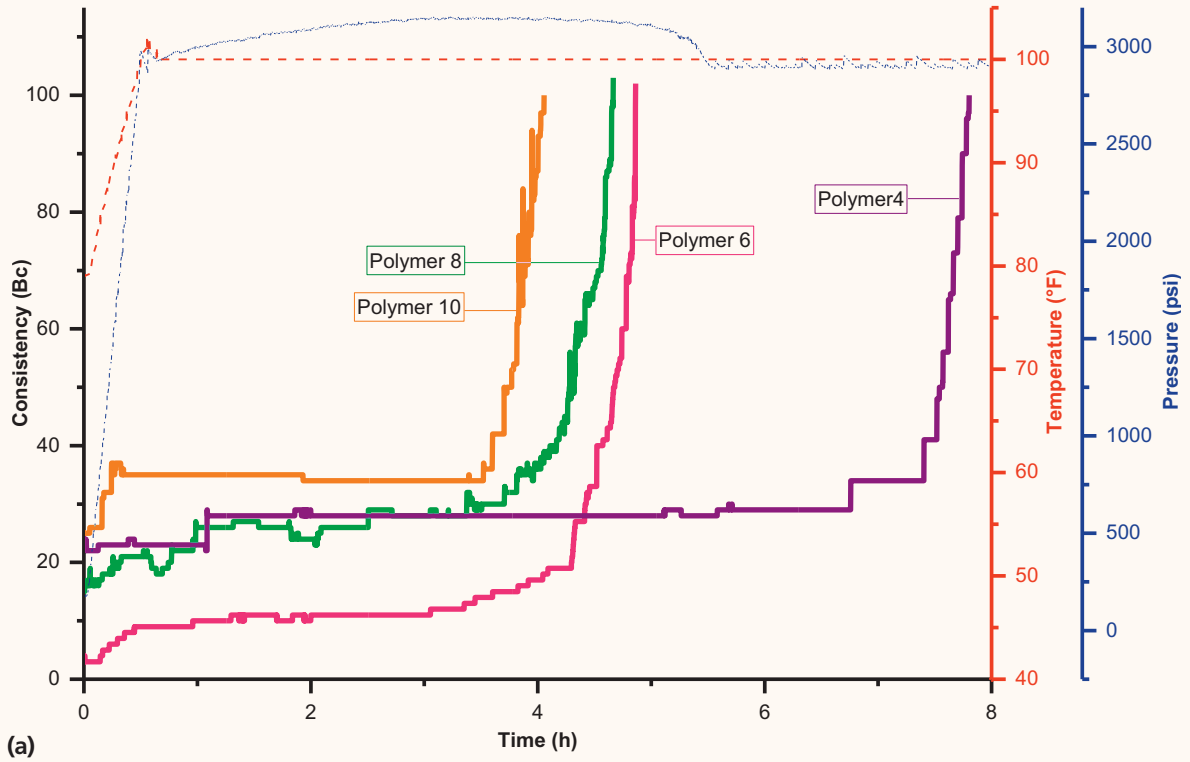

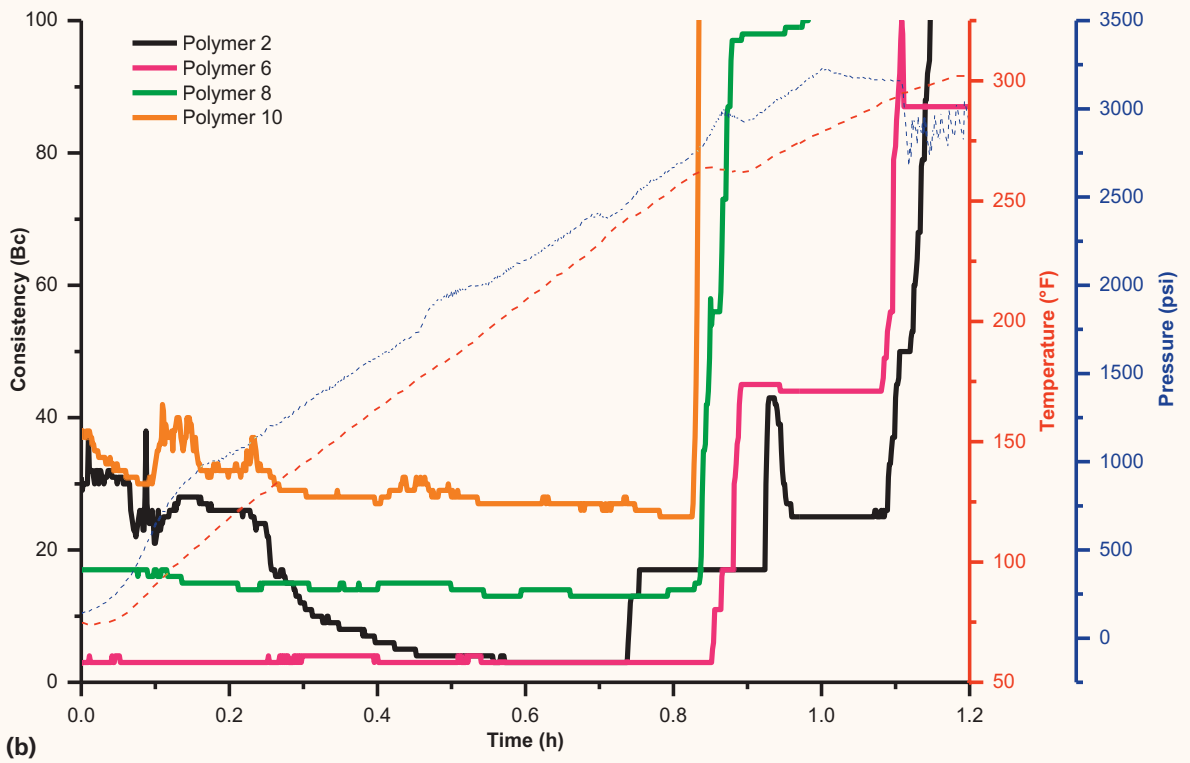

Table 3 *Cement slurry design and thickening times at 100 °F for samples in Fig. 4.*

Polymer Cement	Membrane Composition (BTCAC: co-monomer III) + diamine I	Encapsulated $CaCl_2$	Thickening Times at 70 Bc (hh:mm)
4	(3:2)	1% bwoc	07:39
6	(2:3)	2% bwoc	04:48
8	(1:4)	2% bwoc	04:31
10	(1:0)	2% bwoc	03:52

Table 4 *Cement slurry design and thickening times reaching 300 °F for samples in Fig. 4.*

Polymer Cement	Membrane Composition (BTCAC: co-monomer III) + diamine I	Encapsulated $CaCl_2$	Thickening Times at 70 Bc
(hh:mm:ss)			
2	(4:1)	2% bwoc	01:08:05
6	(2:3)	2% bwoc	01:05:20
8	(1:4)	2% bwoc	00:51:50
10	(1:0)	2% bwoc	00:50:00

Fig. 5 *SEM of broken vesicle 280 µm in external diameter, with 4 µm wall thickness. Insert TEM image.*

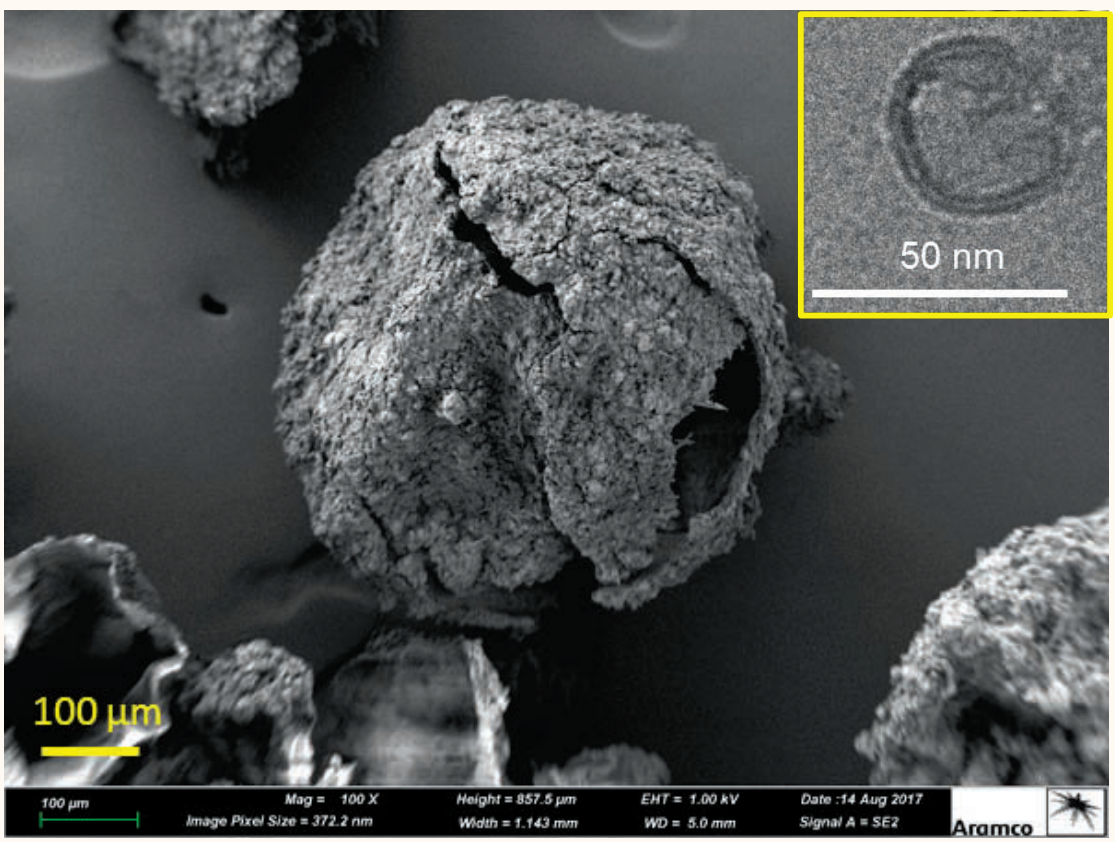

Table 5 *Unconfined CS of cements with embedded spent capsules.*

Polymer Cement	CS (psi)
40	4,724
60	3,641
80	5,090
Elasticrete cement	4,525
Neat cement	4,225

in Table 4 are ongoing to allow for the development of the next generation of additives in cementing.

Cement Mechanical Properties from Spent Vesicles

Polyaramide vesicles serve to deliver additives and reagents into the slurry when required. Once this task is complete, the spent vesicles remain intact and do not dissolve or degrade as is commonly found in commercial products, Fig. 5. Subsequently, once embedded in hard set cement, the polymer membrane remains intact. These spent capsules continue to characteristically enhance cement performance for long-term integrity[9]. Embedded in the set cement, the empty polymer shells continue to impart beneficial mechanical properties to the cement sheath during the lifetime of the oil well, Table 5. The upcycling of this technology after the encapsulant is spent makes this technology unique.

This technical solution serves dual functions for the controlled release of chemicals into the slurry and the enhancement of the lifespan of the well. This system exhibits a promising prospect for a variety of cement slurry applications.

Conclusions

Vesicle systems are particularly appealing for the delivery of beneficial agents, such as chemical additives and small molecules. The many components of a vesicle lends to the design of the chemical shell and hollow interior for the encapsulation of additives to control the properties of any fluidic or solid system, such as cement slurries and sheaths, respectively. In this report we showed how the design of a vesicle helped control cement properties, such as rheological, thickening time, setting time, and mechanical properties. The vesicles are versatile and a topic of interest, due to potential breakthrough applications in different fields of interest. In addition, the formation of capsules or vesicles in a cost-effective and time saving manner allows for the design of high temperature resistant chemical additives for more challenging environments.

Polymeric additives are an effective means to designing complex systems to deliver chemical reagents under challenging conditions and to impart favorable physical properties to the slurry and the set states of cement. From chemical delivery and their controlled release of chemical additives during placement of a slurry downhole, these vesicles prove useful in the preparation of cement slurry formulations.

Acknowledgments

The authors would like to thank the management of Saudi Aramco and Aramco Services Company for their support and permission to publish this article.

This article was presented at the SPE International Conference on Oil Field Chemistry, Galveston, Texas, April 8-9, 2019.

References

1. Reddy, B.R., Santra, A.K., McMechan, D.E., Gray, D.W., et al.: "Cement Mechanical Property Measurements under Wellbore Conditions," *SPE Drilling & Completion*, Vol. 22, Issue 1, March 2007, pp. 33-38.
2. Thiercelin, M.J., Dargaud, B., Baret, J.F. and Rodriquez, W.J.: "Cement Design Based on Cement Mechanical Response," *SPE Drilling & Completion*, Vol. 13, Issue 4, December 1998, pp. 266-273.
3. Sabins, F.L., Tinsley, J.M. and Sutton, D.L.: "Transition Time of Cement Slurries between the Fluid and Set States," *SPE Journal*, Vol. 22, Issue 6, December 1982, pp. 875-882.
4. Bonett, A. and Pafitis, D.: "Getting to the Root of Gas Migration," *Oilfield Review*, Vol. 8, Issue 1, March 1996, pp. 36-49.
5. Contreras, E.Q., Reddy, B.R., Maimani, F., Alhassanalsayed, H., et al.: "Intelligent Cement Slurry Design Based on Molecular Level Understanding," paper AADE-16-FTCE-11, presented at the American Association of Drilling Engineers Fluids Technical Conference and Exhibition, Houston, Texas, April 12-13, 2016.
6. Song, Y., Fan, J-B. and Wang, S.: "Recent Progress in Interfacial Polymerization," *Materials Chemistry Frontiers*, Vol. 1, Issue 6, January 2017, pp. 1028-1040.
7. Quevedo, E., Steinbacher, J. and McQuade, D.T.: "Interfacial Polymerization within a Simplified Microfluidic Device: Capturing Capsules," *Journal of the American Chemical Society*, Vol. 127, Issue 30, August 2005, pp. 10498-10499.
8. Mathiowitz, E. and Cohen, M.D.: "Polyamide Microcapsules for Controlled Release. II. Release Characteristics of the Microcapsules," *Journal of Membrane Science*, Vol. 40, Issue 1, January 1989, pp. 27-41.
9. Contreras, E.Q., Rasner, D., Martinez, R.F. and Thaemlitz, C.J.: "Novel Aromatic Polyamides and its Application in Enhancing the Integrity of Oil Well Cement Sheath," SPE paper 194118, presented at the SPE/IADC International Drilling Conference and Exhibition, The Hague, the Netherlands, March 5-7, 2019.

About the Authors

Dr. Elizabeth Q. Contreras

Ph.D. in Chemistry,
Rice University

Dr. Elizabeth Q. Contreras joined the Drilling Technology Team at the Aramco Research Center-Houston as a Research Scientist in 2015. She works with upstream chemistry research to develop cementing and drilling technologies.

Elizabeth received her M.S. degree in Chemistry and Chemical Biology from Cornell University, Ithaca, NY. In 2012, she received a Ph.D. degree in Chemistry from Rice University, Houston, TX, where her research topics focused on polymer synthesis, and advanced materials development of flow through devices, and on the inorganic synthesis and physicochemical characterization of engineered nanoparticles and their impact on the environment.

Kenneth Dejuan Johnson

B.S. in Biology,
University of Arkansas at Pine Bluff

Kenneth Dejuan Johnson currently works as a Laboratory Technician Specialist at Aramco Services Company, Houston, TX. Previously, he worked for BJ Services and Baker Hughes as a Research Design and Development Scientist III specializing in cementing. One of Kenneth's key areas of focus was enhancing pay zone recovery by optimizing the transition time of cement. Prior to these positions, he worked for Core Laboratory as a Lead Core Analyst.

Kenneth's research includes formulating cement designs for better bonding between the casing and the wellbore, pore pressure depletion, and wellbore stability. He has worked in the oil and gas industry for over 18 years.

Kenneth received his B.S. degree in Biology from the University of Arkansas at Pine Bluff, Pine Bluff, AR.

Diana Rasner

B.S. in Chemistry,
University of Washington

Diana Rasner is a Laboratory Technician supporting the Drilling Technology Team at the Aramco Research Center-Houston, TX. She spent three years working for Solvay Chemicals before transitioning into an R&D role in the oil and gas industry. Diana's focus include oil well cement characterization, synthesis, and analytical support.

She received her B.S. degree in Chemistry (ACS Certified) from the University of Washington, Seattle, WA.

Carl J. Thaemlitz

M.S. in Chemistry,
Texas State University

Carl J. Thaemlitz founded and leads the Research and Development Team for drilling technology at the Aramco Services Company: Research Center-Houston, TX. Previously, he held scientist, patent liaison, operations management, and strategic business management roles within Halliburton's technology, drilling operations, and strategic business organizations over a 23-year span.

Carl has more than 30 issued patents related to chemistries for drilling and completion operations and a Hirsch index of 12. He serves the Society of Petroleum Engineers (SPE) as a member of the Drilling Advisory Committee, and as an Associate Editor for the *SPE Drilling & Completion* journal; from 2012 to 2015, Carl was the Executive Editor.

He received his B.S. degree from Missouri State University, Springfield, MO, and an M.S. degree from Texas State University, San Marcos, TX, both in Chemistry.

Advanced Wellbore Stability Analysis for Drilling Naturally Fractured Rocks

Dr. Yanhui Han, Dr. Chao Liu, Dr. Dung Phan, Dr. Khalid M. Al-Ruwaili, and Dr. Younane N. Abousleiman

Abstract /

An advanced wellbore stability analysis software product has been developed in-house at Aramco. This product offers three analysis modules: (1) The classical mechanical module (elastic); (2) The time-dependent analysis module (poroelasticity); and (3) The time-dependent analysis of naturally fractured rock module (dual porosity and dual permeability poroelasticity). The stress and pressure analyses are integrated with four rock failure criteria (Mohr-Coulomb, Drucker-Prager, Modified Lade, and Hoek-Brown) to calculate critical mud densities.

The basic mechanical module is similar to the wellbore stability module provided in the most frequently used drilling geomechanics software. What sets this product apart from the others is that no commercial drilling software to date has the time-dependent stress and pressure analyses modeled by this product's poroelastic and dual porosity poroelastic modules, which can capture real-time phenomena introduced by the time-dependent fluid pore pressure perturbation and the wellbore time-dependent failures in tension and/or compression. The dual porosity poroelastic module is uniquely developed to compute safe mud weight windows for drilling in fractured formations through coupling dual porosity, dual permeability with the Hoek-Brown failure criterion.

Introduction

As the oil industry has moved to exploring and producing oil and gas from offshore and unconventional reservoirs, the identification, quantification, and assessment of natural fractures have been becoming key factors in the drilling operations[1, 2]. It is well understood that the stability of a drilled wellbore is affected by the in situ stresses and pore pressure, the mechanical properties of the drilled formation, the trajectory of the well to be drilled, and the selected drilling mud[3, 4].

The influence of natural fractures in the formation on wellbore stability can be very complicated as they will modify the stresses/pore pressure distributions around the wellbore and the mechanical/hydraulic properties of the source rock. Both the rock matrix and natural fractures are in contact with drilling mud in the wellbore, and the pressure difference between the wellbore and the reservoir will induce fluid diffusion. Due to their higher conductivity, the fluid pressure diffuses much faster in natural fractures than in rock matrix. The pressure difference between the rock matrix and fractures will cause tertiary fluid diffusion between fractures and rock matrix — in addition to the primary diffusion between the wellbore and fractures and secondary diffusion between the wellbore and rock matrix. Subsequently, the effective stresses will evolve with the pore pressures in the fractures and rock matrix. Evidently, the presence of natural fractures introduces a few more coupling processes around the wellbore and makes the stability of the wellbore a time-dependent problem[5, 6].

No commercial drilling software to date offers any time-dependent stress and pressure analysis model that can capture the coupling processes described here. To bridge this gap, we developed advanced wellbore drilling geomechanics software at Aramco for real-time wellbore stability analysis. The salient advantage of this software package is that it is built on the rigorous poromechanics theory and can take into account more realistic mechanical properties of rocks. It will therefore be more appropriate for the modeling of challenging source rocks, thereby providing better predictions of the stresses and pore pressure around the wellbore in these formations, and the optimal design of the wellbore drilling problems.

As previously mentioned, in the evaluation of wellbore stability and computation of safe mud weight windows, three sets of inputs are required, i.e., well trajectory, in situ stresses, and rock properties. The well trajectory is available as predrill data. Three principal stresses and pore pressure need to be known in the wellbore stability analysis. The overburden pressure can be computed from density logging data. The pore pressure can be estimated from logging data. The two horizontal stresses can be measured from or calibrated with well tests, e.g., mini-fracture test. The rock properties should be measured in the laboratory experiments if core samples, lab equipment and well trained technicians are available. Because of economic, time and/or technical constraints, very few laboratory experiments are conducted in drilling practice.

Even if lab tests are performed, the number of tested spots along the borehole is still very limited. A more common, alternative approach is to estimate rock properties from well logging data and calibrated with available lab data. Many correlations for this purpose have been proposed and applied in wellbore stability analysis over the last few decades. In this software, the rock properties can be inputted directly if available, or estimated from logging data using extensively verified correlations in the oil industry if not.

Mechanical properties of rocks can be categorized into elastic properties (stiffness) and plastic properties (strength). Depending on the failure criterion to be used in the analysis, different plastic properties are required. In wellbore stability analysis, the Mohr-Coulomb criterion is the most widely used one. In this criterion, cohesive strength and frictional angle are required properties. Since different rocks follow different constitutive laws they fail differently; some other failure criteria, such as Drucker-Prager and Modified Lade, have also been used in wellbore stability analyses. Besides mechanical properties, other factors, such as thermal expansion/contraction, chemical reaction, fluid penetration and diffusion, rheology of source rock, can also impact the stability of the drilled hole. In many cases, these factors can have a dominant impact on the wellbore stability. In the long run, all these factors will be included in this software.

The software, Saudi Aramco Geomechanics Expert: Wellbore Stability Analyzer (SAGE:WSA) was planned to be developed and released in an incremental manner over several years. In the current version, which is the first release as described later, a user-friendly, mouse-click driven graphical user interface (GUI) is developed to pre-process users' inputs, perform computation, display computational results at the post-processing stage, and export data and results to specified files. The mechanical elements implemented in this version include three analysis modules: (1) the classical mechanical module (elastic); (2) the time-dependent analysis module (poroelasticity); and (3) the time-dependent analysis of naturally fractured rock module (dual porosity and dual permeability poroelasticity); and four failure criteria: (1) Mohr-Coulomb; (2) Drucker-Prager; (3) modified Lade; and (4) Hoek-Brown.

In the following sections, first, the software architecture is described; next, the analysis modules and failure criteria implemented in this software are briefly reviewed; next, the correctness and accuracy of the stress and pore pressure solutions are verified through comparison with published data in the open literature; next, the software is used to revisit some published case studies; and last, the ongoing and future development plan is discussed.

Software Architecture

This advanced software platform, SAGE-WSA, was developed in-house using a poromechanics system engineering approach. The structure of SAGE-WSA comprises two parts. The front-end, or the GUI, is a menu-driven environment with which a user communicates by entering different values in the input dialogs. The back-end, or the computation engine, contains the routines to generate numerical results. The computation engine receives calculation requests from the GUI, interprets these, performs computation, and generates results accordingly. Upon receiving the results from the computation engine, the front-end visualizes them in various plots.

Mechanical Models

Stress and Pore Pressure Models

In this software, an analytical solution approach is used in the evaluation of wellbore stability, which makes the computation very efficient. This is of critical importance when performing wellbore stability analysis at thousands of points with complicated physics involved.

Static stress model (elasticity). The source rocks are assumed to be linearly elastic materials — before reaching plastic yielding stress domain. In the elastic domain, the mechanical behaviors of the rocks are governed by constitutive law, equilibrium equations, and strain displacement relations:

$$\sigma'_{ij} = 2G\varepsilon_{ij} + \frac{2Gv}{1-2v}\varepsilon_{kk}\delta_{ij} \quad (1)$$

$$\sigma_{ij,j} = 0 \quad (2)$$

$$\varepsilon_{ij} = \frac{1}{2}\left(u_{i,j} + u_{j,i}\right) \quad (3)$$

In Eqns. 1 to 3, σ_{ij} is the component of the total stress tensor; ε_{ij} is the component of the strain tensor; G is the shear modulus; v is Poisson's ratio; u_i is the displacement in the x_i direction; δ_{ij} is the Kronecker delta; σ'_{ij} is the effective stress tensor:

$$\sigma'_{ij} = \sigma_{ij} - \alpha p\delta_{ij} \quad (4)$$

where p is pore pressure and α is Biot's coefficient of effective stress[7]. In the traditional effective stress concept developed in soil mechanics by Terzaghi (1925)[8], α is equal to 1, which is reasonable because soil mass is much more compressible than individual soil solid grains.

Time-dependent stress model (poroelasticity). If the pore pressure variation caused by fluid flow in the source rocks or rock deformation is non-negligible, the hydro-mechanical interaction can impose significant impact to the wellbore stability. Due to the time-dependent nature of fluid diffusion in porous media, the stability of the wellbore becomes time-dependent. Two key mechanisms, i.e., pore pressure buildup/drop-down by mechanical contraction/expansion, and effective stress change induced by pore pressure variation, can be captured by Biot's poroelasticity theory[7,9], in which some coupling equations are added to the classic elasticity theory, including fluid transport equation (Darcy's law), continuity equation:

$$q_i = -\frac{k}{\mu}\frac{\partial p}{\partial x_i} \quad (5)$$

$$\frac{\partial \varsigma}{\partial t} + \frac{\partial q_i}{\partial x_i} = 0 \quad (6)$$

and pore pressure-mechanical deformation coupling equation:

$$p = M(\varsigma - \alpha \varepsilon_{kk}) \quad (7)$$

where k is the intrinsic permeability of porous media; μ is the dynamic viscosity of pore fluid; ς is the volumetric variation of fluid content in the porous media; q_i is the component of the pore fluid discharge vector; M is Biot's modulus:

$$M = \frac{2G(v_u - v)}{\alpha^2(1-2v_u)(1-2v)} \quad (8)$$

where v_u is undrained Poisson's ratio, it can be calculated from the drained Poisson's ratio, v, Biot's coefficient, α and Skempton pore pressure coefficient, B:

$$B = \frac{3(v_u - v)}{\alpha(1-2v)(1+v_u)} \quad (9)$$

The mathematical derivation and resulted poroelastic solutions of stresses, pore pressure, etc., can be found in Detournay & Cheng (1988)[9] for vertical wellbore and Cui and Abousleiman (1997)[4] for inclined wellbore.

Fractured formation model (dual poroelasticity). For porous media that contains extensive microfractures, such as naturally fractured shales, the hydro-mechanical responses of the materials can be well described by the dual porosity, dual permeability (or, dual poroelasticity) theory[10, 11].

The fractured porous medium may be imagined as superposition of two sets of porous materials — matrix and fractures — each with its own hydraulic conductivity. If the pore pressures in matrix and fractures are different, fluid transfer will take place between the matrix and fractures. Correspondingly, Eqns. 10 and 11 are the fluid transport and continuity equations for porous medium "*I*"; Eqns. 12 and 13 are the fluid transport and continuity equations for porous medium "*II*"[5, 12]:

$$q_i^I = -\frac{k^I}{\mu}\frac{\partial p^I}{\partial x_i} \quad (10)$$

$$\frac{\partial \varsigma^I}{\partial t} + \frac{\partial q_i^I}{\partial x_i} = \Gamma(p^{II} - p^I) \quad (11)$$

$$q_i^{II} = -\frac{k^{II}}{\mu}\frac{\partial p^{II}}{\partial x_i} \quad (12)$$

$$\frac{\partial \varsigma^{II}}{\partial t} + \frac{\partial q_i^{II}}{\partial x_i} = -\Gamma(p^{II} - p^I) \quad (13)$$

where k^I and k^{II}, ς^{II} and q_i^I, and q_i^{II}, p^I and p^{II} are the intrinsic permeability, the volumetric variation of fluid content of matrix and fractures, the component of the pore fluid discharge vector, and the fluid pressure of matrix and fractures, respectively; Γ is the fluid transfer coefficient between the matrix and fractures.

The compressibility of the fractured porous media is taken as the average of matrix and fractures:

$$\frac{1}{G} = \frac{v^I}{G^I} + \frac{v^{II}}{G^{II}}; \frac{1}{K} = \frac{v^I}{K^I} + \frac{v^{II}}{K^{II}} \quad (14)$$

where K^I and K^{II}, G^I and G^{II} are the bulk and shear moduli of the matrix and fractures, respectively; G and K are the overall shear and bulk moduli of the fractured porous medium; and v^I and v^{II} are the volume fractions of the matrix and fractures, respectively.

Collapse Failure Criteria

Mohr-Coulomb (MC) criterion. The Mohr-Coulomb criterion is written as:

$$\sigma_1' = \sigma_3' N_\phi + 2c\sqrt{N_\phi} = \sigma_3' N_\phi + UCS \quad (15)$$

where $N_\phi = \frac{1+\sin\phi}{1-\sin\phi}$; ϕ is frictional angle; c is cohesive strength; σ_1' and σ_3' are major and minor effective principal stresses, i.e., the same as σ_{11}' and σ_{33}'. Note that the second term in the right-hand side, i.e., $2c\sqrt{N_\phi}$, is equivalent to unconfined compressive strength (UCS).

Drucker-Prager (DP) criterion. The expression of Drucker-Prager criterion is similar to Mohr-Coulomb in shear stress-normal stress domain:

$$\tau_{oct} = \tau_0 + m_d \sigma_{oct} \quad (16)$$

$$\tau_{oct} = \sqrt{(\sigma_1 - \sigma_2)^2 + (\sigma_2 - \sigma_3)^2 + (\sigma_3 - \sigma_1)^2} \quad (17)$$

$$\sigma_{oct} = \frac{1}{3}(\sigma_1 + \sigma_2 + \sigma_3) \quad (18)$$

Modified Lade (MD) criterion. The Modified Lade failure criterion[13] can be described by:

$$\frac{(I_1'')^3}{I_3''} = 27 + \eta_L \quad (19)$$

where $I_1'' = \sigma_1' + \sigma_2' + \sigma_3' + 3S_L$ and $I_3'' = (\sigma_1' + S_L)(\sigma_2' + S_L)(\sigma_3' + S_L)$ are stress and strength related invariants; S_L and η_L and are strength related material constants.

Hoek-Brown (HB) criterion. The Hoek-Brown failure criterion[14, 15] may be expressed as:

$$\sigma_1' = \sigma_3' + \sigma_{ci}\left(m_b \frac{\sigma_3'}{\sigma_{ci}} + s\right)^a \quad (20)$$

where σ_{ci}, m_b, s, and a are material constants (strength parameters).

Tensile Failure Criteria

If the minor effective principal stress turns into tension at a point and its magnitude exceeds the material's tensile strength, the material will fail in tensile yielding mode:

Fig. 1 *Measuring cohesive strength and the frictional angle from triaxial test results.*

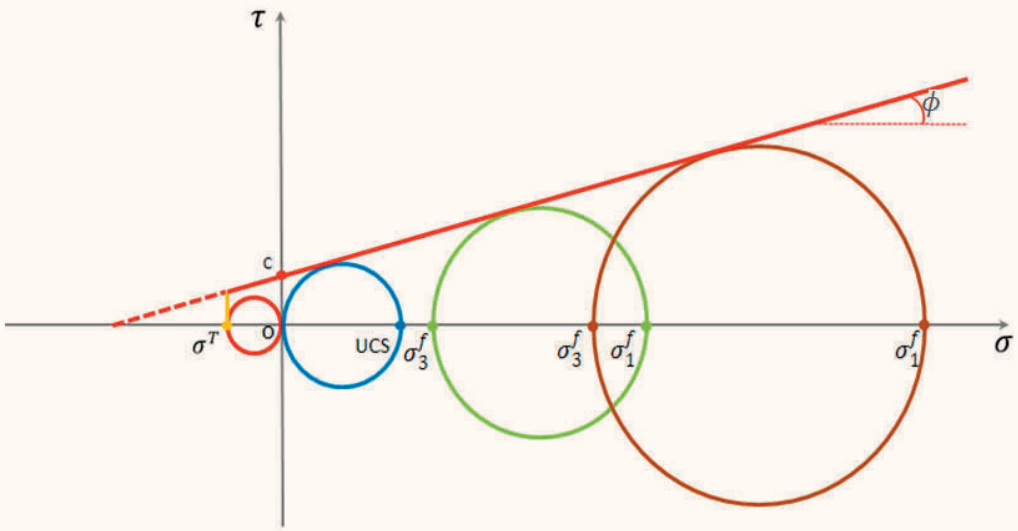

$$\sigma_3' = -\sigma^T \quad (21)$$

where σ^T is the material's tensile strength.

In the wellbore problem, drilling mud inside the well induces tensile hoop stress in the wellbore wall. Once the combination of this mud induced tensile hoop stress and the hoop stress introduced by the in situ stresses and pore pressure reaches the tensile strength, the wellbore wall will fail in tension.

Determination of Strength Parameters

The MC criterion is the most widely used failure criterion to describe the compressive failure behaviors of soil and rock materials. The two parameters in MC criterion, cohesive strength and frictional angle, can be measured by triaxial compression tests on cylindrical samples. Evidently, since there are two parameters needed to be determined, at least two tests, each with a different confining stress, are required. In each test, the cylindrical sample is loaded by an increasing axial load under confinement of a constant stress until the sample collapses. Using the confining stress (σ_3^f) and collapsing axial stress (σ_1^f), a Mohr cycle can be drawn in the shear stress — normal stress ($\tau - \sigma$) coordinate system, Fig. 1. Note that if there is no confining stress, the axial stress measured at the collapse point is UCS. The tensile strength in theory can be measured by direct tension test (e.g., the red cycle in Fig. 1), but in practice, the direct tension test is very difficult to perform, so tensile strength is often measured indirectly in Brazilian disc setup[16, 17].

Strength parameters of HB failure criterion, m_b, s and a, can be estimated from the Geological Strength Index (GSI) and rock damage (D), which is a factor depending on the disturbance degree that rock mass has experienced[18]:

$$m_b = m_i e^{\frac{GSI-100}{28-14D}} \quad (22)$$

$$s = e^{\frac{GSI-100}{9-3D}} \quad (23)$$

$$a = \frac{1}{2} + \frac{1}{6}\left(e^{-\frac{GSI}{15}} - e^{-\frac{20}{3}}\right) \quad (24)$$

The strength parameters of HB, DP, and ML criteria can be linked to the cohesive strength and frictional angle. Unlike the MC failure criterion, the HB criterion is nonlinear in the major stress – minor stress ($\sigma_1' - \sigma_3'$) space, so the equivalent cohesive strength and frictional angle are different at the different stress level, i.e., they are dependent on σ_3'[20, 21]. The equivalence relations between them are provided in Table 1. The strength parameters of ML criterion, S_L and η_L, can be directly derived from the cohesive strength and frictional angle[13]. Figure 2a shows the criterion envelopes of the DP and MC criteria in principal stress space. In π-plane, MC criterion is hexagonal and DP criterion is circular, Fig. 2b. The parameters of the DP circles that coincide with the outer apices ("outer circle"), the inner apices ("middle circle") and touches the insides of the MC hexagon ("inner circle") can also be directly computed from cohesive strength and frictional angle using formulations provided in Table 1.

GUI

Figure 3 illustrates the key feature in the current version of SAGE-WSA, i.e., to study the stability of a wellbore with arbitrary trajectory drilled in fractured formations. The well trajectory is defined by the azimuth (relative to north) and inclination angle. The stress field is described by three principal stresses and the azimuth of the maximum

Table 1 *Relationship of strength parameters to cohesive strength and frictional angle.*

Failure Criterion	Parameters	References
Hoek-Brown	$N_\phi = 1 + am_b\left(m_b\frac{\sigma_3'}{\sigma_{ci}} + s\right)^{a-1}$ $UCS = \sigma_3'(1 - N_\phi) + \sigma_{ci}\left(m_b\frac{\sigma_3'}{\sigma_{ci}} + s\right)^a$	Itasca (2011)[20]
Drucker-Prager	Outer circle: $m_d = \frac{2\sqrt{2}\sin\phi}{3-\sin\phi}$; $\tau_0 = \frac{2\sqrt{2}\,c\cos\phi}{3-\sin\phi}$ Middle circle: $m_d = \frac{2\sqrt{2}\sin\phi}{3+\sin\phi}$; $\tau_0 = \frac{2\sqrt{2}\,c\cos\phi}{3+\sin\phi}$ Inner circle: $m_d = \frac{\sqrt{6}\sin\phi}{\sqrt{9+3\sin^2\phi}}$; $\tau_0 = \frac{\sqrt{6}\,c\sin\phi}{\sqrt{9+3\sin^2\phi}}$	McLean and Addis (1990)[19]
Modified Lade	$S_L = \frac{c}{\tan\phi}$; $\eta_L = \frac{4\tan^2\phi(9-7\sin\phi)}{1-\sin\phi}$	Ewy (1998)[13]

Fig. 2 *Projection of DP and MC criteria in: (a) principal stress space, and (b) π–plane[19].*

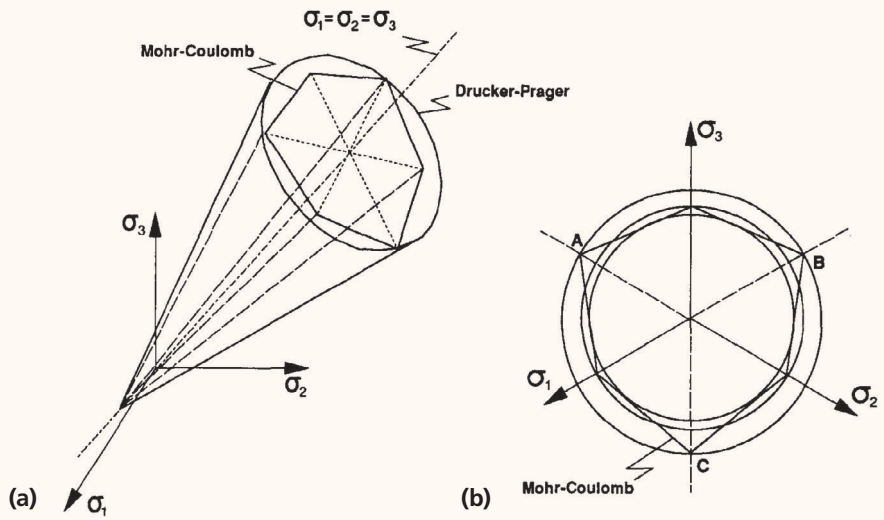

Fig. 3 *Splash picture of SAGE-WSA.*

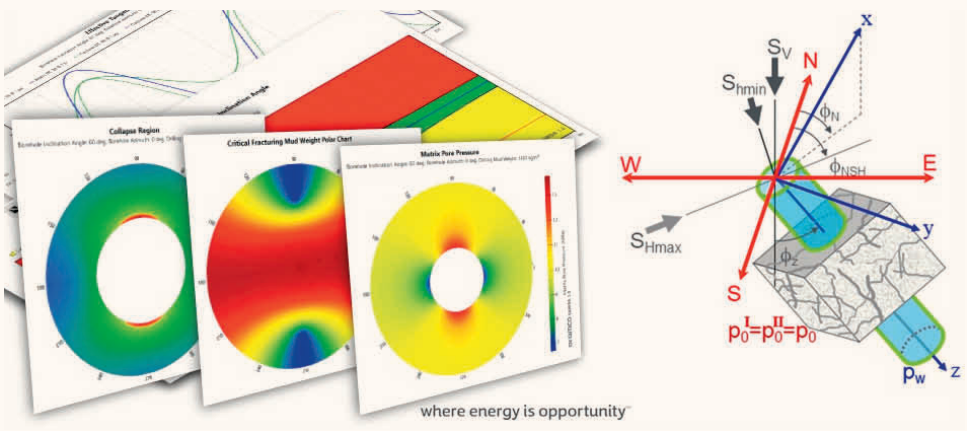

Fig. 4 *GUI: layout and input dialog.*

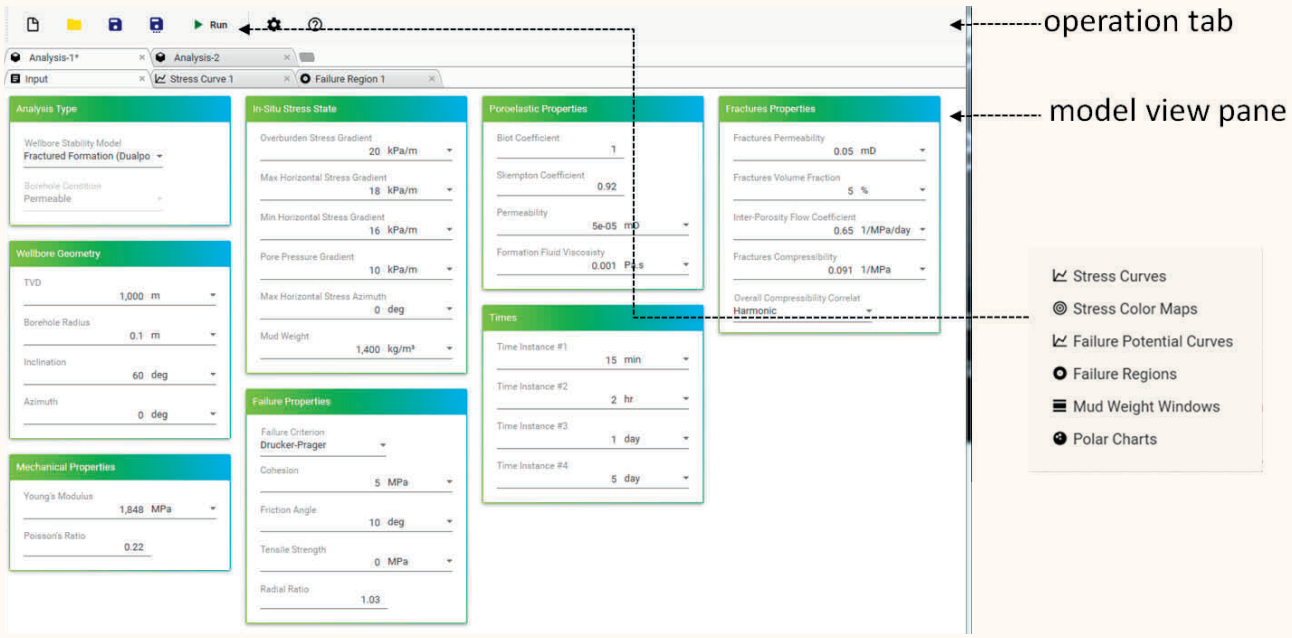

Fig. 5 *Example calculation output.*

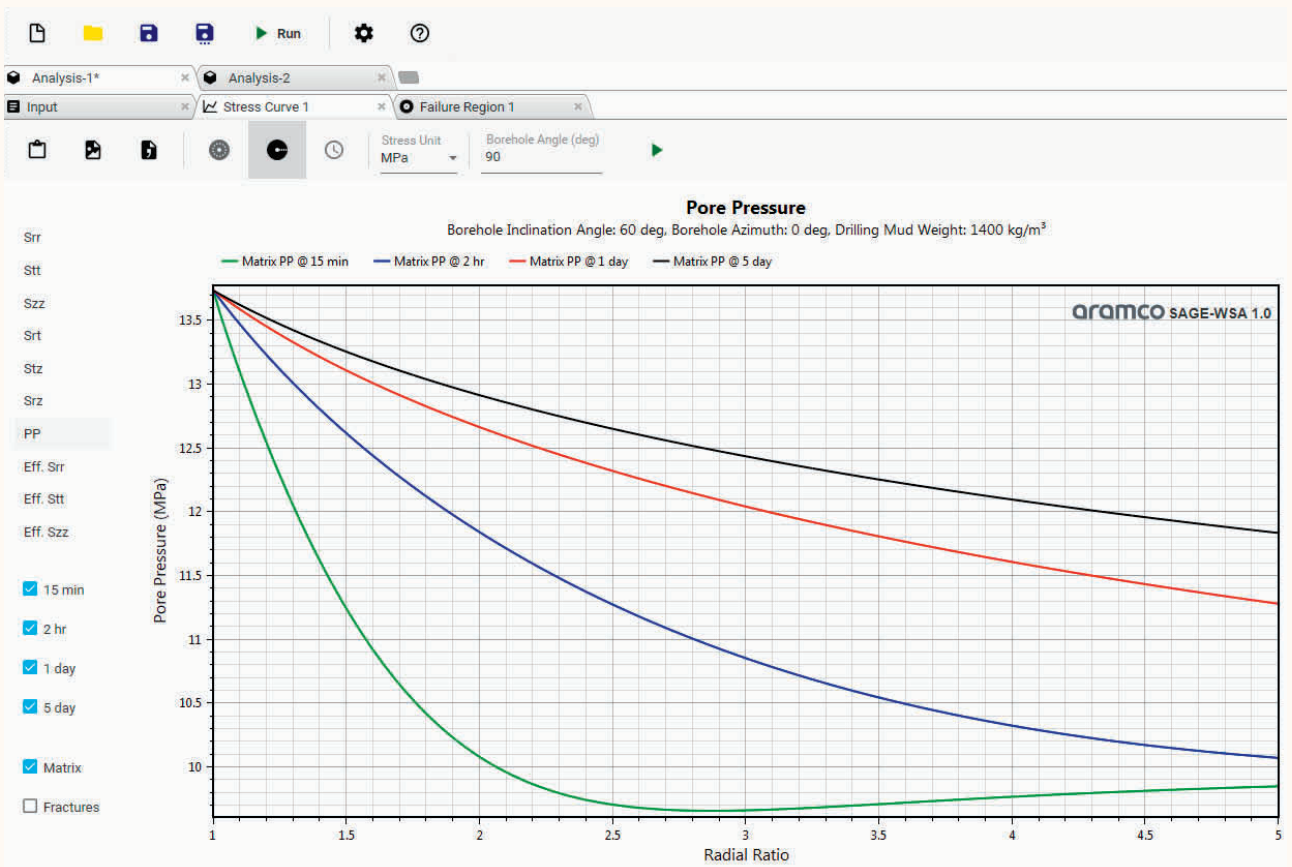

Table 2 *Input parameters for the case study in Cui et al. (1997)[4].*

Wellbore Geometry	In Situ Stresses and Pore Pressure	Rock Properties	Mud Pressure
TVD = 1,000 m φ_N = 60° β = 30°	dSV = 25 kPa/m dSH = 29 kPa/m dSh = 20 kPa/m dPp = 9.8 kPa/m φ_{NSH} = 0°	E = 1,652 MPa v = 0.219 α = 0.968 B = 0.915 k = 10^{-4} md ρ_w = 1,000 kg/m^3 (μ = 1 cP)	P_w = 0

horizontal stress. The fluid pressure in the rock matrix and natural fractures are initially identical. The wellbore stability is maintained by applying appropriate mud pressure inside the wellbore.

Figure 4 shows the layout of the GUI, which consists of two parts. The bar on the top part holds seven clickable icons for operating the software. From left to right, icons offer functionalities of "New Analysis," "Open," "Save," "Save As," "Run," "Settings," and "Help" (their functionalities are self-explained by their names). The model view pane below the top bar has multiple tab layouts, so many case studies can be performed in one SAGE-WSA window.

Each tab corresponds to one analysis case and can have multiple subtab panes; the first subtab pane is added automatically, it is the input dialog for the current analysis case, e.g., the first subtab pane of "Analysis-1" lists the required input parameters for analyzing the stability of the wellbore drilled in fractured formations; the calculation is triggered by clicking and choosing the computation type from the drop-down menu of the "Run" icon, including "Stress Curves," "Stress Color Map," "Failure Potential Curves," "Failure Regions," "Mud Weight Windows," and "Polar Charts," as shown on the right side in Fig. 4. After the desired computation is finished, a new subtab pane will be added to the current tab and the computed results will be plotted in this new subtab pane, e.g., Fig. 5 shows that two subtab panes have been added under the tab of "Analysis-1," one from the "Stress Curves" computation; the other from the "Failure Regions" computation.

Fig. 6 *Comparison of distribution of the effective radial stress along the radial direction calculated by SAGE-WSA with Fig. 6 in Cui et al. (1997)[4].*

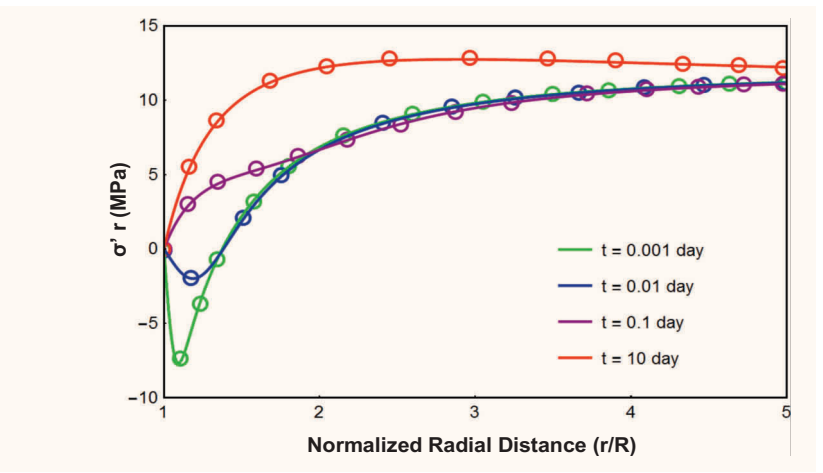

Verification Examples

Poroelastic Solution (Time Dependent Stress)

The poroelastic analysis module is verified with a case study presented in Cui et al. (1997)[4], for which the input parameters of well geometry, in situ stresses and pore pressure, rock and fluid properties and mud pressure inside the well are duplicated in Table 2.

All the stress components and pore pressure can be computed in SAGE-WSA and compared with results presented in the referred publication. For example, the effective radial stress distributions along radial direction at various times, 0.001-, 0.01-, 0.1-, and 10-day, are compared in Fig. 6, where the lines are calculated results

Table 3 *Input parameters for the case study in Abousleiman and Nguyen (2005)[5].*

Wellbore Geometry	In Situ Stresses and Pore Pressure	Rock Properties	Mud Pressure
TVD = 1,000 m φ_N = 60° β = 0°	dSV = 22.6 kPa/m dSH = 18 kPa/m dSh = 14 kPa/m dPp = 10.4 kPa/m φ_{NSH} = 0°	E = 1,853 MPa v = 0.219 α = 0.968 B = 0.915 k = 10^{-4} md ρ_w = 1,000 kg/m^3 (μ = 1 cP)	P_w = 0

given by SAGE-WSA and cycle symbols are solutions digitized from Fig. 6 in Cui et al. (1997)[4]. Clearly, SAGE-WSA can accurately reproduce the published results, which verifies the correctness of the implementation of poroelastic solutions of stresses and pore pressure around the wellbore.

The second example is taken from Abousleiman and Nguyen (2005)[5]. In that work, after they derived the complete analytical solutions for an inclined wellbore drilled through a naturally fractured rock formation, they demonstrated that the dual poroelastic solutions converged to the poroelastic solutions if the hydro-mechanical behaviors of fractures are suppressed. The input parameters for this case study are listed in Table 3. The pore pressure profiles along radial direction at various times, 0.001-, 0.1-, and 1-day, computed by SAGE-WSA where the lines are compared with their counterparts, cycle symbols, given by Abousleiman and Nguyen (2005)[5] in Fig. 7, which shows excellent agreements. Similarly, effective radial stress distributions along the radial direction are compared in Fig. 8.

Dual Poroelastic Solution (Fractured Formations)

In a case study in Nguyen and Abousleiman (2009)[12], the time evolution of pore pressure in the rock matrix near the wellbore drilled in fractured formation is presented. The input parameters used in that case study are duplicated in Table 4. The time-evolution of pore pressure at $r = 1.1R$ and $=0°$ computed by SAGE-WSA (the line) is compared with its counterpart (the cycle symbols) in Nguyen and Abousleiman (2009)[12] in Fig 9.

Application of SAGE-WSA in Mud Weight Computation

Basic Mechanical Analysis (Time Independent)

In this application example, a set of field data for some inclined offshore wellbore drilled in the Gulf of Mexico is revisited, using both TECHLOG 2016.2 and SAGE-WSA. The water depth is 7,846 ft. The hydraulic pressure gradient for the water depth is 0.447 psi/ft. The profiles of wellbore trajectory, stresses, pore pressure, and rock properties along the measured depth (MD) are displayed in the left and central sections in Fig. 10. Using the geomechanics module of TECHLOG, the safe mud weight window, i.e., confined by critical collapse mud weight (CMW) as lower bound and fracturing mud weight (FMW) as upper bound, can be calculated, as presented in the right section in Fig. 10.

Since a multiple depth analysis module has not been implemented in SAGE-WSA yet, the calculation of the mud weight window needs to be conducted for each depth

Fig. 7 Comparison of pore pressure distribution along the radial direction calculated by SAGE-WSA with Fig. 4 in Abousleiman and Nguyen (2005)[5].

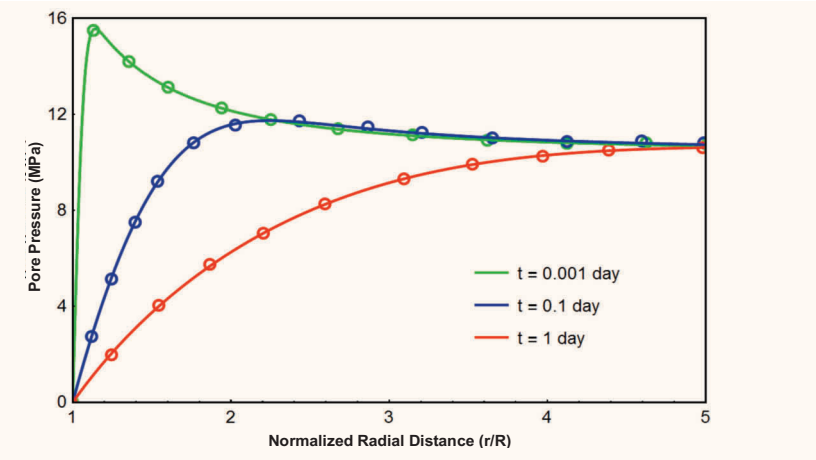

Fig. 8 Comparison of effective radial stress distribution along the radial direction calculated by SAGE-WSA with Fig. 4 in Abousleiman and Nguyen (2005)[5].

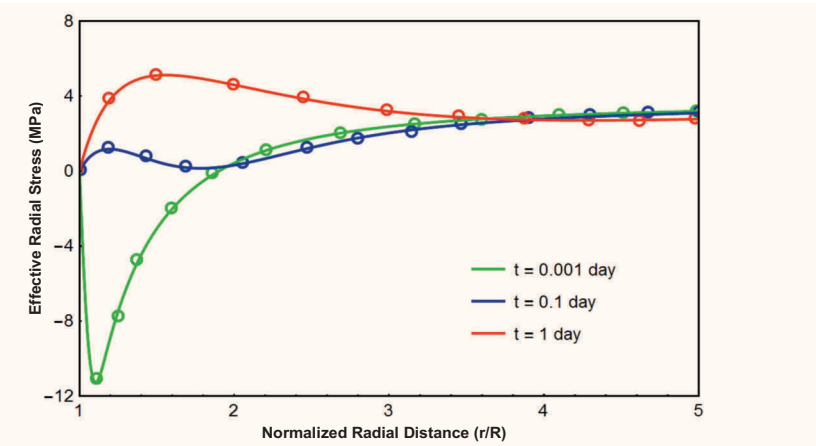

Table 4 Input parameters for the case study in Abousleiman and Nguyen (2009)[12].

Wellbore Geometry	In Situ Stresses and Pore Pressure	Rock Properties	Fracture Properties	Mud Pressure
TVD = 1,000 m $\varphi_N = 0°$ $\beta = 0°$	dSV = 20 kPa/m dSH = 18 kPa/m dSh = 16 kPa/m dPp = 10 kPa/m $\varphi_{NSH} = 0°$	E = 1848 MPa v = 0.22 α = 0.96 B = 0.92 $k = 5 \times 10^{-4}$ md (μ = 1 cP)	E = 18.48 MPa v = 0.22 α = 1 B = 0.99 $k = 5 \times 10^{-2}$ md	$P_w = 0$

Fig. 9 *Comparison of time-evolution of pore pressure in rock matrix at r = 1.1R and θ = 0° calculated by SAGE-WSA with Fig. 2 in Nguyen and Abousleiman (2009)[12].*

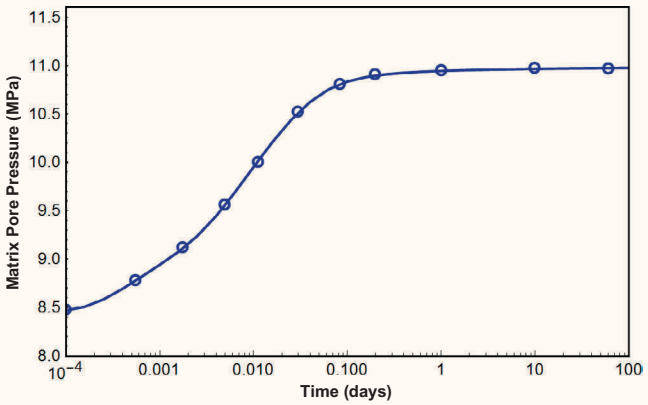

separately. To run analysis in SAGE-WSA, we need to convert psi to psi/ft for the inputs of in situ stresses and pore pressure gradients. Also, for offshore wells, the water depth needs to be considered in the stress and pore pressure conversion. For example, at a true vertical depth (TVD) of 8,899.08 ft, the equivalent in situ stresses and pore pressure gradients can be calculated as follows:

$$dSV = SV/TVD = 0.471 \text{ psi/ft}$$

$$dSH = SH/TVD = 0.469 \text{ psi/ft}$$

$$dSh = Sh/TVD = 0.466 \text{ psi/ft}$$

$$dPp = Pp/TVD = 0.462 \text{ psi/ft}$$

Fig. 10 *Mud weight window predicted by Techlog 2016[2].*

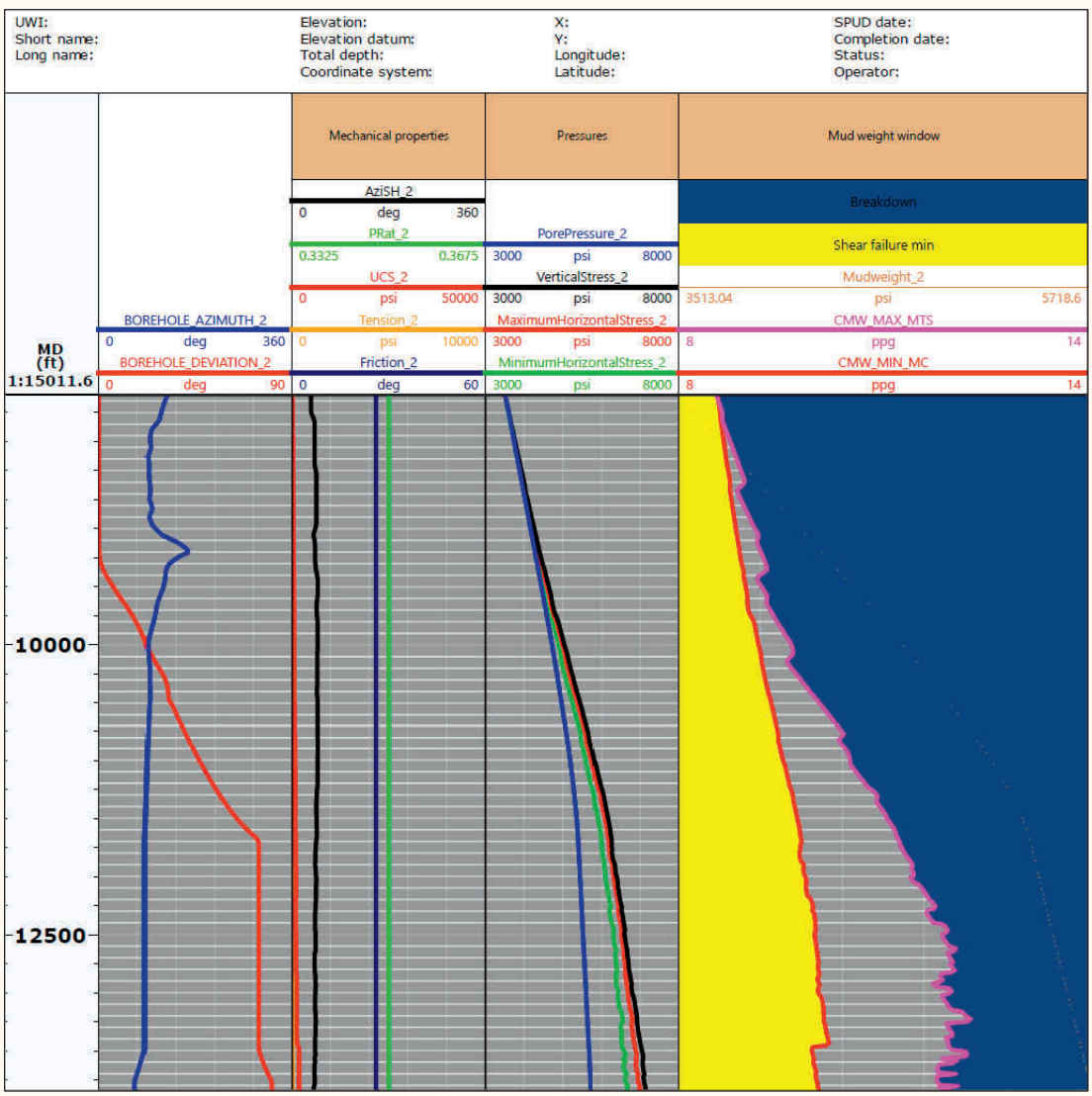

Fig. 11 *Mud weight window calculation for a TVD of 9,865.20 ft (MD = 9,879.44 ft) in SAGE-WSA: (a) input, and (b) output.*

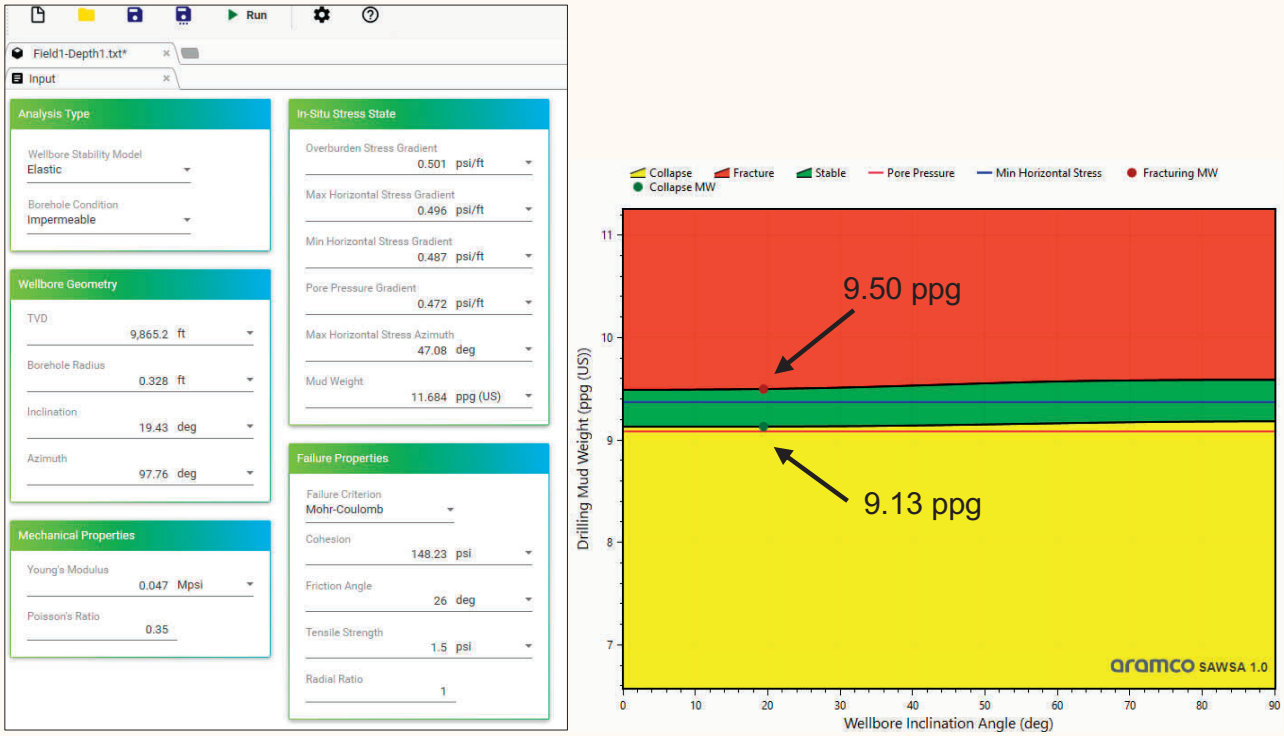

Table 5 *The set of data chosen for running SAGE-WSA.*

MD (ft)	TVD (ft)	Incl (deg)	Azi-muth (deg)	SV (psi)	SH (psi)	Sh (psi)	Pp (psi)	AziSH (deg)	Cohe-sion (psi)	E (Mpsi)	SAGE-CMW (ppg)	SAGE-FMW (ppg)
9,879.44	9,865.20	19.43	97.76	4,944.49	4,897.95	4,805.03	4658.26	47.08	148.23	0.047	9.13	9.50
11,857.45	11,355.93	58.15	88.21	6,265.33	6,179.05	5,996.73	5482.18	44.86	249.96	0.08	9.71	10.87
13,838.80	11,991.36	74.36	85.74	6,804.85	6,736.24	6,511.01	5814.19	43.77	293.35	0.094	9.87	11.46
15,869.78	12,538.82	74.36	85.74	7,279.40	7,193.49	6,951.03	6092.90	43.27	292.23	0.094	10.07	11.85
17,825.66	13,066.05	74.37	85.74	7,761.41	7,599.02	7,289.28	6364.58	42.51	355.20	0.114	10.18	11.89
19,862.41	13,605.44	76.49	78.92	8,240.35	8,051.55	7,717.21	6643.93	42.94	558.98	0.179	10.11	12.04

Some constant parameter: R = 0.328 ft; v = 0.35; φ = 26°; σ^T = 1.5 psi.

Note that due to the water column above the well surface, the calculated equivalent in situ stress gradients are smaller than the typical values of onshore well data. Figure 11 displays the input and output of SAGE-WSA for computing the mud weight window for the first point listed in Table 5, i.e., at TVD of 9,865.20 ft.

The mud weight windows at all 180 depths computed by TECHLOG and SAGE-WSA are plotted together and compared in Fig. 12. Evidently, TECHLOG and SAGE-WSA gave essentially the same "CMW" and "FMW" at all depths.

Fractured Formation

In the case study taken from Nguyen and Abousleiman (2009)[12] that we revisited, the variations of the safe mud weight window along with the borehole inclination angle were also presented. SAGE-WSA offers features of directly computing safe mud weight windows for varying wellbore inclination, azimuth or time. As shown in Fig. 13, the safe mud weight windows for varying wellbore inclination angles calculated by SAGE-WSA are essentially identical to the solutions given by Nguyen and Abousleiman (2009)[12].

Conclusions and Future Work

This article reviews the governing equations of classic continuum mechanics, poroelasticity and dual poroelasticity theories and four failure criteria developed in an advanced wellbore stability software in-house at Aramco, called SAGE-WSA. A couple of examples are documented on the validation of these modules, i.e., the poroelastic and dual poroelastic modules in SAGE-WSA are validated through comparing solutions from the software with data published in the open literature. Time-dependent distribution and evolution of stress and pore pressure around wellbore computed by SAGE-WSA are compared with published solutions, which consistently showed that for the same input parameters, SAGE-WSA gives identical solutions as those publications.

In the first case study, the basic mechanical analysis module in SAGE-WSA is applied to compute the safe mud weight window for drilling a well through reservoir formations. The safe mud weight window for drilling the offshore well was calculated in both TECHLOG and SAGE-WSA and they gave essentially the same solutions. In the second case study, the mud weights for drilling a fractured formation is employed to revisit a case presented in a journal article and solutions given by SAGE-WSA are found identical to the reported results.

SAGE-WSA is perhaps the only advanced geomechanics software capable of addressing very challenging drilling problems encountered in fractured formations. The ongoing development work includes a multiple depth analysis module and a logging correlation module. In the long run, other advanced modules, such as viscoelastic (rheology), bedding planes, chemo, and thermo, will be incrementally added to the software.

Fig. 12 *Comparison of mud weight windows calculated by SAGE-WSA and Techlog 2016[2].*

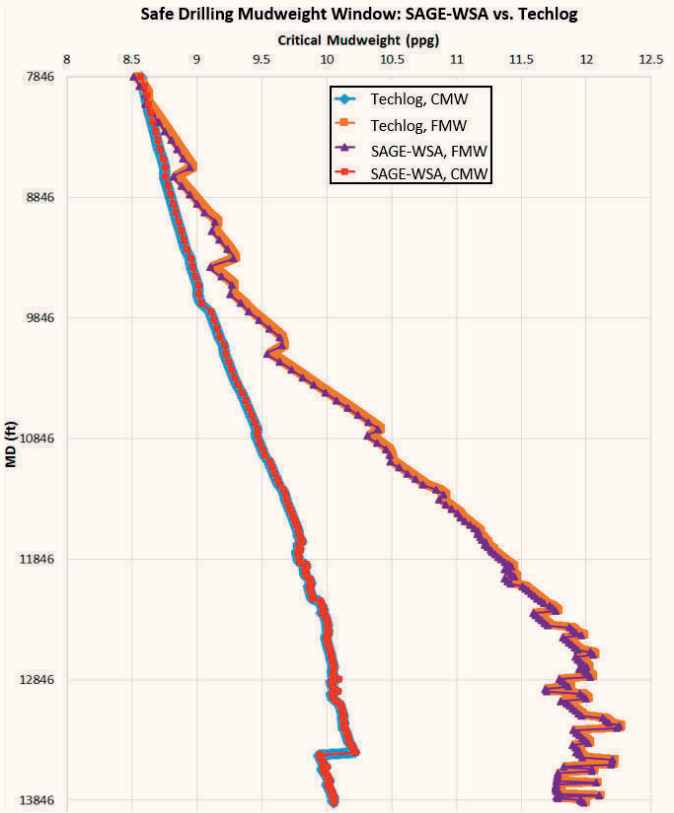

Fig. 13 *Comparison of safe drilling mud weight window vs. the wellbore inclination angle calculated by SAGE with Fig. 12 in Nguyen and Abousleiman (2009)[12].*

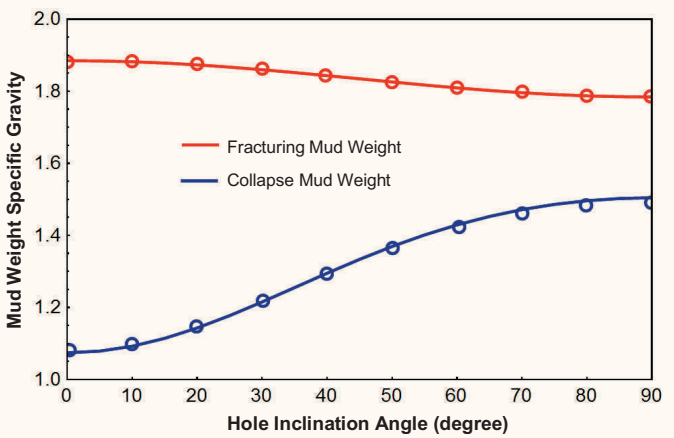

Acknowledgments

The authors would like to thank the management of Saudi Aramco and Aramco Services Company for their support and permission to publish this article. The authors would also like to thank their colleagues, Khaqan Khan, Adel Qahtani, and Osman Hamid in the Gas Reservoir Management Department for the great assistance and efforts that they put into the evaluation and field deployment of this advanced wellbore stability software.

This article was presented at the SPE Middle East Oil & Gas Show and Conference, Manama, Kingdom of Bahrain, March 18-21, 2019.

References

1. Lyngra, S., Widjaja, D.R., Al-Shammeri, F.M., Al-Otaibi, U.F., et al.: "A Complex Naturally Fractured Reservoir Case Study: Fracture System Understanding is Key to Development Drilling Success," SPE paper 178011, presented at the SPE Saudi Arabia Section Annual Technical Symposium and Exhibition, al-Khobar, Saudi Arabia, April 21-23, 2015.

2. Ahmed, M., Al-Shehri, H.A., Haidary, S.A. and Povstyanova, M.: "A Comprehensive Geomechanical Study to Understand Drilling Challenges in the Manifa Field Offshore, Saudi Arabia," SPE paper 182833, presented at the SPE Kingdom of Saudi Arabia Annual Technical Symposium and Exhibition, Dammam, Saudi Arabia, April 25-28, 2016.

3. Fjaer, E., Horsrud, P., Raaen, A.M., Risnes, R., et al.: *Petroleum Related Rock Mechanics,* Vol. 33, 1st edition, Elsevier, 1992, 337 p.

4. Cui, L., Cheng, A.H-D. and Abousleiman, Y.N.: "Poroelastic Solution for an Inclined Borehole," *Journal of Applied Mechanics*, Vol. 64, Issue 1, March 1997, pp. 32-38.

5. Abousleiman, Y. and Nguyen, V.: "Poromechanics Response of Inclined Wellbore Geometry in Fractured Porous Media," *Journal of Engineering Mechanics*, Vol. 131, Issue 11, November 2005, pp. 1170-1183.

6. Liu, C. and Abousleiman, Y.N.: "Multiporosity/ Multipermeability Inclined Wellbore Solutions with Mud Cake Effects," *SPE Journal*, Vol. 23, Issue 5, October 2018, pp. 1723-1747.

7. Biot, M.A.: "General Theory of Three-Dimensional Consolidation," *Journal of Applied Physics*, Vol. 12, Issue 2, 1941, pp. 155-164.

8. Terzaghi, K.: *Principle of Soil Mechanics: A Summary of Experimental Studies of Clay and Sand*, McGraw-Hill, 1925, 98 p.

9. Detournay, E. and Cheng, A.H-D.: "Poroelastic Response of a Borehole in a non-Hydrostatic Stress Field," *International Journal of Rock Mechanics and Mining Sciences & Geomechanics Abstracts*, Vol. 25, Issue 3, June 1988, pp. 171-182.

10. Barenblatt, G.I., Zheltov, I.P. and Kochina, I.N.: "Basic Concepts in the Theory of Seepage of Homogeneous Liquids in Fissured Rocks [Strata]," *Journal of Applied Mathematics and Mechanics*, Vol. 24, Issue 5, 1960, pp. 1286-1303.

11. Aifantis, E.C.: "Introducing a Multi-Porous Medium," *Developments in Mechanics*, Vol. 8, Issue 37, 1977, pp. 209-211.

12. Nguyen, V.X. and Abousleiman, Y.N.: "Poromechanics Response of Inclined Wellbore Geometry in Chemically Active Fractured Porous Media," *Journal of Engineering Mechanics*, Vol. 135, Issue 11, November 2009, pp. 1281-1294.

13. Ewy, R.T.: "Wellbore Stability Predictions by Use of a Modified Lade Criterion," *SPE Drilling & Completion*, Vol. 14, Issue 2, June 1999, pp. 85-91.

14. Hoek, E. and Brown, E.T.: *Underground Excavations in Rock*, 1st edition, CRC Press, 1980, 532 p.

15. Hoek, E. and Brown, E.T.: "Practical Estimates of Rock Mass Strength," *International Journal of Rock Mechanics and Mining Sciences*, Vol. 34, Issue 8, December 1997, pp. 1165-1186.

16. Jaeger, J.C., Cook, N.G.W. and Zimmerman, R.: *Fundamentals of Rock Mechanics*, 4th edition, Wiley-Blackwell, 2007, 488 p.

17. Han, Y., Lai, B., Liu, H-H. and Li, H.: "Measurement of Elastic Properties in Brazilian Disc Test: Solution Derivation and Numerical Verification," *Geomechanics and Geophysics for Geo-Energy and Geo-Resources*, Vol. 4, Issue 1, March 2018, pp. 63-77.

18. Hoek, E., Carranza-Torres, C. and Corkum, B.: "Hoek-Brown Failure Criterion — 2002 Edition," *Proceedings of NARMS-Tac Conference*, Vol. 1, Issue 1, January 2002, pp. 267-273.

19. McLean, M.R. and Addis, M.A.: "Wellbore Stability Analysis: A Review of Current Methods of Analysis and their Field Application," SPE paper 19941, presented at the SPE/IADC Drilling Conference, Houston, Texas, February 27-March 2, 1990.

20. Itasca Consulting Group: "Fast Lagrangian Analysis of Continua (FLAC), Version 7.0," Minneapolis, Minnesota, 2011.

21. Hoek, E.: "Estimating Mohr-Coulomb Friction and Cohesion Values from the Hoek-Brown Failure Criterion," *International Journal of Rock Mechanics and Mining Sciences & Geomechanics Abstracts*, Vol. 27, Issue 3, June 1990, pp. 227-229.

About the Authors

Dr. Yanhui Han

Ph.D. in Computational Geomechanics, University of Minnesota

Dr. Yanhui Han is a Petroleum Engineer at the Aramco Research Center-Houston. His research interests are computational geomechanics related research, development, and applications. Yanhui's previous positions include the primary FLAC Developer and Geomechanics Consultant at Itasca Consulting Group for 10 years, Principal Technical Professional at Halliburton for 1 year and Production Technologist at Shell for 2 years.

Yanhui is the recipient of the 2013 N.G.W. Cook Award from the American Rock Mechanics Association. He is also a Registered Professional Engineer in the United States. Yanhui is currently serving as an Associate Editor for the *Journal of Petroleum Science and Engineering*.

He received his Ph.D. degree in Computational Geomechanics from the University of Minnesota, Minneapolis, MN.

Dr. Chao Liu

Ph.D. in Petroleum Engineering, University of Oklahoma

Dr. Chao Liu is a Petroleum Engineer at the Aramco Research Center-Houston. Formerly, he was a Research Associate at the PoroMechanics Institute, where he performed research on poromechanics and its applications in the oil and gas industry.

Chao received his B.S. degree in Mathematics from the East China Normal University, Shanghai, China, and his Ph.D. degree in Petroleum Engineering from the University of Oklahoma, Norman, OK.

Dr. Dung Phan

Ph.D. in Computer Science, Stony Brook University

Dr. Dung Phan is a Petroleum Engineer at the Aramco Research Center-Houston. He has extensive experience in software development, especially in the geomechanics domain. Dung's research interests include machine learning, artificial intelligence, formal methods in system design, and software verification.

He received his B.S. degree from Hanoi University of Science and Technology, Hanoi, Vietnam, an M.S. degree from the University of Oklahoma, Norman, OK, and his Ph.D. degree from Stony Brook University, Stony Brook, NY, all in Computer Science.

Dr. Khalid M. Al-Ruwaili

Ph.D. in Petroleum Engineering, Heriot-Watt University

Dr. Khalid M. Al-Ruwaili is a Petroleum Engineer leading and supporting several research projects in the Production Technology Division of Saudi Aramco's Exploration and Petroleum Engineering Center – Advanced Research Center (EXPEC ARC). He joined Saudi Aramco in 2006 as a Petroleum Engineer working in various technical positions for the Northern Area Reservoir Management at Berri field. After this assignment, Khalid worked on the ultimate development plan of the Upper Fadhili reservoir, a tight carbonate reservoir. His area of research is borehole mechanics, wellbore stimulation, hydraulic fracturing, and reservoir geomechanics.

He is an active member of the Society of Petroleum Engineers (SPE) and a technical contributor to the American Rock Mechanics Association. Khalid has authored and coauthored several technical papers.

He received his B.S. degree in Petroleum and Natural Gas Engineering from King Saud University, Riyadh, Saudi Arabia, an M.S. degree in Petroleum Engineering (Geomechanics) from the University of Calgary, Calgary, Alberta, Canada, and a Ph.D. degree in Petroleum Engineering (Geomechanics) from Heriot-Watt University, Edinburgh, Scotland, U.K.

Dr. Younane N. Abousleiman

Ph.D. in Civil Engineering, University of Delaware

Dr. Younane N. Abousleiman is the Director of the PoroMechanics Institute and a Professor in the Mewbourne School of Petroleum and Geological Engineering, ConocoPhillips School of Geology and Geophysics, and School of Civil Engineering and Environmental Science at the University of Oklahoma. His principal research focuses on poroelasticity and its applications to reservoir compaction and subsidence, inclined boreholes, rock and shale anisotropy, geomechanics of naturally fractured reservoirs, and sanding.

Younane received his B.S. degree from the American University of Beirut, Beirut, Lebanon, an M.S. degree from Columbia University, New York, NY, and his Ph.D. degree from the University of Delaware, Newark, DE, all in Civil Engineering.

Notes

Got an article you would like to publish? Here are our guidelines.

These guidelines are designed to simplify and help standardize submissions. They need not be followed rigorously. If you have any questions, please call us.

Length

Average of 2,500-4,000 words, plus illustrations/photos and captions. Maximum length should be 5,000 words. Articles in excess will be shortened.

What to send

Send text in Microsoft Word format via email plus one hard copy. Send illustrations/photos and captions separately but concurrently, both as email and as hard-copy (see file format section for more information).

Procedure

Notification of acceptance is usually within three weeks after the submission deadline. The article will be edited for style and clarity and returned to the author for review. All articles are subject to the company's normal review. No paper can be published without a signature at the manager level or above.

Format

No single article need include all of the following parts. The type of article and subject covered will determine which parts to include.

Working Title
Lorem Ipsum here.

Abstract
Usually 150-300 words to summarize the main points.

Introduction
Different from the abstract in that it sets the stage for the content of the article, rather than telling the reader what it is about.

Main body
May incorporate subtitles, artwork, photos, etc.

Conclusion/Summary
Assessment of results or restatement of points in introduction.

Endnotes/References/Bibliography
Use only when essential. Use author/date citation method in the main body. Numbered footnotes or endnotes will be converted. Include complete publication information. Standard is *The Associated Press Stylebook*, 52nd ed. and *Wesbter's New World College Dictionary*, 5th ed.

Acknowledgments
Use to thank those who helped make the article possible.

Illustration/Tables/Photos and explanatory text

Submit these separately. Do not place in text. Positioning in the text may be indicated with placeholders. Initial submission may include copies of originals; however, publication will require the originals. When possible, submit both electronic versions and printouts. Color is preferable.

File Format

Illustration files with .EPS extensions work best. Other acceptable extensions are .TIFF/.JPEG/.PICT.

Permission(s) to reprint, if appropriate

Previously published articles are acceptable but can be published only with written permission from the copyright holder.

Author(s)/Contibutor(s)

Please include a brief biographical statement.

Submission/Acceptance Procedures

Papers are submitted on a competitive basis and are evaluated by an editorial review board comprised of various department managers and subject matter experts. Following initial selection, authors whose papers have been accepted for publication will be notified by email.

Papers submitted for a particular issue but not accepted for that issue may be carried forward as submissions for subsequent issues, unless the author specifically requests in writing that there be no further consideration.

Submit articles to:

Editor
The Saudi Aramco Journal of Technology
C-11B, Room AN-1080
North Admin Building #175
Dhahran 31311, Saudi Arabia
Tel: +966-013-876-0498
Email: *william.bradshaw.1@aramco.com.sa*

Submission deadlines

Issue	Paper submission deadline	Release date
Winter 2019	August 1, 2019	December 31, 2019
Spring 2020	November 12, 2019	March 31, 2020
Summer 2020	February 11, 2020	June 30, 2020
Fall 2020	May 12, 2020	September 30, 2020

There is more.

Monitoring Waterflood Front Movement by Propagating High Frequency Pulses through Subsurface Transmission Lines

Jesus M. Felix Servin

Abstract / This article describes a novel approach to monitor waterflood front movement using proximity sensing in conjunction with contrast agents. Our technique exploits the presence of resistive layers between reservoirs, which act as a transmission line for electromagnetic (EM) signals, to achieve increased propagation range. This work focuses on numerical simulations to evaluate the potential of this approach to monitor water movement in the reservoir under different conditions.

Completion Challenges in Unconventional Resources during the Transition Period

Almaz Sadykov, Syed Muhammad, Nayef I. Al-Mulhim, Pavan Dharwadkar, Dr. Lionel B. Small, Sohrat Baki, and Kenneth M. McClelland

Abstract / Initial exploratory wells in the unconventional program utilized existing well menus that have traditionally been successful for conventional wells. As the unconventional program matured, intensifying stage count, stage volumes, and greater pump rates, it became apparent that the standard accepted practices would no longer be valid. This article addresses the safety and operational challenges that resulted from utilizing a wellhead isolation tool (WHIT) to stimulate unconventional wells completed with 10 Kpsi wellhead components, and provides lessons learned and internally developed best practices.

A More Sustainable Approach: Nanofiltered Seawater-based High Temperature Fracturing Fluids

Dr. Leiming Li, Dr. Fakuen F. Chang, and Dr. Rajesh K. Saini

Abstract / In recent decades, the widespread implementation of horizontal drilling and multistage hydraulic fracturing in unconventional plays has increased the use of freshwater in oil field operations. The formulation of fracturing fluids with non-freshwater sources such as seawater or produced water are attracting more attention, due to the long-term sustainability of non-freshwater use.

Nanocomposite Resin Coated Proppant for Hydraulic Fracturing

Dr. Mohammad H. Haque, Dr. Rajesh K. Saini, and Dr. Mohammed A. Sayed

Abstract / Proppant, such as sand and ceramics, is used in keeping fractures open for hydrocarbon production in hydraulic fracturing operations. Its ability to withstand reservoir closure stresses and provide high conductivity is one of its key selection criteria. Sand is preferred over ceramics in unconventional plays due to its low cost and overall abundance. The lower crush strength of sand compared to ceramics limits its application to wells having lower closure stresses.

To read these articles and others, go to www.saudiaramco.com/jot

أرامكو السعودية
saudi aramco

Aramco
Journal
of Technology

Liked this issue? Sign up. It's free.

To begin receiving the *Aramco Journal of Technology* please complete this form, scan and send by email to ***william.bradshaw.1@aramco.com*.**

Got questions?

Just give us a call at +966-013-876-0498 and we'll be happy to help!

Scan the QR code to go straight to your email and attach the form!

Subscription Form

Name

Title

Organization

Address

City

State/Province

Postal code

Country

Email address

Number of copies